SANDIA REPORT
SAND2001-1303
Unlimited Release
Printed May 2001

The Use of Twist-Coupled Blades to Enhance the Performance of Horizontal Axis Wind Turbines

Don W. Lobitz, Paul S. Veers, G. Richard Eisler,
David J. Laino, Paul G. Migliore, and Gunjit Bir

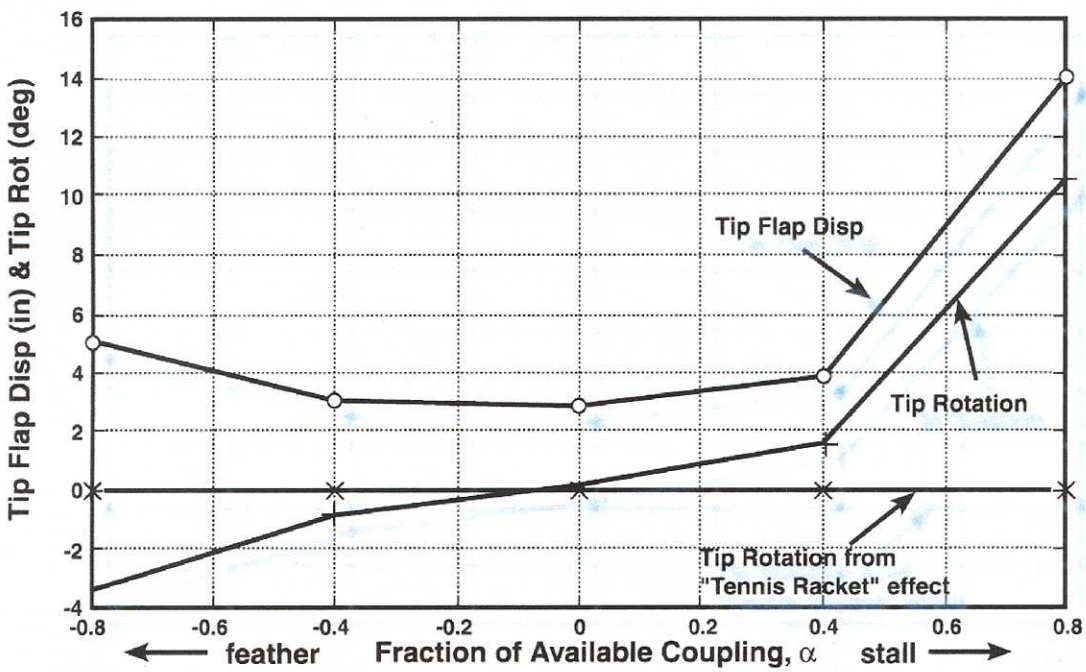

Tip Motion of the bending twist-coupled CEB Turning at 72 rpm in Still Air.

Prepared by
Sandia National Laboratories
Albuquerque, New Mexico 87185 and Livermore, California 94550

Sandia is a multiprogram laboratory operated by Sandia Corporation, a Lockheed Martin Company, for the United States Department of Energy under Contract DE-AC04-94AL85000.

Sandia National Laboratories

Issued by Sandia National Laboratories, operated for the United States Department of Energy by Sandia Corporation.

Available to DOE and DOE contractors from
U.S. Department of Energy
Office of Scientific and Technical Information
P.O. Box 62
Oak Ridge, TN 37831

Telephone: (865)576-8401
Facsimile: (865)576-5728
E-Mail: reports@adonis.osti.gov
Online ordering: http://www.doe.gov/bridge

Available to the public from
U.S. Department of Commerce
National Technical Information Service
5285 Port Royal Rd
Springfield, VA 22161

Telephone: (800)553-6847
Facsimile: (703)605-6900
E-Mail: orders@ntis.fedworld.gov
Online order: http://www.ntis.gov/ordering.htm

SAND2001-1303
Unlimited Release
Printed May 2001

The Use of Twist-Coupled Blades to Enhance the Performance of Horizontal Axis Wind Turbines

Don W. Lobitz
Structural Dynamics Engineering

Paul S. Veers
Wind Energy Technology

G. Richard Eisler
Engineering and Manufacturing Software

Sandia National Laboratories
P.O.Box 5800
Albuquerque, NM 87185-0847

David J. Laino
Windward Engineering
Salt Lake City, Utah 84117

Paul G. Migliore and Gunjit Bir
National Renewable Energy Laboratory
Golden, Colorado 80401

Abstract

This paper reviews issues related to the use of aeroelastic tailoring as a cost-effective, passive means to shape the power curve and reduce loads. Wind turbine blades bend and twist during operation, effectively altering the angle of attack, which in turn affects loads and energy production. It is possible to build a small amount of desirable twisting into the load response of a blade with proper asymmetric fiber lay up in the blade skin. The tailored twisting can create an aeroelastic effect that has payoff in either better power production or in vibration alleviation, or both. Several research efforts have addressed different parts of this issue. Research and development in the use of aeroelastic tailoring on helicopter rotors is reviewed. Potential energy gains as a function of twist coupling are reviewed. The effects of such coupling on rotor stability have been studied and are presented. Fatigue damage estimates due to turbulent inflow have been computed for rotors employing several different control schemes, with and without twist-coupled blades. Energy output and maximum loads are also computed and compared

Contents

Figures and Tables

Figures and Tables (cont.)

Figures and Tables (cont.)

Figures and Tables (cont.)

Figures and Tables (cont.)

Executive Summary

Whenever wind turbine blades twist, there is a direct influence on the angle of attack, changing loads and affecting output power. This is directly exploited in classic pitch control used in not only wind turbines but in rotors of all types. When the pitch changes are rapid enough, they can affect not only average loads and power, but vibratory loads as well, influencing fatigue life throughout the system. Even quite small angles of twist can have significant impact.

Several investigators, including Corbet and Morgan, (1992), Karaolis et al. (1988, 1989) and Kooijman (1996) have explored the use of various blade loads to effect pitch changes. These pitch changes are primarily aimed at regulating and/or increasing power output.

The reorientation of the fiber directions in the blade skin or spar to achieve either flap-load or extension-load coupling with blade twist, has potential to be a cost effective and reliable aeroelastic tailoring approach. We seek here to investigate modest blade rotations produced by elastic twist coupling of the blade as it bends or extends without any additional mechanisms or devices. Following the lead of the helicopter industry which long ago saw potential for aeroelastic tailoring, there are a number of possible uses of aeroelastic tailoring in wind turbine applications. They include stall enhancement to permit larger diameter rotors for improved average energy capture and load alleviation through twist coupling toward feather. In pursuing these potential uses, dynamic effects including stability issues, and manufacturing constraints must be addressed.

Effects on Annual Energy Capture in a Steady Wind Regime, Twisting toward Stall:

For constant speed rotors, enhanced stall control of wind turbines has been used in the past to improve the energy capture of rotors by allowing the rotor size to grow while maintaining a low maximum rating on other components in the system. Tangler and Somers (1995) and Klimas (1984) have published families of airfoils that have since been used to stall regulate turbines at lower power levels with the associated reduced system cost of energy. An aeroelastically tailored blade that twists to stall in response to flap loads has a similar effect.

Lobitz and Veers (1996) examined generic coupling effects on annual energy production of a nominally 26-meter diameter stall regulated HAWT. The blades were assumed to twist to stall, reducing maximum power. The rotor diameter was then increased to bring maximum power back up to its initial level. Twist distributions were specified by prescribing a maximum tip amplitude and a spanwise variation, varying with wind speed in either a linear or quadratic fashion. A twist proportional to power was also used. It was discovered that the details of spanwise variation or how the twist varied with wind speed (or power) had only minor impacts. The twist-coupled blades combined with larger rotors increase power in the important middle-range of wind speeds while power in high winds remains the same. Studies which investigated the increase in annual energy as a function of the annual average wind speed showed that for a maximum twist angle of one degree the energy capture is increased by about 5% and for two degrees, about 10%. The improvements are not overly sensitive to the wind resource.

Large maximum twist angles leading to large increases in rotor diameter were also investigated. For maximum twist angles of less than seven degrees the per cent energy increase actually exceeds the per cent increase in swept ar-

ea. For larger maximum twist angles the benefits drop off substantially.

Care needs to be used, however, when predicting performance enhancements based on fine tuning a stall-controlled rotor. Predicting power output in deep-stall has a very high uncertainty. In subsequent work where twist-coupled blades were structurally modelled, results for both steady and turbulent inflow indicated a measure of instability in the stall regime when the coupling produced twist toward stall. For the turbulent inflow the instability appeared to be stall-flutter exhibiting limit-cycle oscillations at a frequency near the frequency of the first twist-coupled mode. Field data will be required to prove that aeroelastic enhancement using twist-coupling toward stall can be achieved in a stable and reliable fashion. However, computational results suggest twist-toward-stall to be a dangerous concept when operating in the stall regime.

For variable speed rotors, particularly when combined with pitch control, it can be argued that there is no need for additional power control from any other source. Even stall-controlled variable-speed systems can theoretically control power by slowing the rotor down to achieve a flat power regulation. The question is whether the twist-coupled blade will achieve enough of the functionality of the active pitch control device to replace it with the more reliable and inexpensive passive approach.

Eisler and Veers (1998) examined the performance gains of adaptive blades that twist under the action of centrifugal loads, installed on a 26 meter diameter variable speed rotor. Gains were compared to the perfect performance of the system running at peak C_p below rated power and at maximum power at higher wind speeds. Converging on this theoretical limit without a pitching system is the goal. Two speed-control approaches were investigated: an "aggressive" approach where no limitations are placed on rotor speed so that the desired power level at a given windspeed is always achieved; and a "conservative" approach that utilizes stall regulation, requiring constant rotor-speed beyond a predetermined windspeed. Below that windspeed, peak efficiency is achieved by requiring the rotor speed to vary linearly with windspeed. For the aggressive case the generator is assumed to instantaneously slow down the rotor in high winds, which is physically impractical if not impossible.

Using an optimization procedure in conjunction with the PROP-PC code (Tangler, 1987), best choices for rotor speed, pitch offset, and a twist coupling coefficient for a full span twist that varies quadratically with the rotor speed (meant to model centrifugally driven twist coupling), were obtained. These choices maximized annual energy subject to a prescribed rotor power limit. In contrast to the work described above for the constant speed rotor, in this study rotor size was held constant. Sites with average windspeeds of 5, 7 and 9 meters/second were used in these investigations.

The baseline conservative approach resulted in a 7-12% (7 for a 5 m/s average wind speed and 12 for a 9m/s one) loss in annual energy relative to perfect performance. An optimal pitch offset reduces that loss to 4-9%. The introduction of twist-coupling with optimal pitch offset further reduces the loss to 3-6.5%, indicating that aeroelastic coupling is more effective in higher wind sites than in lower ones. With the aggressive approach, only minimal improvement was achieved in annual energy capture with either optimal pitch offset alone or in combination with twist-coupling.

Dynamic and Static Stability Issues:

Whenever the wind turbine blade becomes aeroelastically "active," that is, the elastic deformations play a role in the aerodynamic

loading, dynamic stability will be affected. Lobitz and Veers (1998) addressed two of the most common stability constraints, namely classical flutter and divergence. Classical flutter is the condition where the phasing between the aerodynamic load fluctuations and elastic deformations are such that a resonant condition is achieved. Every wing will have a flutter boundary at some speed; for wind turbines the boundary is defined at the rotational speed (typically determined in still air) at which the blade will flutter. The stability margin is the difference between the flutter speed and normal operating speed. Divergence is a quasi-static condition where the blade twists in response to increasing load in a direction that further increases the load. It occurs when an operating speed is reached where the increase in loads caused by the deformation exceeds the ability of the blade to resist the load.

The stability boundaries were determined with respect to the amount of twist coupling built into the blade. A coupling coefficient, α, which varies between -1 and 1, was defined to facilitate the generic examination of stability effects. For a blade with bending twist-coupling and prescribed bending and twisting stiffnesses, this coefficient represents a range for the coupling stiffness wherein the system remains positive definite.

Creating a bending twist-coupled finite element model of the 10-meter diameter NREL Combined Experiment Blade for use in the MSC NASTRAN commercial software, the flutter and divergence stability boundaries were mapped over the range of possible α's. Instability occurs when the design operating speed exceeds these boundaries. Results indicate that the stability boundaries are not exceeded even with coupling levels up to 80% of the theoretical maximum, although the stability margins decrease toward the extreme values of the coupling coefficient. As α approaches one of it extremes, the blade bends and twists toward stall, increasing angle of attack and also loads, and this reduces the divergence stability margin. Conversely, as α approaches the other extreme, the blade twists toward feather reducing aeroloads and increasing the divergence stability margin. However, in this region, the classical flutter stability margin decreases, although not as severely as the divergence margin for the prior extreme where the blade twisted toward stall.

Another important stability constraint, stall-flutter, is yet to be investigated for twist-coupled blades.

Load Alleviation, Twisting toward Feather:

Twisting to feather in response to increasing winds is a potential means to reduce the dynamic loading on the blades, and hence the rest of the system. Eggers et al. (1996) demonstrated load reductions by linking a pitch control system to flapwise blade loads using simple integral control. The results indicate the potential to reduce the root-mean-square (rms) blade bending response to turbulent winds by about half. And this was accomplished with rms pitching angles of 3 degrees for 1/3 span ailerons, and substantially less with full-span pitch control. The fatigue implications of such a substantial decrease in cyclic loading are enormous, measured in increased lifetime or reduced blade weight. Additional studies reported by Moriarty et al. (2001) indicate that for a spatially uniform turbulent inflow the effects of rotor scale and control system lag do not significantly diminish the above findings.

An aeroelastically twisting blade is similar to the control system investigated by Eggers in that the blade pitch angle would respond to bending loads in a way similar to a proportional, rather than an integral, controller. The ability of bending twist-coupled blades to attenuate (or exacerbate) the cyclic loading has been investigated by Lobitz and Laino (1999), and Lobitz, Veers and Laino (2000) for a

33-meter diameter rotor employing three different control strategies: constant speed stall-controlled, variable speed stall-controlled and variable speed pitch-controlled. Transient structural dynamic simulations of the bending twist-coupled rotor were carried out using the ADAMS commercial software modified to include twist-coupling. Ensembles of 10-minute turbulent wind histories were generated with the SNLWIND-3D software and used to drive the rotor. Average windspeeds of 8, 14 and 20 m/s (peak power for stall-control occurs near 17 m/s, and for pitch-control near 12 m/s) were investigated for both high and low turbulence intensities. Material damage exponents of 3, 6 and 9 were applied to the load cycles for computing damage.

Results for the constant speed stall-controlled case indicate that twist-coupling toward stall produces significant increases in fatigue damage, and for a range of wind speeds in the stall regime apparent stall flutter behavior is observed. For twist-coupling toward feather with a coupling coefficient of magnitude, 0.6, fatigue damage is decreased by 20% to 70% with the higher percentages occurring at the lower average windspeeds. Concurrent with lower fatigue damage estimates for twist-coupling toward feather, maximum loads decreased slightly, especially for the lower average windspeeds. For the case where the pitch offset is altered to bring the power curve of the twist-coupled rotor into better agreement with that of the uncoupled one, differences in average power are minimal (< 1%).

For the variable speed stall-controlled case, some steady wind results were obtained showing that for variable speed operation the twist coupled rotor (α=0.6 toward feather) can be almost as efficient as the uncoupled one if a slightly altered rpm versus windspeed schedule is followed. Turbulent wind simulations show that fatigue damage is decreased by 20% to 50% with, as above, the higher percentages occurring at the lower average windspeeds. Maximum loads also decreased slightly. With the power curves for the two rotors adjusted to be essentially equivalent through a designed pitch offset distribution, power production for the twist-coupled rotor was equivalent to the uncoupled one in all cases. Thus, substantial fatigue damage reductions prevail for the rotor in variable speed operation as in the case for constant speed, and with no loss in power output.

As the introduction of twist-coupling generally softens the blade, additional computations were performed on a rotor with the same amount of softening but with no twist-coupling to determine its impact. Results indicated that for the 8 m/s average windspeed where the turbine operates primarily in the linear aerodynamic range, damage reductions were less than half of those for the twist-coupled rotor. At higher average windspeeds where stall is prevalent, the damage actually exceeded that of the original uncoupled rotor and greatly exceeded that of the twist-coupled one.

Results for the variable speed pitch-controlled case indicate reductions in fatigue damage from 20% to 80% for twist coupling toward feather with α=0.6. Contrary to the previous cases, the larger reductions here correspond to the higher average wind speeds, probably due to the fact that this rotor operates primarily in the linear aerodynamic range for all three of the average windspeeds. As before, with the power curves for the two rotors adjusted to be essentially equivalent through a designed pitch offset distribution, energy capture was nearly identical for all cases. Reductions in maximum loads were significantly greater than that of the rotors discussed above.

Design and Manufacturing:

Although the design and manufacture of twist-coupled blades will not be addressed in the body of this report, for completeness a few paragraphs will be provided here with refer-

ences cited for obtaining additional information.

The fact that there are potential benefits from aeroelastic tailoring does not necessarily mean that the blades can be manufactured to produce the desired coupling. There are limits to the amount of coupling that can be achieved with asymmetric fiber lay ups. The best direction and the maximum coupling are a function of the fiber and matrix properties. Tsai and Ong (1998) indicate that stiffer fiber materials result in the higher coupling levels, with maximum α for flat plates just below 0.8 for a graphite-epoxy system and 0.6 for a glass-epoxy system. The carbon system achieves maximum coupling with all the fibers at about 20 degrees to the axis of bending while the glass maximum is at about 25 degrees. These theoretical maxima, however, do not account for the need for off-axis strength and toughness, nor do they apply directly to cross sections other than flat plates.

Karaolis (1988) mapped out the best combinations of two directional lay ups to maintain strength and produce twist-coupling in an airfoil shape. His results indicate that the best coupling can be achieved with the off-axis fibers oriented at about 20 degrees to the spanwise axis of the blade. Tsai and Ong (1998) found the same result for the D-spar shape. Karaolis predicts that with this configuration, twists on the order of one degree per meter of span can be achieved based upon limits of maximum strain in the blade. The Tsai and Ong results indicate that graphite-epoxy D-spars have maximum couplings around $\alpha = 0.55$ while glass-epoxy D-spars are around $\alpha = 0.4$. Interestingly, hybrid glass and graphite lay ups, using the graphite to obtain the coupling and the glass to provide off-axis strength, do just as well as all graphite. The major reasons for the reduction from the flat plate α's are the need for fibers in other orientations (to provide robust, omnidirectional strength and panel buckling resistance) and the vertical "web" of the spar. Kooijman (1996), who also recommends 20-degree reinforcement, suggests that the coupling is maximized by avoiding 45-degree lay ups in the web.

The manufacturing process will depend on the type of coupling to be produced. Fiber winding is well suited to producing extension twist-coupling in a spar, while clam shell construction with the top and bottom skins manufactured separately is best suited to bending twist-coupling.

Report Synopsis:

The table on the following page provides a condensed overview of the chapters that follow this executive summary. Major findings from each chapter are identified in the table.

Chapter 1: Background	• A number of investigators have studied the use of aeroelastic coupling in HAWTs and helicopters.
Chapter 2: Improved Energy Capture from HAWTs Using Adaptive Blades	• By moderately twisting the blade toward stall through twist-coupling and simultaneously growing the rotor diameter, significant increases in annual energy can be achieved.
Chapter 3: Parameter Optimization Applied to a Variable Speed HAWT with Adaptive Blades for Optimizing Energy Capture	• By optimally selecting blade pitch and twist-coupling parameters, energy capture for a variable speed stall-controlled rotor can approach that of a variable speed variable-speed-controlled rotor.
Chapter 4: Aeroelastic Behavior of Twist-Coupled HAWT Blades	• Twist-coupled blades tend to be less stable with regard to divergence (twist to stall) and classical flutter (twist to feather), but not prohibitively so.
Chapter 5: Load Mitigation with Twist-Coupled Blades on a Constant Speed Stall-Controlled Rotor	• Twist-coupling to stall significantly increases fatigue damage and can promote stall flutter. • Twist-coupling to feather significantly decreases fatigue damage without reducing power output (especially at the lower windspeeds).
Chapter 6: Load Mitigation with Twist-Coupled Blades on Rotor Using Modern Control Strategies	• For variable speed pitch-controlled rotors, twist-coupling to feather substantially decreases fatigue damage without reducing power output (for <u>all</u> windspeeds).

The Use of Twist-Coupled Blades to Enhance the Performance of Horizontal Axis Wind Turbines

Chapter 1: Background

Wind Turbine Experience

Whenever wind turbine blades twist, there is a direct influence on the angle of attack, changing loads and affecting output power. This is directly exploited in classic pitch control used in not only wind turbines but in rotors of all types. When the pitch changes are rapid enough, they can affect not only average loads and power, but vibratory loads as well, influencing fatigue life throughout the system. Even quite small angles of twist can have significant impact.

The concept of building blades that passively adapt to the incident wind loading is not new. Mechanisms that adjusted blade angle of attack in response to the thrust loading were quite popular in the early days of the modern wind energy push. Approaches and objectives were quite varied. Cheney and Speirings (1978) regulated power with a centrifugally loaded mass on an elastic arm. Bottrell (1981) had a system for cyclically adjusting pitch for per rev load balancing. The North Wind 4 kW turbine (Currin, 1981) had a system for passively adjusting pitch for both power and load control. Hohenemser and Swift (1981) studied alleviating yaw loads with cyclic pitch adjustments.

A Garrad-Hassan report (Corbet and Morgan, 1992) evaluates the use of all available blade loads to effect pitch changes that would regulate the power output of a turbine, aiming at a flat power curve in high winds. Only pitching to feather is evaluated to avoid the vagaries of predicting power output in the post-stall regime. They report that several manufacturers were already using some form of passive power control in their designs (Lagerwey, NPS, Berewoud, Flexhat, Swedewind, Carter). The conclusion is that perfect regulation is very difficult to achieve, and that even less than perfect regulation is a challenge. These approaches also depend on quite substantial blade rotations to achieve perfect regulation.

Karaolis et al. (1988, 1989) introduced the concept of using biased lay ups in blade skins to achieve different types of twist coupling for wind turbine applications. Figure 1.1 shows how different fiber orientations in a blade skin can be used to achieve bend-twist or stretch-twist coupling. By changing the blade skin from an orthotropic to a biased fiber lay up, the blade can be aeroelastically tailored with minimal disturbance to the beam stiffness properties or manufacturing costs. Karaolis suggests that in addition to using the flapwise or centrifugal loading to twist a blade, it might be useful to internally pressurize a spar and use changes in the pressure to actively control the angle of blade twist. Interestingly, Corbet and Morgan (1992) mention aeroelastic tailoring as a possible method for improved power control, but dismiss it because of the perceived inability of current manufacturing processes to produce blades with sufficient repeatability to make the concept reliable.

A Kooijman (1996) report on aeroelastic tailoring concludes that “the use of aeroelastic tailoring of the Fibre Reinforced Plastics to control limited torsional deformation is a promising way to improve rotor blade design.” Kooijman evaluates building the elastic coupling into the blade skin. Some of his conclusions for blades designed for the “Smart Rotor” are that:

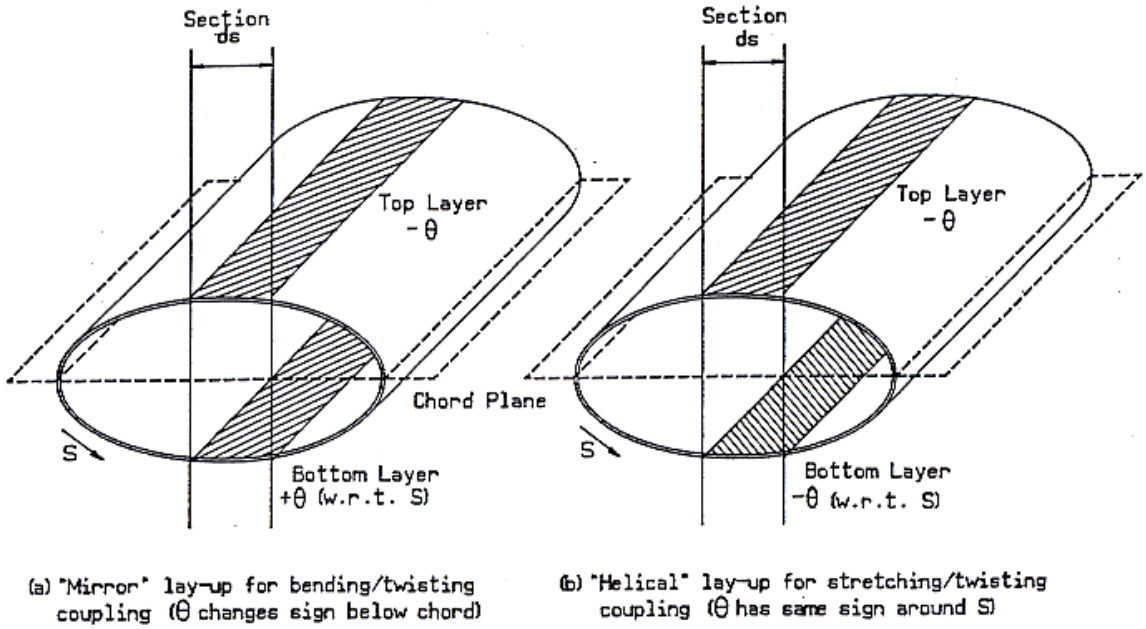

Figure 1.1. Type of asymmetric lay ups required to produce (a) bending twist-coupling and (b) extension twist-coupling (from Karaolis, et al., 1988).

1. bending twist-coupling gives the potential for a few percentages of energy yield improvement for constant-speed pitch-controlled turbines and improves starting torque by 10%.

2. Optimal constant-speed pitch-controlled rotor production is obtained with the inboard span twisting to feather and the outboard 60% of the span twisting toward stall as wind speed increases.

3. The coupling is best achieved with hybrid carbon/glass reinforcement in the cross-ply direction.

4. Bending-torsion stiffness is about 10% less than a standard construction.

Middleton et al. (1998) and Infield et al. (1999) designed, analysed, fabricated and tested a "stretch-twist coupled" blade developed to control the rotor in a runaway scenario. Their composite blade was fabricated using a helical layup with layers of glass and carbon fibers. Measured twist coupling agreed well with predictions and measured runaway speeds were actually less than predicted.

A recent *Windpower Monthly* (Feb. 1998) reported that some Lagerwey turbines will include the "TenTorTube" device for passively controlling power and reducing run-away risk. This tube, shown in Figure 1.2, attaches a pitchable tip to the blade and twists in response to centrifugal loads caused by rotor-speed changes. The mechanism can be locked at low speeds and then used to produce a large change in power at higher rotor speeds. The aramid-epoxy device can be made as long as is needed to produce the desired magnitude of tip rotation. Therefore, large twist angles can be achieved, even with an entirely elastic device.

The ability to design in a few degrees of blade twist was encouraged by a report by Stoddard, et al. (1989) which found a few degrees of elastic twist in blades not intended to have any. They concluded that up to 2.5 degrees of twist can occur in the blades of the study group (UTRC – 2.6 deg., ESI – 0.4 deg., Carter – 2.0 deg.). Therefore, it should be possible to design in desirable elastic twist in response to rotor loads, either centrifugal or flap, that enhance energy capture performance.

The reorientation of the fiber directions in the blade skin or spar to achieve either flap-load or extension-load coupling with blade twist, has potential to be a cost effective and reliable aeroelastic tailoring approach. We seek to investigate modest blade rotations produced by elastic twist of the blade itself without any additional mechanisms or devices. The helicopter industry long ago saw the potential in aeroelastic tailoring. The next section includes a summary of helicopter experience. There are a number of possible uses of aeroelastic tailoring in wind turbine applications, each of which is discussed in subsequent sections. Stall enhancement to better regulate and permit larger diameter rotors and improved average energy capture are discussed first. Then dynamic effects including load alleviation and stability issues are reviewed. The manufacturing constraints and opportunities are just beginning to be addressed.

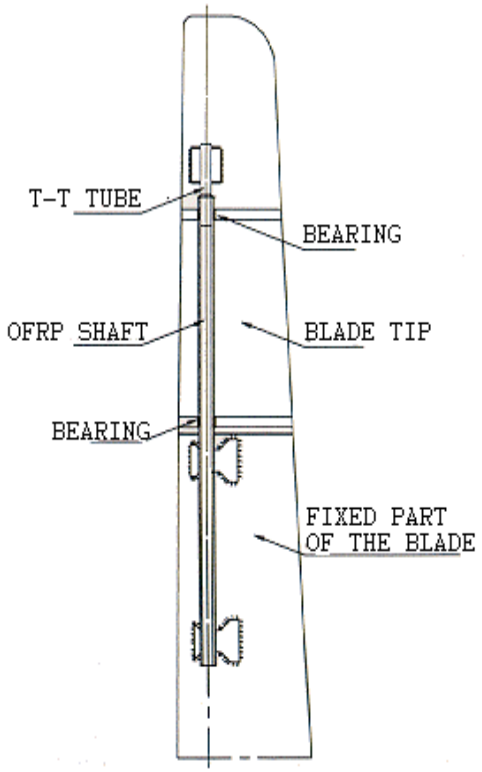

Figure 1.2. TenTorTube schematic (from Joose and van den Berg, 1996)

Helicopter Experience

Wind turbines and helicopters, though designed for different objectives, share similar aeroelastic problems. A sizeable rotor dominates behavior of both the systems. Its rotary blades elastically couple with surrounding air and other system components to influence overall performance, vibration, loads, and stability. Because of these similarities, the aeroelastic tailoring techniques developed for helicopter blades can be readily applied to wind turbine blades.

Earlier structural tailoring attempts in the helicopter field (Miller 1956, Hirsch 1956, McCarthy 1955, Daughaday 1957) were limited to tuning of blade chordwise and spanwise mass distributions with a single objective of blade vibration reduction. Later, as the art of blade manufacturing became more sophisticated, aerodynamic means such as blade twist and swept tips were introduced (Blackwell 1983) as a means for controlling vibration.

Most of the subsequent aeroelastic tailoring research is heavily linked with optimization techniques and understandably so. Aeroelastic tailoring is a multidisciplinary problem dealing with a strong coupling amongst blade elasticity, aerodynamics, dynamics, and controls. We cannot, for example, hope to enhance performance without influencing vibration or stability. We must use a multi-objective criterion encompassing conflicting demands such as performance enhancement, vibratory response, and load reduction subject to multidisciplinary constraints like aeroelastic stability, resonances, system weight, and aerodynamic shape. Friedman (1983, 1984) and Shanthakumaran (1982) present the first documented optimum structural tailoring efforts to reduce helicopter vibration subject to aeroelastic constraints. The studies considered a four-bladed hingeless rotor (much like most of the wind turbine rigid-blade rotors except that the helicopter blades are softer in the plane of rotation). The design variables consisted of the blade box-spar geometric parameters, and the blade structural and non-structural masses.

The constraints consisted of the flap, lag, and torsion frequencies, and the aeroelastic stability margins. The objective function contained peak-to-peak oscillatory hub shears and hub rolling moments. A general-purpose constrained optimization package (Miura 1979) was used to solve the optimization. Results showed a reduction of 38% in hub shear and a reduction of 25% in hub rolling moment. The blade mass decreased by 20%. Celi et al. (1988, 1987) extended these studies to include double-cell box sections and swept tips. Results indicated vibration reduction between 20-50%; tip sweep reduced vibration by an additional 10%.

Lim and Chopra (1988, 1987) tackled the vibration reduction problem using a more comprehensive formulation. This study included a number of substantial contributions, in particular the formulation of a direct analytical approach (1987) for the calculation of the derivatives of hub loads and the blade stability with respect to the design variables. Studies using 25 design variables showed a 20-77% reduction in hub shear and moments. In addition to these fairly comprehensive studies, a number of less ambitious studies, too numerous to be cited, were conducted at universities and industry, wherein the main objective was to explore fundamental aspects of the optimal tailoring problem. Some notable contributions are the study of blade frequencies placement (Peters 1986, 1988), weight reduction (Bielawa 1971), improvement of handling qualities (Celi 1989), and vibration reduction using modal shaping or modal vibration indices (Taylor 1982, Davis 1988, Weller 1988,1989).

As these optimal tailoring techniques were maturing, metallic blades were rapidly giving way to composite blades. Composites offer several advantages over metals, such as superior fatigue characteristics, higher stiffness-to-weight ratio, fabricability of complex-geometry blades, and potential for aeroelastic tailoring. Composite-blade elastic anisotropy can not only be tightly controlled but also varied over the span by appropriate selection of ply angles, thickness, and spanwise lay up. Resulting anisotropy provides direct bending-axial-torsion elastic couplings not possible with metallic blades.

Early studies on the aeroelastic behavior of composite blades (Hong 1985, Panda 1987) showed that the elastic couplings could have a powerful influence on aeroelastic stability, blade stresses, and loads. These studies, however, did not model precisely the non-classical phenomena like shear and warping. Smith and Chopra (1991) addressed this limitation. Later, Chandra and Chopra (1991, 1992) used Vlasov theory to extend composite blade modeling to include composite beams of arbitrary sections, including open sections and closed multi-cell sections. These models were integrated into a comprehensive aeroelastic code (Bir, 1990) and used as a starting point for all the subsequent aeroelastic tailoring efforts carried out at the University of Maryland. Friedman et al (1992) were also involved in the development of an aeroelastic-tailoring capability for composite straight-tip and swept-tip blades, but results though have not yet been presented. While it had been amply demonstrated that composite couplings can significantly influence rotor vibration and stability, Ganguli and Chopra (1992, 93, 94) were the first to apply a systematic optimization approach to composite tailoring of helicopter blades. The analytical formulation of sensitivity derivatives, a key step in the optimal tailoring process, was extended to cover composite blades. Hitherto, aeroelastic tailoring efforts had been confined to minimization of hub loads only, which at times resulted in higher blade bending moments, leading to higher stresses and reduced blade fatigue life. Ganguli and Chopra (1997) extended aeroelastic-tailoring research to simultaneously minimize both hub loads and blade-bending moments. Constraints were imposed on blade stability, rotating-blade frequency placement, and autorotational inertia. Results showed significant reductions in both hub and blade loads. Reductions resulted from elastically introduced couplings. Positive flap/torsion elastic coupling, equivalent to a delta-3 of about 35 degrees, reduced hub loads. Reduction of

flap, lag, and torsion stiffness at the blade root decreased the blade dynamic stresses. Negative lag/torsion elastic coupling, equivalent to a delta-4 of about -10 degrees, enhanced the lag-mode stability (some readers may be aware that rotor-lag instability is a major issue for helicopters).

Recent research has shown that the blade geometry may also be tailored to gain performance, loads, and stability benefits (Celi 1988). Bir and Chopra (1994) developed a comprehensive model of an advanced geometry blade that involves variable sweep, anhedral, taper, and twist along the blade span. Ganguli and Chopra (1997) integrated this advanced geometry blade with aeroelastic optimization schemes, then simultaneously tailored blade geometry and composite anisotropy to minimize blade stresses and vibration. They performed the tailoring studies on a four-bladed, soft-inplane, hingeless rotor with variable sweep, taper, and anhedral, and with a two-cell composite box spar. The tailored blade achieved a reduction of 40-60% in the 4/rev hub loads, and a reduction of 15-25% in the peak-to-peak vibratory blade flap and lag bending moments.

As noted earlier, the objective function for a helicopter rotor design differs somewhat from that for a wind turbine blade. For a mission-driven helicopter design, the emphasis is on maximizing rotor in-plane stability and minimizing vibration without deteriorating performance and fatigue life. For a cost-driven wind turbine design, the emphasis is on enhancing or regulating power without adversely affecting fatigue loads, blade response, and system stability. The general optimal aeroelastic tailoring approach however is similar for both systems. The nature of design variables is also the same for both helicopter and wind turbine blades. Wind turbine research can save substantial time and developmental cost by adapting well-established tailoring/optimization and code-integration techniques developed for helicopters over the last two decades.

Improved Energy Capture from HAWTs Using Adaptive Blades

Chapter 2

Introduction

The concept of building blades that adapt to the incident wind loading is not new. Many blade concepts that twist to change their angle of attack in response to the thrust loading were produced in the early days of the wind energy rush of the late twentieth century with quite varied objectives and approaches. Cheney and Spierings (1978) presented a power regulation design that used a centrifugally loaded mass on an elastic arm to adjust the full span pitch. Bottrell (1981) had a design for cyclically adjusting pitch for per rev load balancing. The North Wind 4kW turbine (Currin, 1981) had a system for passively adjusting the blade pitch for both power and load control. Hohenemser and Swift (1981) studied a design for alleviating the high loads due to yaw control by cyclic pitch adjustments. Most of the early attempts relied on pitching the blades to feather to reduce the power output and loads. Elastic deformation of turbine blades has also been documented (Stoddard, et al., 1989) with elastic twist due to normal operating loads well over two degrees noted.

Stall controlled rotors have experienced renewed interest in the past decade with the advent of designer airfoils (Klimas, 1984; Tangler and Somers, 1987) that enhance the stall regulation of a wind turbine. These airfoils have been quite successful in reducing the maximum power output of a given sized rotor allowing the rotor diameter to be increased without increasing plant capacity. The larger rotor produces more net energy without proportional increases in system cost.

Our aim in this feasibility study is to investigate the enhanced stall approach using an adaptive blade to limit maximum power. This will enable both rotor diameter and system energy increases without proportional increases in system cost. The purpose of this study is to investigate the potential for energy increases. The question to be answered is "How much energy production can be gained by adaptive blades twisting to stall?" Only constant speed options are considered in this investigation.

If the energy increases prove large enough (5-10%) follow-on work will be required to design a blade with the desired twisting characteristics and to identify methods for its manufacture. In the design process, aeroelastic instability issues will be addressed as it is quite possible that a response to load which increases load (in the linear angle of attack range) could lead to amplified structural response.

Method of Analysis

The aerodynamic performance of various HAWT configurations was established using PROP for personal computers (Tangler,1987). The PROP family of codes is somewhat of an industry standard and the "personal computer" version is relatively easy to modify due to its simplicity.

In this study, a modified version of the PROP software is used in a mode wherein the turbine rpm is fixed and the windspeed is allowed to vary over a specified range, the result of interest being a power curve for the turbine. Normally for these computations, the geometry of the rotor is fixed, but for this study

the blade twist is prescribed as a function of windspeed and spanwise location on the blade. As an example, the tip of the blade might undergo rotations of zero to two degrees as a linear function of windspeed over a specified range. For each tip rotation, spanwise blade twist might vary linearly from 0 degrees at the hub to the tip value. The goal is to simulate blade motion that might be achieved with an adaptive blade without actually designing the blade or computing its response to the aerodynamic loads. Thus, the blade twist prescription as a function of windspeed and spanwise location is strictly an educated guess of what might be possible. If these twisting scenarios promote stall in such a way that the captured energy can be significantly increased by extending the blade length, without an increase in maximum power output, a proof of concept is established.

Two options are provided for twist as a function of blade position: constant with span and linear with span. For constant twist with span, the twisting is assumed to take place locally near the hub in a specially designed blade segment. For linear twist, the blade is assumed to be designed so that under the action of the various loadings it twists in a linear fashion from the hub to the tip. It is hoped that the twisting behavior can be accomplished using strictly passive methods, but active methods may also need to be pursued.

For each of the above spanwise twisting strategies, two options are investigated for the manner in which the the maximum blade twist at the blade tip varies with windspeed: linearly and quadratically. A third option is also investigated where the blade tip twists linearly with the output power of the turbine. With these three options it is hoped that the most likely scenarios for the twisting of the blade under load are captured as the wind speed varies. The two blade-twist configurations along with the three twisting schedules are implemented via modifications to the PROP software.

The procedure followed is first to establish a power curve for the turbine of interest with a rigid rotor (i.e. no twisting). From this curve a maximum power output is selected that should not be exceeded due to the design limitations of the turbine gearbox and generator. After selecting a maximum blade tip twist, a twisting schedule and a twist configuration, the PROP performance code is run iteratively, increasing the blade length until the maximum power output matches that of the one with the rigid rotor. The blade chord is not increased proportionately with the blade length. This new power curve is output from PROP in a format readable by the MATLAB software (The Math Works Inc., 1992) for additional processing and graphical visualization.

The additional processing in MATLAB consists primarily of multiplying the power curve by a windspeed probability distribution and integrating the result to obtain annual energy estimates. A Rayleigh probability distribution which is characterized by the average windspeed at the site of interest (Equation 2.1) is used for this purpose. In Equation 2.1, V is the windspeed and $\overline{V}$ is the site average windspeed. Typical Rayleigh

$$f(V) = \frac{2}{V} \times \frac{\pi}{4}\left(\frac{V}{\overline{V}}\right)^2 \exp\left[-\frac{\pi}{4}\left(\frac{V}{\overline{V}}\right)^2\right] \qquad (2.1)$$

probability distributions with average windspeeds of 5.0, 6.5 and 8.0 m/s are shown in Figure 2.1. To determine the effect of the site-average windspeed on the annual energy capture, computations are completed over a range of average windspeeds from 5.0 m/s to 8.0 m/s.

For each turbine configuration, including the rigid one, a curve for the annual energy capture versus average windspeed is computed. From these curves the new curves for the percent

increase in annual energy over the untwisted configuration are obtained. Such curves are obtained for a generic utility scale turbine (~300 kw) and are presented in the next section.

Results

First a credible power curve (electric) had to be developed for the generic turbine, using available information from the National Renewable Energy Laboratory (NREL) for the blade geometry, airfoil data and drive train efficiency. The various options of the PROP software were exercised in an attempt to produce a reasonable power curve. Tangler and Smith et. al. (1991) provided valuable insight and guidance in completing this task. The electric power curve that was finally obtained is shown in Figure 2.2.

For the first series of variable-twist rotor configurations, each blade was constrained to twist at its root only, producing a uniform incremental pitch along its length (constant twist). This action is equivalent to full blade pitch control. The maximum incremental twist permitted was set at either one degree or two degrees. For each of these twist values, the three twisting schedules (linear with windspeed, quadratic with windspeed, and linear with power) were applied to the rotor. After adjusting the blade lengths to achieve rated maximum power, new power curves were generated and are shown in Figure 2.3 for the two degree maximum twist case. As expected the power curves for the three twisting schedules are skewed to the left, all with a maximum power approximately equal to that of the power curve for the rigid generic turbine. The fact that the three curves deviate only slightly from one another, indicates that the schedule details may not be of great importance. As shown, blade length increases for the three schedules are: 0.716 meters - linear with windspeed; 0.625 meters - quadratic with windspeed.; and 0.792 meters - linear with power. When compared to the original blade length of 13.106 meters, these increases are of the order of 5%.

To obtain the increase in annual energy capture as a function of the site average windspeed, these power curves were used in conjunction with Rayleigh windspeed distributions like the ones shown in Figure 2.1. Results for both a one degree maximum twist and a two degree maximum twist are shown in Figure 2.4. The lower and upper sets of three curves correspond to a maximum twist of one and two degrees, respectively. Generally, the variation of the individual curves over the average windspeed range is of the order of 1% in annual energy, indicating that the annual energy increase is not particularly sensitive to the site average windspeed. As noted from the curves, the annual energy increase is substantial, especially for the configurations with a maximum of two degrees of twist.

For the second series of variable-twist rotor configurations the blades were constrained to twist linearly with span. This action might be achieved through specially designed composite blades which are coupled in bending and/or extension, and torsion. The maximum incremental twist permitted at the tip of the blade was set at either one degree or two degrees, and the three twisting schedules were applied in each case. The power curves that resulted from this process are shown in Figure 2.5 for the two-degree maximum twist case. As for the constant-twist series, the power curves are skewed to the left, although to a lesser degree, and they deviate only slightly from one another. Blade length increases for the three schedules are: 0.533 meters - linear with windspeed; 0.482 meters - quadratic with windspeed; and 0.579 meters - linear with power. When compared to the original blade length of 13.106 meters, these increases are of the order of 4%.

The annual energy increase versus site average

windspeed, associated with these power curves is shown in Figure 2.6. As before, the lower three curves correspond to a maximum twist of one degree and the upper curves correspond to two degrees of twist. As with the constant-twist blades the annual energy increase for the linear-twist blades is also not particularly sensitive to the site-average windspeed. Although the annual energy increases for the linear-twist blades is somewhat less than those for the constant-twist blades, the increases are still significant.

Some final computations were completed to identify limits on the concept of promoting stall to increase annual energy capture. With the blade in a linear-twist configuration on a linear-twisting schedule, the annual energy increase was obtained for maximum twists of five, ten, and fifteen degrees. These were combined with the one- and two-degree results obtained previously and all were averaged over the range of mean windspeeds to obtain an average annual energy capture. The increase in average annual energy capture over the base line design is plotted in Figure 2.7 versus maximum twist. Also plotted in Figure 2.7 is the per cent increase in blade radius required to achieve this increase in performance. While the blade radius increases in an approximately linear fashion, diminishing returns are apparent for the increase in average annual energy capture, which peaks at a maximum twist of ten degrees

As stated previously, the blade chord was not increased proportionately with the blade length. Some trial calculations where the chord was increased proportionately yielded smaller increases in annual energy. The greater solidity resulting from the increased chord caused the blade length increases to be smaller when the maximum power limit was reached, leading to a smaller annual energy increase. The practice of increasing the blade length slightly (~5%) without increasing the chord may produce some structural and/or aeroelastic instability problems.

Conclusions and Recommendations

Using a generic utility-sized rotor as a test case, two blade-twist configurations in conjunction with three twisting schedules were investigated to determine the benefits of blades that twist towards stall with applied loading. In all cases the power curves skewed to the left producing increases in annual energy of the order of 10 -15% for a maximum blade twist of two degrees and 5 -7% for a one degree maximum twist. Although the twisting schedules had marked differences, the annual energy increases differed from one another only modestly for a given blade twist configuration. The predicted annual energy increases were not particularly sensitive to the site average windspeed over the range investigated (5 - 8 m/sec).

This study has indicated that substantial increases in annual energy capture can be achieved if the blades can be made to twist towards stall with increasing applied load. Moreover, if the maximum incremental blade twists that were used in this study can be realized, the system seems to be robust in the sense that the details of the blade twist configuration, the twisting schedule and the site average windspeed are not crucial to achieving a significant increase in annual energy capture. On this basis it is recommended that design studies be initiated to identify blade designs that could passively twist towards stall to the desired levels under the action of the applied loads. It is imperative that these design studies address aeroelastic instability due to the adaptive nature of the blades.

Acknowledgment

The authors are indebted to James Tangler of NREL who provided valuable information,

insight and guidance in the development of a generic utility scale turbine and its associated electric power curve.

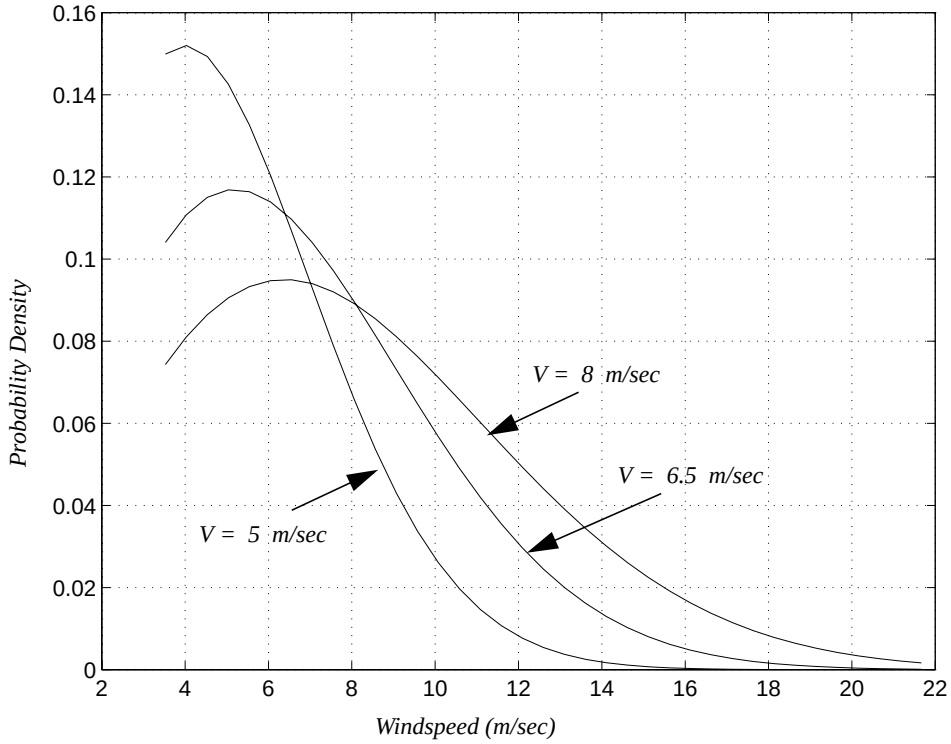

Figure 2.1. *Rayleigh probability distributions for windspeed with average windspeeds of 5.0, 6.5 and 8.0 m/s.*

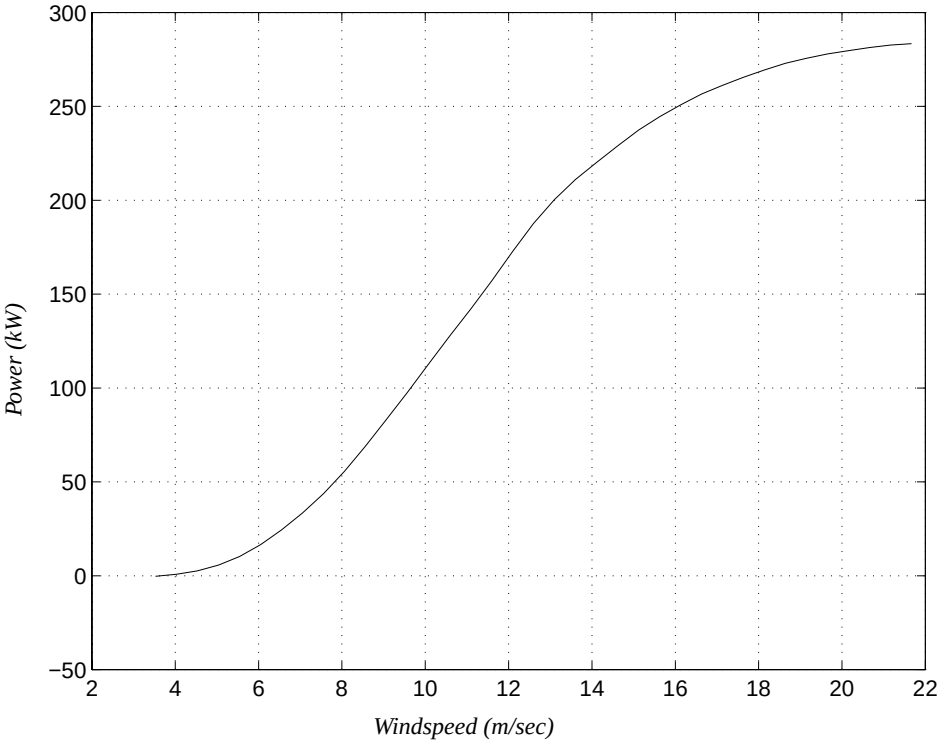

Figure 2.2. *Power curve for the generic rigid rotor.*

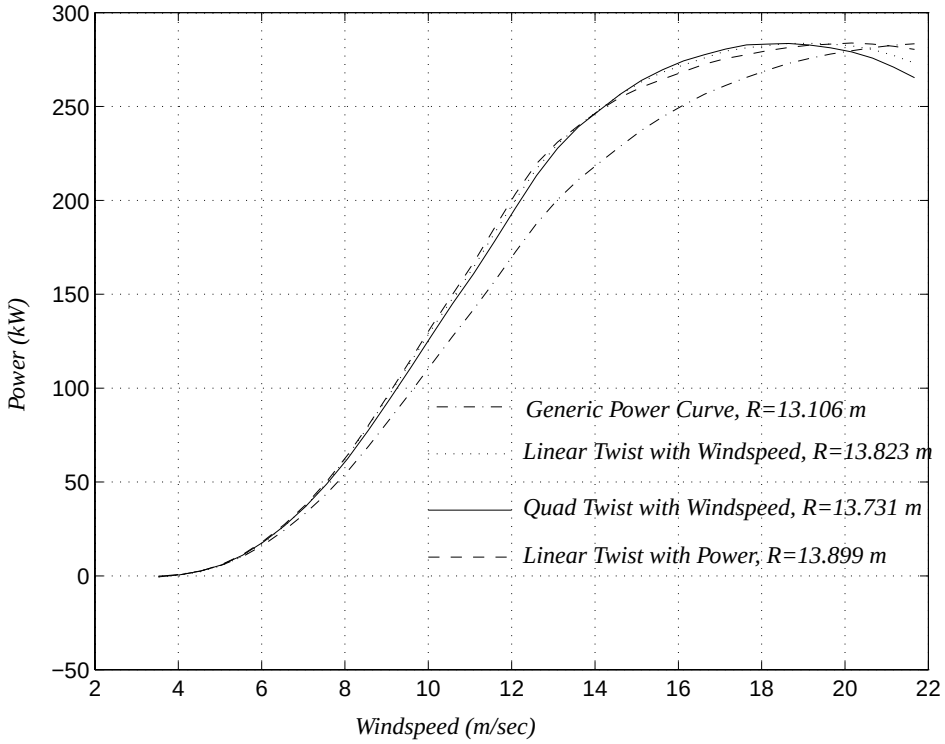

Figure 2.3. *Power curves for the three twisting schedules - constant twist along the span.*

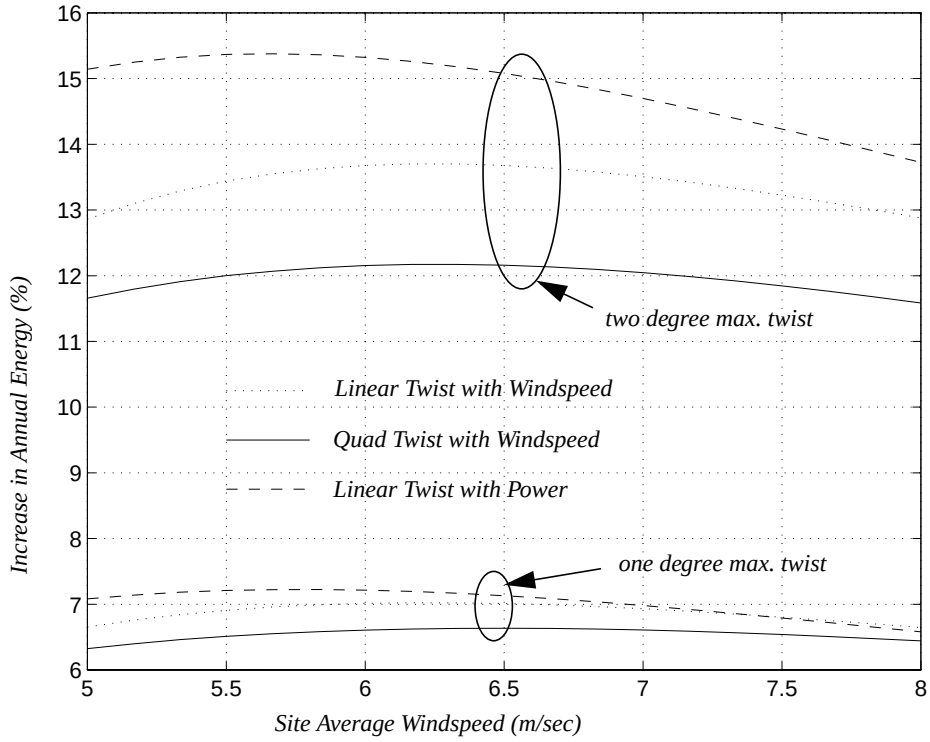

Figure 2.4. *Percent increase in annual energy for the three twisting schedules - constant twist along the span.*

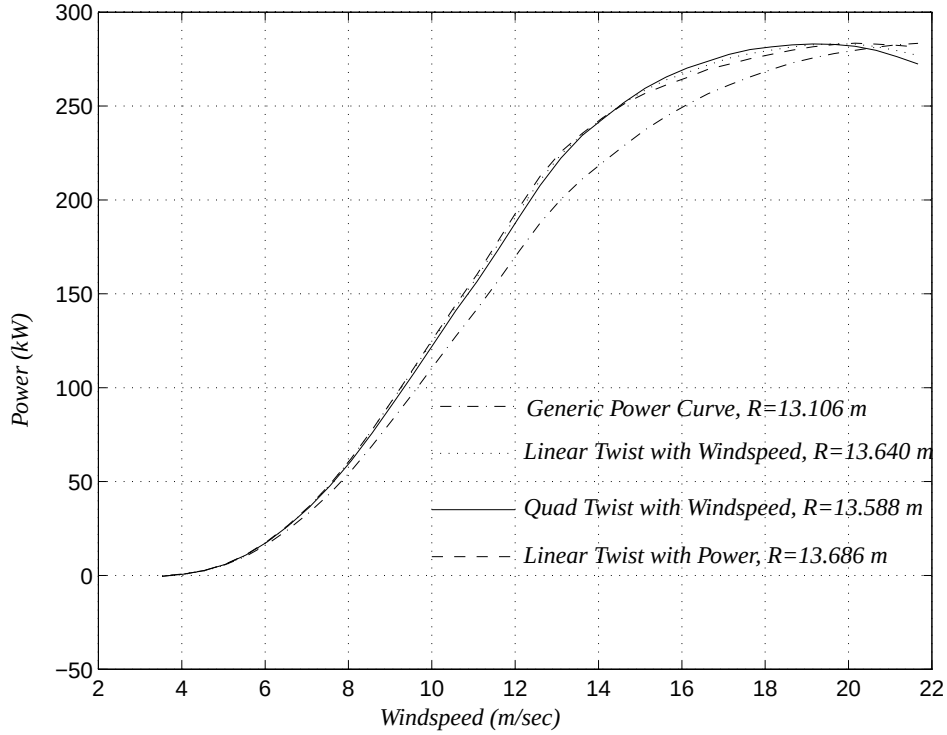

Figure 2.5. *Power curves for the three twisting schedules - linear twist along the span.*

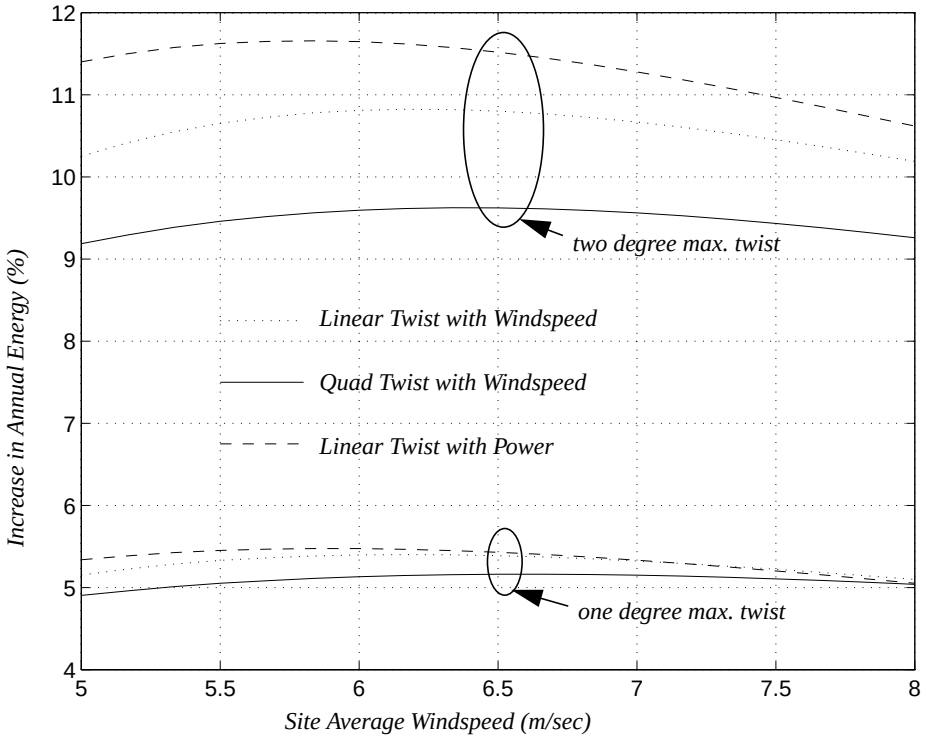

Figure 2.6. *Percent increase in annual energy for the three twisting schedules - linear twist along the span.*

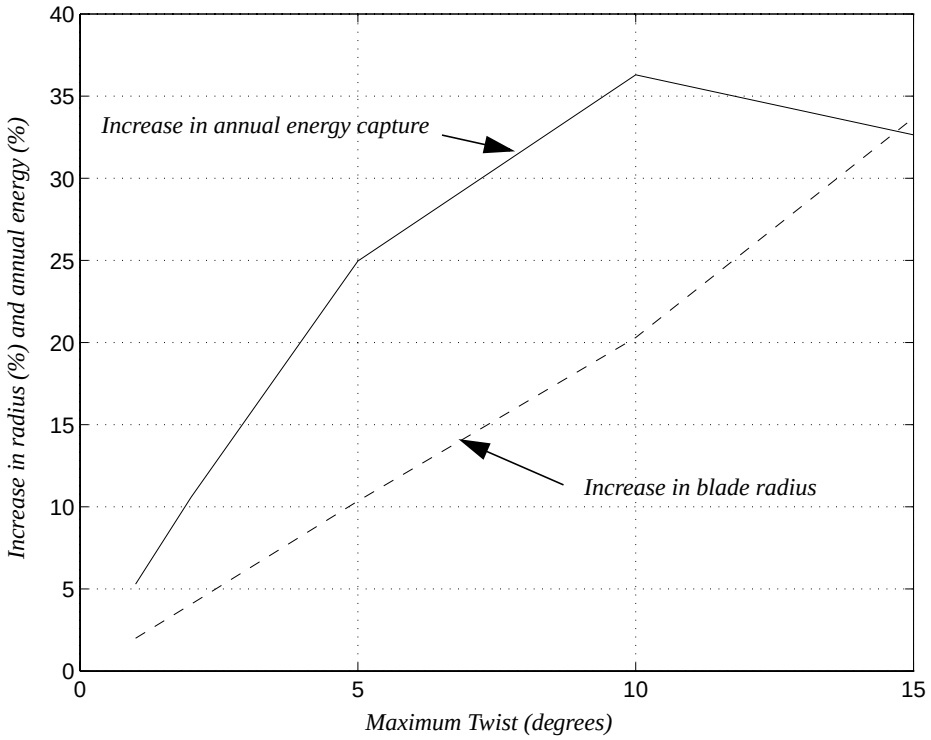

Figure 2.7. *Percent increase in blade radius and average annual energy capture versus maximum blade twist.*

Parameter Optimization Applied to a Variable Speed HAWT with Adaptive Blades for Optimizing Energy Capture

Chapter 3

Introduction

One of the basic requirements of wind turbine control is to ensure that the rotor does not produce more power than the rest of the system (drive train, generator, etc.) can withstand. The simplest approach is passive stall regulation that uses the characteristics of the airfoils to stall in high winds and regulate the power production of the rotor. More advanced controllers use changes to the rotor configuration to maximize system efficiency while the wind speed is fluctuating. Examples are variable speed, variable pitch (either full span or tip actuation), ailerons, passive pitch actuators and the like. There is a balance to be struck between the complexity of the control system, and hence cost and maintainability, and the ability of the controller to limit loads and/or to deliver more energy.

Enhancing stall regulation has long been a strategy for reducing wind turbine cost of energy. Increasing rotor size while holding the power rating constant allows all costs except the blades to remain relatively constant. At the same time an increase in net energy is obtained because the larger rotor captures more energy in low winds where efficiency is high and most of the annual energy is to be found. Tangler (1990) uses this strategy to initially guide the development of the SERI family of airfoils, some of which stall at lower than usual angles of attack and therefore regulate at lower wind speed.

A previous study by Lobitz and Veers (1996) showed how a substantial improvement in system performance can be realized by enhancing the stall regulation of a constant-speed system via adaptive blade twist. The adaptive blade twists elastically in response to loads, creating a change in the angle of attack and thus influencing loads and power production. The approach described in the Lobitz paper assumes that the blade twists toward stall in response to loads that are proportional to either wind speed or power (e.g., flap loads) and therefore enhances power regulation. By increasing the rotor size while enhancing regulation using adaptive blades, a fixed power limit can be maintained while increasing net energy. Energy production grows in excess of the increase in rotor swept area with only modest elastic blade twist (2 degrees). While this result illustrates one specific application of the adaptive twisting blade to improve system performance, many significant issues need to be addressed before the adaptive blade can be proposed as a definite improvement. A more systematic evaluation of the benefits of the adaptive concept needs to be done in a variety of applications. This study looks at improvements in net energy production through systematic optimization of rotor operational parameters. Future work will evaluate dynamic-load effects.

There is a strong sentiment in the U. S. wind-energy community that variable-speed systems will dominate the market in the near future, driven by cost reductions and improvements in power electronics. The value of adaptive blades needs to be evaluated in this variable-speed environment. The question remains whether elastic twist designed into a blade structure can add value to a variable-speed sys-

tem either by improving the theoretical maximum energy delivered in variable-speed operation or by replacing an active control element with an inherently more robust passive element.

The Baseline Configuration

This optimization study uses the AWT-26 rotor as a baseline configuration from which to study adaptive blade enhancements. The airfoil selection and basic layout of the blade are therefore based on a pre-existing design and are not part of the optimization. Only the control features involving variable-speed selections and elastic twist coefficients are included. The AWT-26 turbine (Figure 3.1) is rated at 300 kilowatts (kW) and is a two-bladed, downwind, teetered, free-yaw, fixed-pitch, stall-controlled, constant-speed, horizontal-axis wind turbine. The rotor is 26 meters (m) in diameter. The normal operating speed is 57 revolutions per minute (rpm). For analysis purposes, a blade is divided into ten segments, which have associated twist and airfoil characteristics. Blade twist is displayed as a function of normalized chord (local chord length/blade length) in Figure 3.A-1 in Appendix 3.A. Lift and drag curves per segment as a function of angle of attack are shown in Figure 3.A-2. Blade pitch is fixed at +1.2 degrees; positive implies pitch to feather, negative is pitch to stall.

Figure 3.1. AWT-26 Turbine

Overview of the Study

The point of this study is to see if adaptive blades that enhance stall regulation can achieve substantial benefits in a fixed-pitch, variable-speed environment. Since the baseline turbine already regulates quite well in constant speed mode at 300kw, there is no additional gain to be had under those conditions. In the previous study by Lobitz and Veers (1996) the power limit was held at 300kw while the rotor size was allowed to grow with improving ability to stall regulate. Here, rather than growing the rotor diameter, we reduce the target maximum power from 300kw to 200kw. This ensures that the power bound is violated for obtainable rotor speeds and that the optimization is required to compensate.

A rotor designed to have a high efficiency at a particular tip-speed ratio (TSR = $R\Omega/V$, where R is the rotor radius, Ω is the rotor rotation speed and *V is the* wind speed) can theoretically be operated at that constant tip-speed ratio below rated power to achieve the maximum energy capture. Power can theoretically be maintained at the rated level above the rated wind speed by lowering the speed to reduce the efficiency. (This is essentially what is done with variable pitch, where pitching the blade reduces the efficiency and keeps the rotor from overproducing. Here we focus on fixed pitch to see if the adaptive blades can supply a function similar to active pitch, but without the expense of the mechanism.) The term “theoretically” is

used because, first, the turbine can never be operated exactly at the target tip-speed ratio because of the transient nature of the wind, and, second, it may not be possible to maintain a constant power using speed control alone without substantially oversizing the generator and drive train. The first issue is one for which adaptive blades might have application, but requires dynamic analysis to evaluate and will not be dealt with here. The second issue is the primary focus. It will be shown that the speed variations necessary to limit power output using speed control alone are extreme. In addition, the generator must extract energy from the kinetic energy of the rotor to slow it down, and do it exactly when the generator is already at rated power (Muljadi et al. (1996) and Muljadi et al. (1997)). Such speed variations may not be possible to implement without substantially oversizing the generator and drive train to allow "headroom" for overshooting the rated power. However, Pierce and Migliore (2000) demonstrated experimentally with specialized drivetrain hardware and control designs that the power curve of a variable speed pitch-regulated turbine may be approached using variable speed alone.

This study examines the ability of adaptive blades to regain some of the theoretical advantage of variable speed, but with a conservative and easily implemented control strategy. Two different variable-speed scenarios are therefore examined. The first, or *aggressive* approach, allows rotor speed to assume arbitrary values as a function of wind speed. This gives maximum variable-speed control without regard for whether it is achievable or not. It produces a theoretical maximum against which other results can be compared. The second, or *conservative* approach, allows rotor speed to increase until it reaches a point where the rotor will stall regulate at 200kw at that speed. The rotor speed is fixed at this value in high winds. This provides a lower bound for what variable speed alone can achieve. Adaptive blade effects are applied to both scenarios to see how they can affect the theoretical maximum (in the aggressive approach) and if they can regain some of the lost energy sacrificed in conservatively operating a variable-speed turbine. If sufficient energy can be regained in the conservative approach, it may be possible to operate a variable-speed rotor with stall regulation and without excessive headroom.

Analysis

A gradient-based parameter optimization method is used to query the quasi-steady PROP wind turbine performance analysis code (Tangler (1987)). The decision parameters describe rotor speed variation with wind speed and blade pitch dependencies on current rpm and bending moment. Rotor configuration and airfoil data, shown in the Appendix, are used as input to the PROP analysis code. PROP uses momentum-strip theory to calculate loads and performance. This is a quasi-steady analysis that does not include transient dynamics. PROP was modified from its original configuration of computing over a range of TSR's to computing thrust, moments, and power at a single TSR. An outer loop was wrapped around PROP to compute a TSR from a designated rpm and wind speed . Inside PROP, blade pitch adjustments were simply added to the nominal +1.2 degree value. By varying V and Ω for a given blade pitch, a dependent variable "response" grid can be generated. Two dependent variable responses, for power and blade-root bending moment, are shown below.As energy optimization was the goal of the study, a metric proportional to average annual energy was chosen. By using the power, P, computed in PROP and combining it with a wind-speed probability distribution function, the result can be integrated over wind speed to produce an average annual power. This metric is proportional to average annual energy. A Rayleigh probability distribution that is characterized by an average wind speed

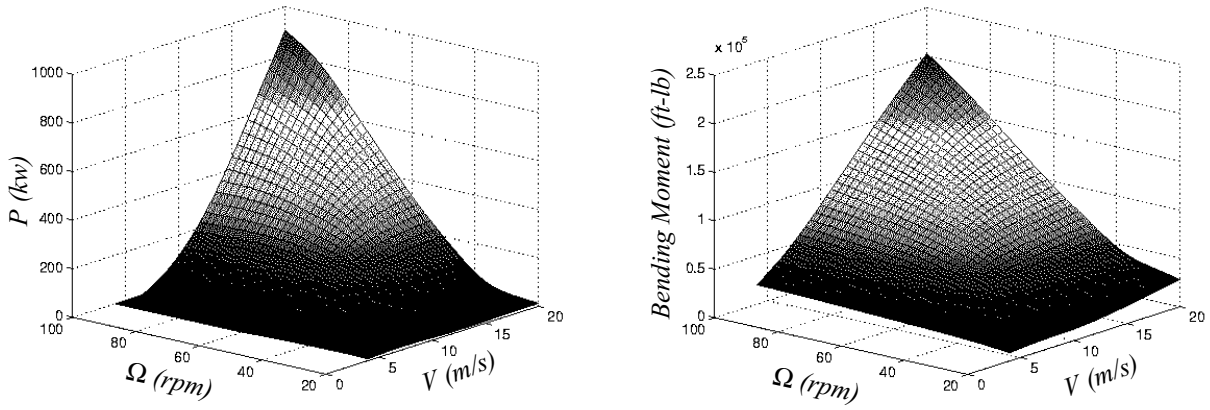

Figure 3.2. PROP output for the AWT-26 model.

at a site is given by Equation 2.1 and reproduced here for conveniece:

$$f(V) = \frac{2}{\bar{V}} \times \frac{\pi}{4}\left(\frac{V}{\bar{V}}\right)^2 \exp\left[-\frac{\pi}{4}\left(\frac{V}{\bar{V}}\right)^2\right]$$

where V is instantaneous wind speed and $\bar{V}$ is the annual average wind speed. The average annual power is then given by

$$\bar{P}(\bar{V}) = \int_{V_{min}}^{V_{max}} P(V)\, f(V)\, dV \qquad (3.1)$$

The power output from PROP is shown in Figure 3.2 and the transformation to the integrand value, *P(V)f(V)*, is shown in Figure 3.3 for $\bar{V} = 5$ meters/sec (m/s). Average wind speeds of 5, 7, and 9 m/s are examined in this study. Note that the result of transforming the power

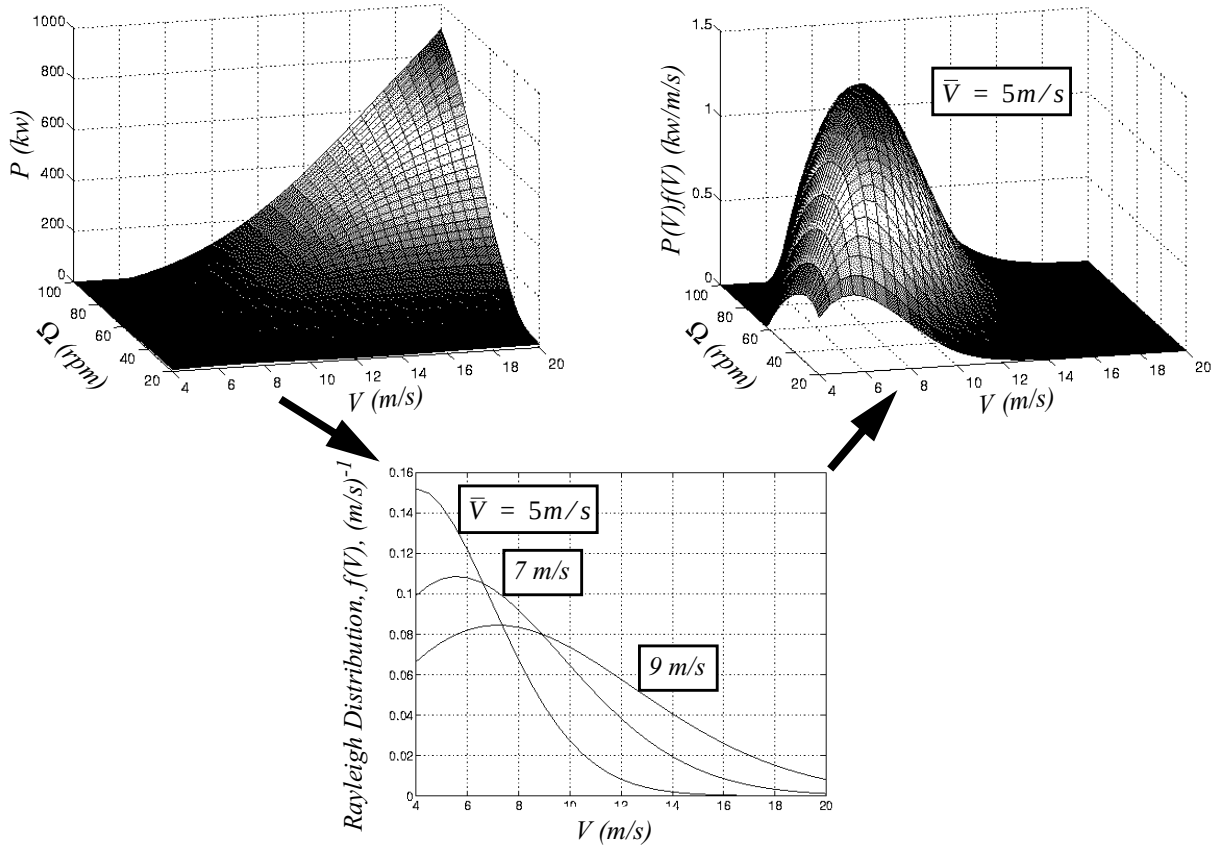

Figure 3.3. Power to Average Power Conversion.

via the Rayleigh distribution accentuates performance in the lower wind speeds and lessens its importance at higher speeds. Therefore, if more power could be generated at the lower wind speeds via variable rotor speed or adaptive blade measures, then $\bar{P}$ will increase. This is the goal of the optimization efforts.

If only rotor speed as a function of wind speed is of interest, the grid shown in Figure 3.3 could be sequentially searched for rotor speed values that would maximize $P(V)f(V)$, as well as maintain power between specified bounds. Since $P(V)f(V)$ is always positive, maximizing its magnitude will also maximize the integral, $\bar{P}(\bar{V})$.

Search results are shown in Figure 3.4, where the maximum values of $P(V)f(V)$ are shown as a solid line superimposed on the surface in three dimensions. An upper power bound for this search was chosen to be 200 kW, as explained above. The projection of the $[P(V)f(V)]_{max}$ curve onto the *wind speed-rpm* plane gives the "control" history that maximizes $\bar{P}(\bar{V})$. The projection of the $[P(V)f(V)]_{max}$ curve onto the $P(V)f(V)$-*wind speed* plane gives the curve whose integral is the annual power performance metric, $\bar{P}(\bar{V})$.

Recall that to test the efficacy of an optimization technique in tuning speed and blade pitch, the power limit of the nominally 300kw turbine was reduced to 200kW for this study. This would insure that the power bound would be violated for obtainable rotor speeds and that the optimization method would be required to compensate. Two different rotor speed scenarios were parameterized and compared to maximize $\bar{P}(\bar{V})$, while maintaining the upper power bound. The first, or *aggressive* approach, allowed rotor speed to assume arbitrary values as a function of wind speed. This required a rotor speed parameter value, $\Omega_i(V_i)$, at each value of wind speed (Figure 3.5). Wind speeds covering the range from 4 to 20 m/s in

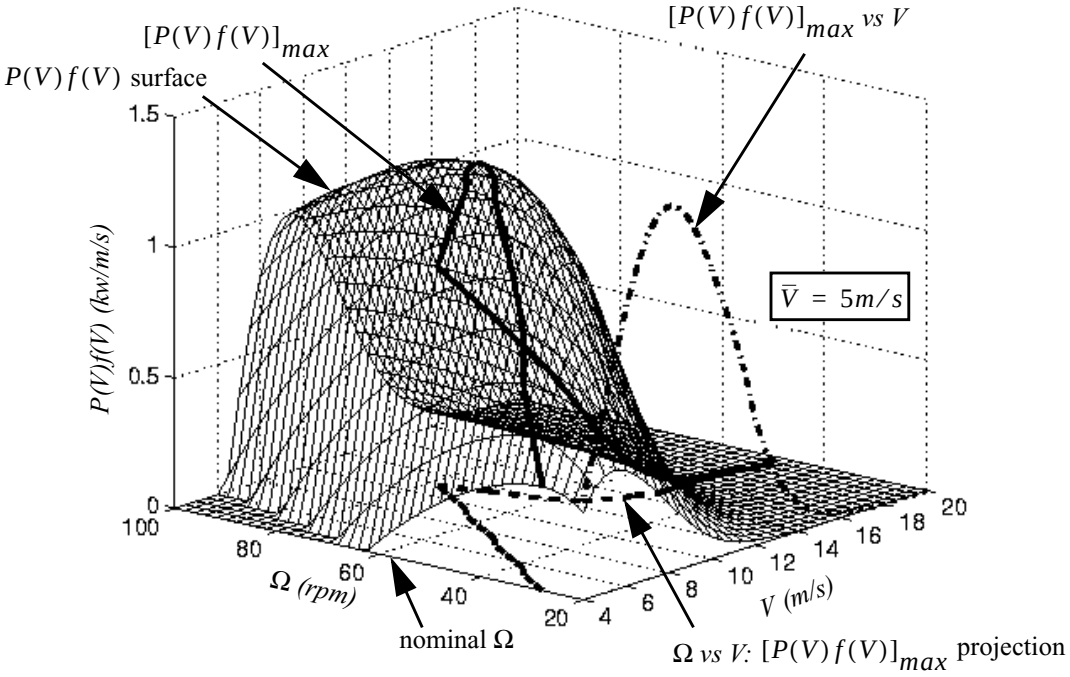

Figure 3.4. Average Power Grid Components.

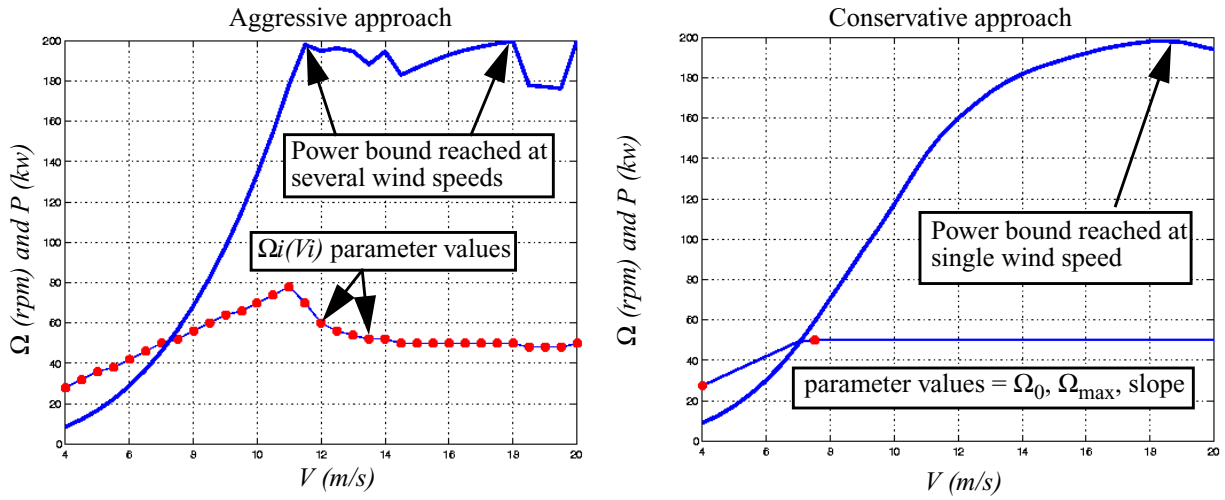

Figure 3.5. Rotor Speed Parameterization Approaches

0.5 m/s increments were selected to provide an accurate numerical computation of the integral $\bar{P}(\bar{V})$. Note that small variations in Ω at the higher wind speeds can cause abrupt variations in power. The second, or *conservative* approach, allowed rotor speed to linearly increase as a function of wind speed until it reached a point that the first violation of the power bound occurred at *any* wind speed. After this point, the rotor speed remained fixed at this value. This approach required only 3 parameters, an initial rotor rpm value (Ω_O), a constant slope, and a final rpm value (Ω_{max}) as shown in Figure 3.5. Ω_O is assumed to be at 4 m/s and the slope places Ω_{max} at the desired wind speed.

As stated previously, the AWT-26 turbine has blades pitched 1.2 degrees to feather, nominally. To assess possibilities for adaptive blade operation, a polynomial combining the effects of a constant angle offset, rotor speed, and bending moment was used to change the effective pitch angle across the range of local wind speeds. The effective pitch angle at a given wind speed, V_i, was

$$\theta_{effective}(V_i) = 1.2 + k_0 + k_1\left(\Omega\frac{(V_i)}{60}\right)^2 + k_2 BendingMoment((V_i)/10^5) \quad (3.3)$$

where k_0 is a constant offset angle and k_1, k_2 are multiplicative constants. These *parameters* are added to those of the chosen speed control approaches described previously to complete a given parameter set for optimization. Ω and bending moment have been normalized to keep values in the zero to one range. The bending moment history was obtained from an optimization history where only Ω was optimized. Therefore, there is no iteration on bending moment; the bending moment without pitching is used to determine the change in pitch due to the bending twist-coupling. Note that the rotor speed effect on $\theta_{effective}$ is quadratic to model the speed-driven centrifugal-force coupling.

The major problem with the model from a numerical standpoint is its use of a nonlinear numerical solution as a prelude to computing forces and moments. One of the avenues of exploration in this study is to search out appropriate Ω's over a range of wind speeds to maximize $\bar{P}(\bar{V})$. As seen in Figure 3.3, increasing *P* at the lower wind speeds is critical to this goal. Figure 3.6 shows an example of PROP power computation for varying rotor speed for a fixed local wind speed of 6 m/s and the nominal 1.2 degree blade pitch angle. On the macro-scale of 40-60 rpm, the power appears to smoothly decrease. However, on examining

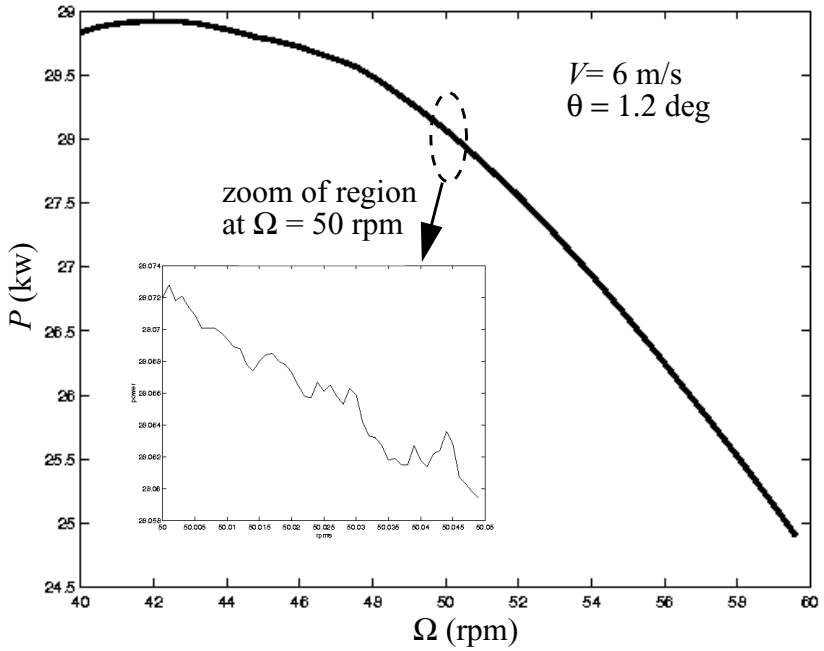

Figure 3.6. Coarse and Fine Scale PROP Output.

a micro-region of the curve, this decrease is really an average behavior of a noisy output. The problem is that noise wreaks havoc with gradient-based numerical optimization techniques. Attempts to use analytic gradient solvers (Bischof et al. (1995)) to generate the partial derivatives, $\frac{\partial P_i}{\partial \Omega_i(V_i)}, \frac{\partial P_i}{\partial k_j}$ failed because of the noise severity. Finite-difference gradient approximations were used instead. Measures taken to alleviate (but not eradicate) this problem included the use of higher solution tolerances for the nonlinear solver, converting PROP to double precision, and the use of larger parameter variations, $\Delta\Omega_i(V_i)$, Δk_i, in the finite-difference computation of the partial derivatives

Optimization Methodology

The optimization method used was the Modified Method of Feasible Directions (MMFD) written by Vanderplaats (1995) and provided as an option in the DAKOTA optimization environment developed at Sandia National Laboratories by Eldred et al. (1996). The MMFD method attempts to minimize a scalar performance metric, $F(\vec{\xi})$, which is a function of parameter vector $\vec{\xi}$, subject to a vector of constraints, $\vec{C}(\vec{\xi}) \le 0$. Since we are seeking to maximize average power (in this minimization environment) and there is only a single active constraint, the problem specifications are:

$$\textit{minimize}: -\bar{P}(\bar{V}) \text{ subject to } P(V, \vec{\xi}) \le 200kw$$
$$\text{for } 4 \le V \le 20 \text{ m/s}, \vec{\xi} = \left[\Omega_i(V_i)\ k_0\ k_1\ k_2\right] \quad (3.4)$$

Power is being sampled from PROP at discrete values of local wind speed, V_i, in order to compile approximations to the performance metric and constraint dissatisfaction. To accommo-

date this sampling, the actual metric and constraint are posed as follows:

Performance Index:

$$F(\vec{\xi}) = -\bar{P}(\bar{V}) \approx \Delta V \sum_{i=1}^{N} P_i(V_i, \vec{\xi})\, f(V_i, \bar{V}) \tag{3.5}$$

Constraint Dissatisfaction:

$$\vec{C}(\vec{\xi}) \approx \sum_{i=1}^{N} max[P_i(V_i, \vec{\xi}) - 200., 0.],$$

where N=33 velocities sampled at ΔV=0.5 m/s increments over the 4-20 m/s range. Note that the individual terms in the constraint dissatisfaction summation will either produce a positive quantity if $P_i(V_i, \vec{\xi}) > 200$ or zero if it is less. Since the MMFD method expects satisfied constraints to be of the form, $\vec{C}(\vec{\xi}) \le 0$, the use of the above approximate form will show satisfaction when $\vec{C}(\vec{\xi}) = 0$ (i.e., the output from PROP, $P_i(V_i, \vec{\xi})$, never exceeds 200 kW). Since only a single constraint exists in this study, the vector arrow over the C will be henceforth omitted.

$F(\vec{\xi})$ and $C(\vec{\xi})$ were of the same form as above for all computations; only the composition of $\vec{\xi}$ changed, as well as the average annual wind speed, $\bar{V}$.

Results

As stated previously, two different rotor speed scenarios, aggressive and conservative, were optimized as shown in Figure 3.5. For both, the following adaptive blade measures were also simultaneously applied:

[Case 1] $\theta_{effective}(V_i) = 1.2$ degrees (nominal blade pitch, no optimization)

[Case 2] $\theta_{effective}(V_i) = 1.2 + k_0$

[Case 3]

$$\theta_{effective}(V_i) = 1.2 + k_0 + k_1\left(\Omega\frac{(V_i)}{60}\right)^2$$

[Case 4]

$$\theta_{effective}(V_i) = 1.2 + k_0 + k_1\left(\Omega\frac{(V_i)}{60}\right)^2 + k_2 BendingMoment((V_i)/10^5)$$

Results were generated for average annual wind speeds of $\bar{V}$ = 5, 7, and 9 m/s.

Figure 3.7 shows results for the baseline optimization of the rotor speed history only for nominal blade pitch (item 1 in the above list). The baseline conservative optimization has only three parameters (Ω_{min}, Ω_{max}, *slope*) that need to be adjusted. The Ω histories rise linearly from 27 rpm to a maximum value of 50 rpm at about 7 m/s.

The Ω histories for this approach are identical because the outcome is only contingent on the lowest Ω value encounter with the 200kW power bound, which occurs at 18 m/s and is not a function of $\bar{V}$. There is no chance of increasing P at lower wind speeds, because of this encounter. Note that the Rayleigh weighted power, *P(V)f(V)*, suffers less high-speed decay and increases in overall value as $\bar{V}$ increases.

The baseline aggressive-approach results in Figure 3.7 show a near linear rise in Ω with wind speed from 27 rpm to 76 rpm, and then falls off precipitously to ensure that the 200kW power bound is not violated. The optimization has, therefore, found a region in the moderate wind speeds where power can be increased via a peak in Ω to affect the annual power integral, $\bar{P}(\bar{V})$. Note that the aggressive approach is

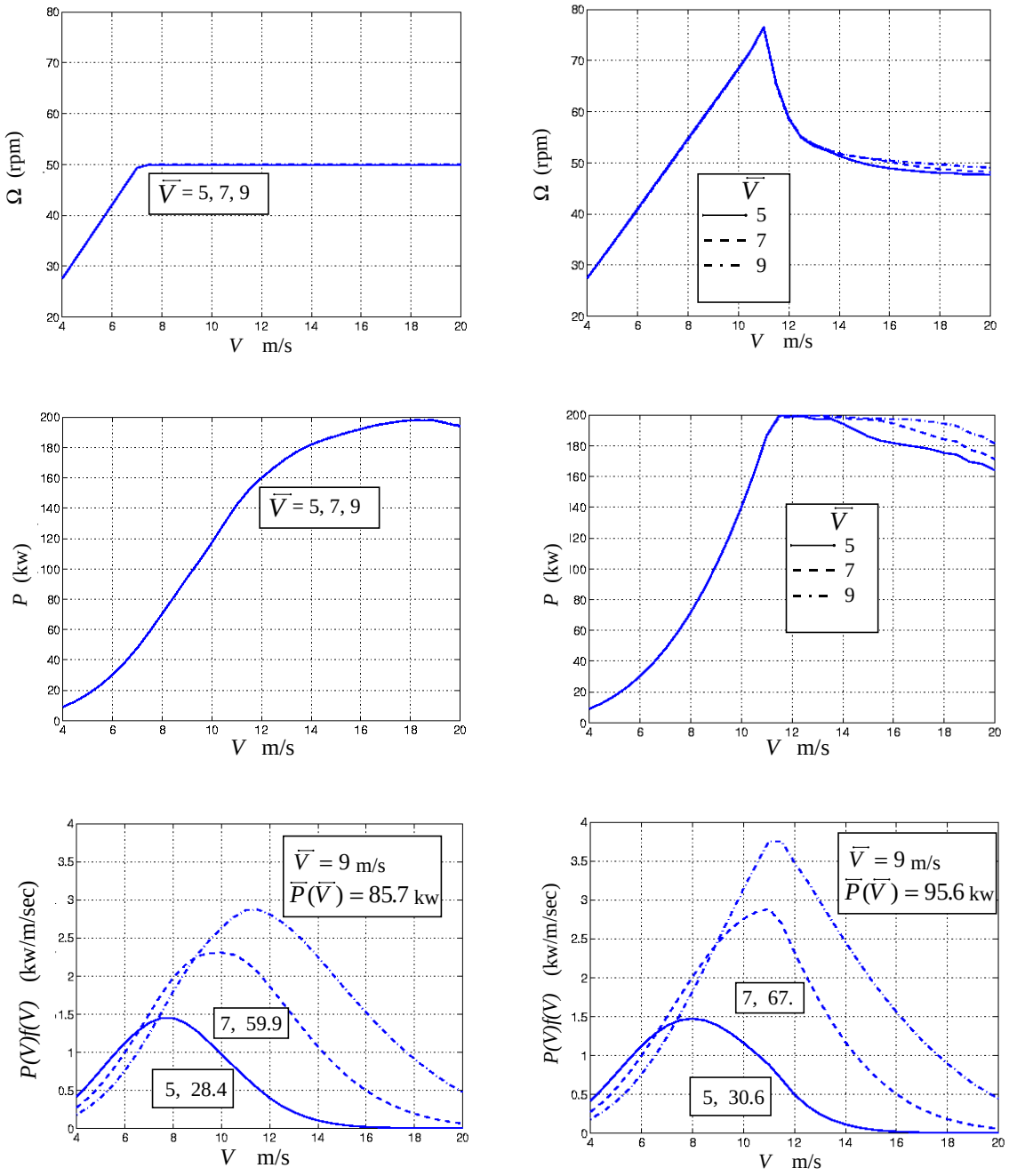

Conservative Ω approach

Aggressive Ω approach

Figure 3.7. Rotor Speed Optimization Results for Nominal Blade Pitch [Case 1]

able consistently to maintain power near the bound if there is significant energy to be gained. The optimization pushes the power closer to the 200kW barrier in high winds as those winds become more important. In the 5 m/s case, for example, power output above 15 m/s is virtually irrelevant. $\overline{P}(\overline{V})$ differences, (aggressive-conservative)/conservative, range from 7-12% for $\overline{V}$ = 5-9 m/s.

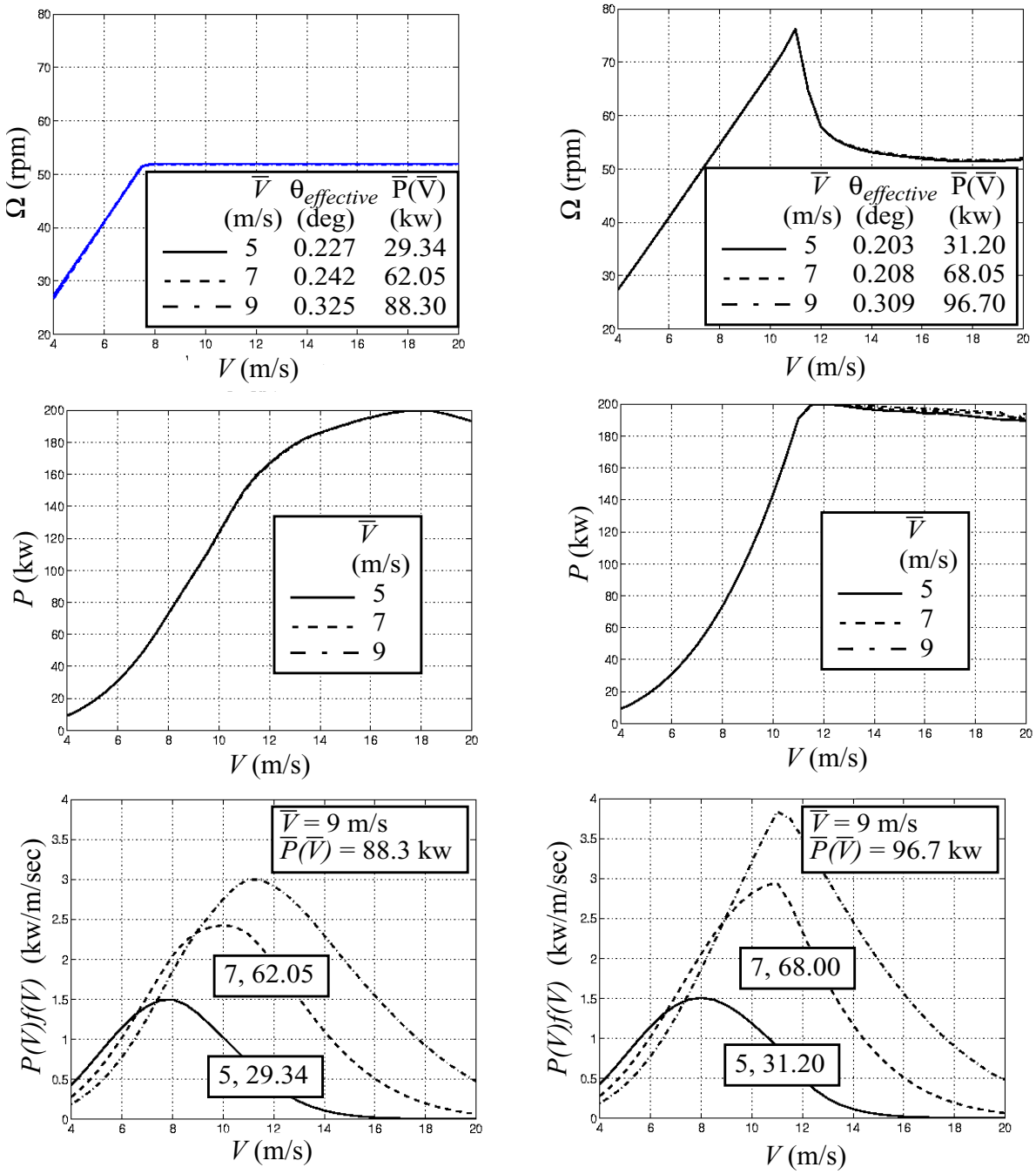

Conservative Ω approach Aggressive Ω approach

Figure 3.8. Rotor Speed Optimization Results for Constant Offset Blade Pitch [Case 2]

Figure 3.8 shows these comparisons for a constant offset (bias) in the pitch angle, where $\theta_{effective}(V_i) = 1.2 + k_0$ (k_0 being the optimized constant offset in degrees). In all cases the tendency was to reduce the blade angle, which was originally pitched to feather. The reduction was on the order of one degree. The conservative Ω histories are again identical, due to the "1st bound contact" at 18 m/s wind speed. However the rpm value to achieve this is now slightly higher at 52 rpm versus the nominal pitch case and occurs at a higher wind

speed. The energy metric, $\bar{P}(\bar{V})$, shows a 3.0-3.6% increase across the span of $\bar{V}$ versus the nominal-pitch, conservative-Ω case.

The aggressive-approach results have changed in this case to display nearly identical rotor speed histories characterized by the familiar linear increase at the low and moderate wind speeds, followed by a rotor speed drop-off to satisfy the power bound. Ω at the higher wind speeds is asymptotic to the 52 rpm value found in the conservative approach. *P* more closely "hugs" the bound for all $\bar{V}$'s versus the nominal pitch case. $\bar{P}(\bar{V})$ shows only a 1-2% increase versus the nominal-pitch, aggressive-Ω case. Because the conservative approach benefits more from a readjustment of the pitch offset, the advantage of the aggressive speed control has dropped to 4-8%, with the least advantage still in the 5 m/s average winds.

Figure 3.9 shows the results of adding an Ω^2 dependency into the blade pitch equation. This term reflects an adaptive blade that twists in response to centrifugal loads. Use of this term produced many local $\bar{P}(\bar{V})$ maxima [as a function of $\Omega_i(V_i)$, k_0, k_1] of nearly the same value, depending on the initialization of the k_0, k_1 constants. This signifies that a "flat" region in the parameter space has been reached. In this region, sensitivity to some part of the parameter set has been lost. The optimization algorithm is forced to generate an answer with insensitive parameters and has minimal good derivative information to change parameter values from the initial "guesses." This behavior was more evident for the aggressive approach.

The conservative approach with Ω^2 blade dependency increases rpm linearly with wind speed to a value greater than the constant-offset blade-angle case. The changeover from variable to constant speed also occurs at a higher wind speed, about 8 m/s. A spread of several rpm exists between the $\bar{V}$ = 5 m/s case and the 7 and 9 m/s cases. Power curves are still roughly the same. $\bar{P}(\bar{V})$ values show about a 2% difference versus the constant offset case. A comparison of θ histories is shown in Figure 3.10. For all $\bar{V}$'s the tendency is to pitch the blade to stall for the 4-20 m/s local wind speed range. A $\Delta\theta$ difference of 1.0 degree exists between the 5 m/s, the 7 m/s and the 9 m/s curves, where the higher $\bar{V}$ histories are pitched further into the stall region.

The aggressive Ω approach with Ω^2 blade dependency displays almost no change from the constant offset case. Ω histories for all $\bar{V}$'s are essentially identical, which in turn show the same small power differences at the higher wind speeds. The blade histories in Figure 3.10 demonstrate the *insensitivity* of the $\bar{P}(\bar{V})$ values with respect to this added adaptive blade feature. The optimization turned off the Ω^2 dependency at $\bar{V}$=5 and 7 m/s leaving the blade with the constant offsets found previously. Clearly these are cases of over-parameterization or of the use of multiple terms in the modeling that have similar effects.

At $\bar{V}$ = 9 m/s the optimization activates the Ω^2 blade angle dependence, creating a θ history that looks very much like the Ω curve. However, the effect on $\bar{P}(\bar{V})$ is negligible. Obviously, another local maximum has been found with no advantage over the constant offset case.

A comparison with the conservative

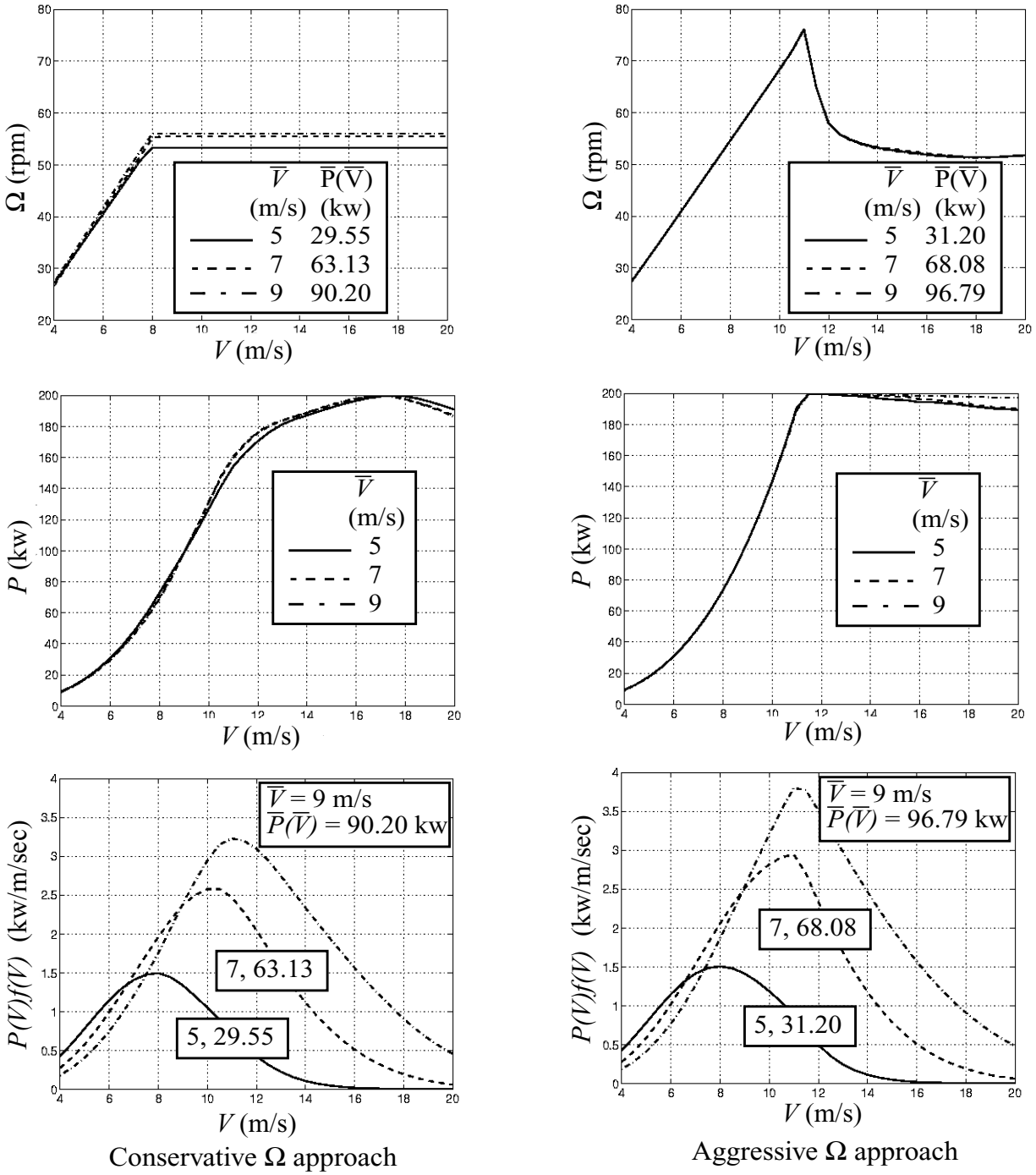

Conservative Ω approach

Aggressive Ω approach

Figure 3.9. Rotor Speed Approaches with Offset + Ω^2 Blade Pitch Dependencies [Case 3]

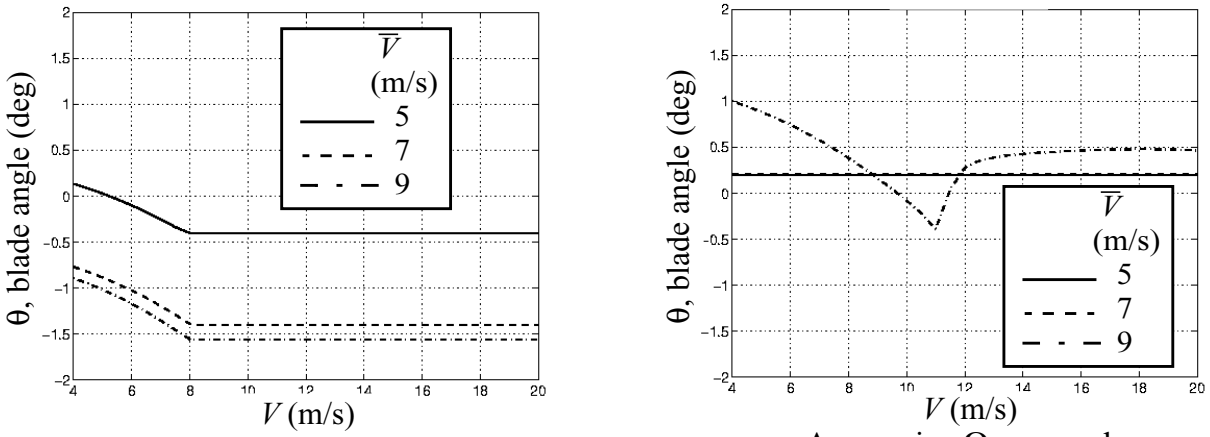

Conservative Ω approach Aggressive Ω approach

Figure 3.10. Adaptive Blade Angle Histories for Offset + Ω^2 Dependencies [Case 3]

offset + Ω^2 approach was made by replacing the Ω^2 dependency with a linear dependence on nominal bending moment to assess any advantage. The $\bar{P}(\bar{V})$ results for the latter idea compared with those in Figure 3.9 are shown in the following table.

Table 3.1. Comparison of average annual power using Ω^2 and bending moment (BM) deendencies.

$\bar{V}$ (m/s)	$\bar{P}(\bar{V})$ (kw) $\theta = k_0 + k_1\Omega^2$	$\bar{P}(\bar{V})$ (kw) $\theta = k_0 + k_1 BM$
5	29.55	29.69
7	63.13	63.31
9	90.20	90.29

The change to bending moment (BM) shows only a slight improvement (< 1%) across the $\bar{V}$ range and with the inherent noise in the model is deemed to have an equivalent (but not superior) effect to that of rotational speed.

Attempts were made to include the bending moment dependency (k_2) into the θ formulation as a third term (together with the *offset* and Ω^2 terms [Case 4]). This produced a variety of local maxima in both variable-Ω approaches, which demonstrated *no* advantage over less involved blade adaptations. The results were not plotted. These maxima entailed tradeoffs in value between the k_0, k_1, k_2 parameters much like the $\bar{V}$ = 9 m/s blade history shown previously in Figure 3.10. This scenario is an example of *over-parameterization,* where the modeled behavior can be successfully captured with fewer parameters and dependencies.

Figure 3.11 displays previously shown parameterizations isolated for $\bar{V}$ = 7 m/s and both Ω approaches. As seen before, rpm at higher wind speeds increases if the blade is pitched from its nominal 1.2 degree setting toward stall. With the conservative Ω approach, there is more chance to affect the $\bar{P}(\bar{V})$ performance measure via blade adaptation versus the aggressive approach. This comparison demonstrates that variable speed and adaptive blade measures for average annual power increase are intertwined, and that one can compensate for constraints on the other. In the conservative Ω approach, speed is moderately-to-severely constrained and blade adaptation has an impact [5% in $\bar{P}(\bar{V})$ values]. In the aggressive case, no constraints (other than maximum power)

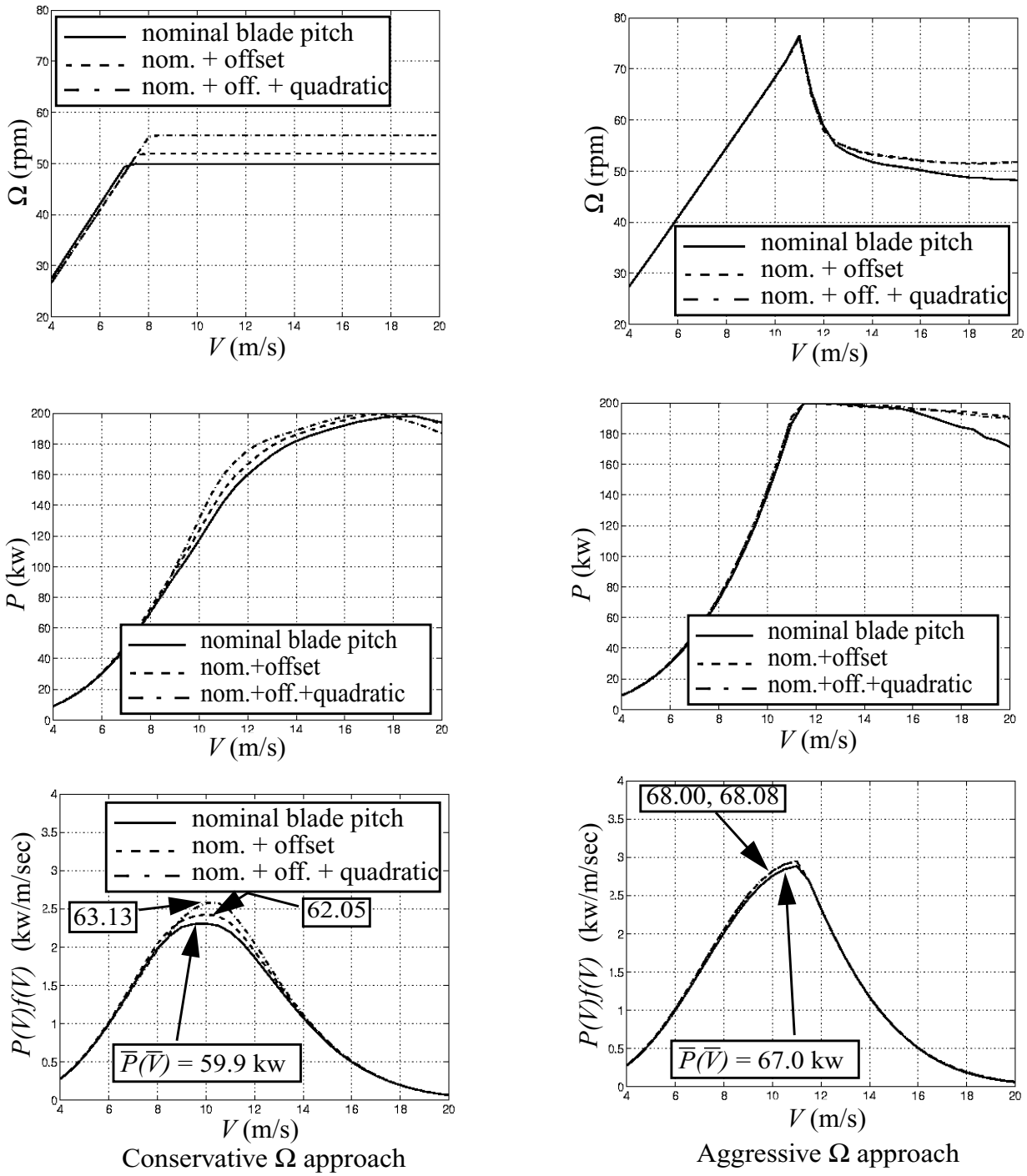

Conservative Ω approach

Aggressive Ω approach

Figure 3.11. Comparison of Variable Speed/Adaptive Blade Schemes for $\overline{V}$ = 7 m/s.

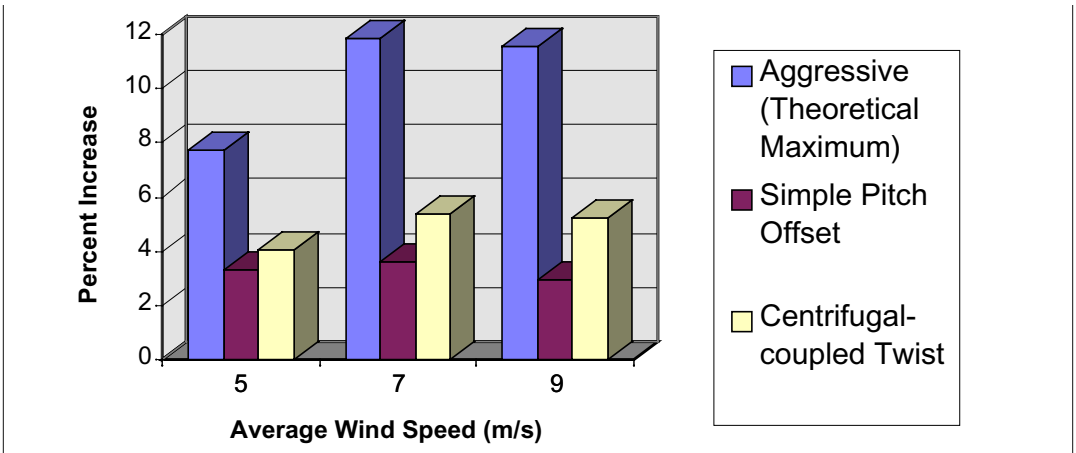

Figure 3.12. Increase in annual energy capture above baseline conservative speed-control case ("Aggressive" allows any rotor speed at each wind speed; the other two are cases with the conservative speed-control enhanced as stated).

are put on rotor speed and the impact of blade adaptation is minimal (1%).

Figure 3.12 illustrates that simple pitch offsets and an adaptive blade with centrifugal twist-coupling are able to partially compensate for a conservative approach to variable-speed control. A simple pitch change can recover some of the theoretical losses of conservative speed control. In a low wind site (5 m/s) a simple pitch change may be sufficient; additional improvements are marginal. In higher wind sites, the adaptive blade can capture 45% of the difference between the baseline conservative and aggressive (theoretical maximum) cases.

Conclusions

This study sought to increase simulated annual energy capture for the AWT-26 turbine via a combination of variable speed and adaptive blade-pitch measures. Gradient-based, numerical optimization was used to solve for parameters in function models for these two measures. The variable-speed models were composed of 1) a conservative approach characterized by a linear rotor-speed rise with local wind speed to a constant rpm; and 2) an aggressive model that had no behavioral constraints on speed other than to maintain an upper bound on power. Blade pitch models were summation combinations of the nominal blade setting, constant offsets, quadratic-in-rotor-speed dependency, and bending-moment dependency. The optimization problem consisted of maximizing average annual power (which is proportional to annual energy capture) while maintaining an upper bound on the power curve.

Average annual power is increased by operating at speeds that maintain maximum efficiency below rated power and are arbitrarily adjusted to regulate power above rating. This aggressive speed-control approach represents an upper bound on performance, although it may not be realizable due to the extreme changes in rotor speed required as a function of wind speed. This aggressive approach cannot be improved substantially by adaptive blade schemes. The greatest improvement was about 1%.

The conservative speed-control approach produces an average annual power 7-12% lower than the theoretical maximum. However, most of the losses resulting from the more workable speed control can be regained with some simple adaptations. A simple resetting of the pitch toward stall recovers about 3% of the total average power in all wind speed cases. This is 25% to 45% of the total difference between

conservative and aggressive approaches. Relating the blade pitch changes to the square of rotor speed (centrifugal coupling) results in average powers 4% to 5.5% higher than the conservative case, a 45% to 52% recovery of the difference between conservative and aggressive approaches. The greatest improvement due to adaptive blade coupling is in the higher (7 and 9 m/s) average wind speeds. Results for a simple pitch change and an adaptive blade are about the same in the 5 m/s case. The improvements stem from an increase in maximum rotor speed and an increase in the wind speed at which the rotor switches to constant-speed operation, resulting in a greater range of operation at peak efficiency and higher efficiencies in the middle of the wind-speed operating range. The power curve is therefore boosted where the greatest annual energy is available in the higher wind cases.

It appears that adaptive pitch changes can compensate for constrained rotor speed operation in the regimes covered in this study to improve average annual power output. Where rotor speed is unconstrained, as in the aggressive approach, blade-pitch compensation showed no ability to improve average annual power output.

Appendix 3.A: AWT-26 Blade Aerodynamic and Twist Data

Tables of lift, drag, and twist data for the AWT-26 blades are used by the PROP code to compute performance. The AWT-26 rotor blades are 43 ft in length. Each is modeled as 20 segments ordered from hub to blade tip. Twist data as a function of normalized blade chord is shown in . Segment 1 (closest to hub) and segment 2 have identical twist values. Segment 7 has the largest blade chord. Blade segment lift and drag data as a function of angle of attack are shown in Figure 3.A-2. Aerodynamic data are approximated as duplicated for every two adjacent segments from hub to tip for a total of 10 individual curves. Note that the lift data are highly variable and indicate a maximum where blade chord is the largest. Drag data display small variations from one segment pair to the next, except when the tip pair is reached.

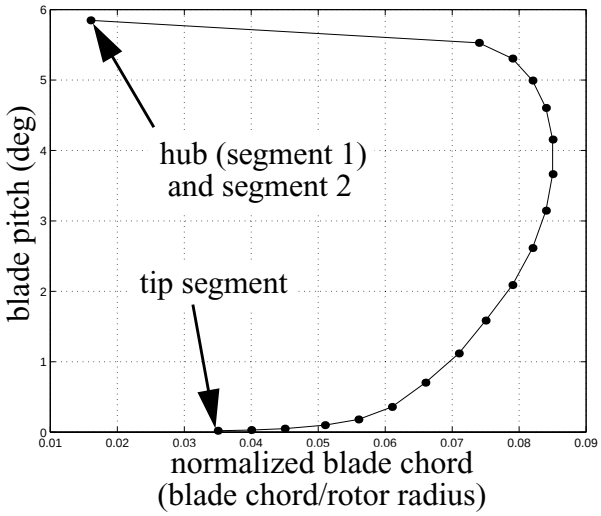

Figure 3.A-1. AWT-26 Blade Twist Data.

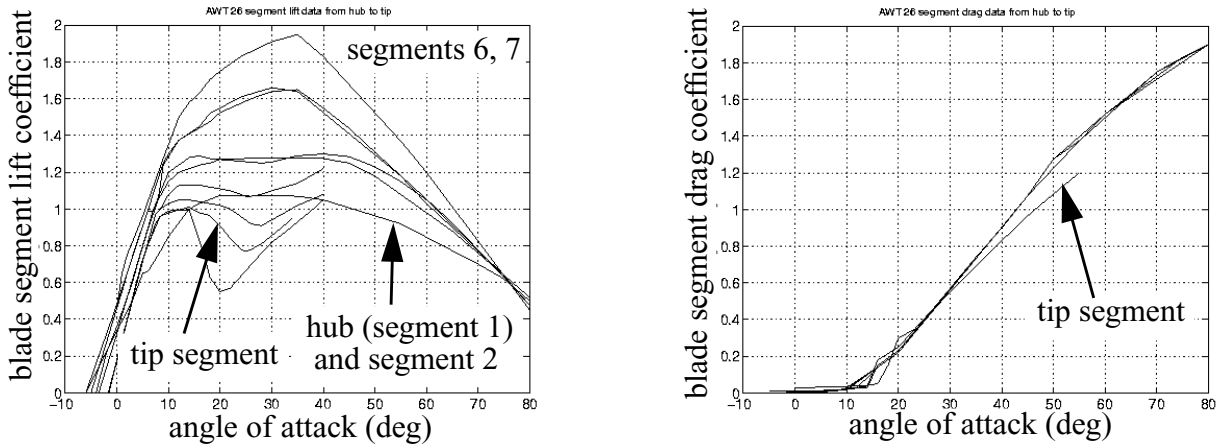

Figure 3.A-2. AWT-26 Blade Aerodynamic Data.

Aeroelastic Behavior of Twist-Coupled HAWT Blades
Chapter 4

Previous Work

There have been many efforts aimed at creating adaptive blades using material elastic coupling to replace mechanical devices with passive techniques. Several have used the composite lay up structure to create a coupling between the twisting of the blade (directly affecting angle of attack) and various other inherent forces. Karaolis et al. (1988, 1989) illustrates how to achieve power control with such a blade on a small system and even provides optimum composite ply structures to provide maximum coupling. Joose and van den Berg (1996) and van den Berg et al. (1994) have publicized efforts to develop a special axial twist-coupled spar that will rotate a tip mechanism through large enough angles to control power and provide some over speed protection. Infield and Feuchtwang (1995) and Feuchtwang and Infield (1995) show how small turbines can have improved speed regulation with extension twist-coupling. A common feature in these works is to provide relatively large rotations to achieve substantial amounts of power regulation. Most have used extension twist-coupling on variable speed systems to assist in over speed control or power regulation and rely on large angles of twist to accomplish complete control of high wind loads. Lobitz et al. (1996), however, demonstrated that even with relatively small twists (that incidentally also enhance regulation), a stall controlled, fixed pitch system could be operated with a larger rotor to achieve net energy enhancements without increasing the maximum power rating.

An excellent report evaluating a great variety of passive methods of achieving power control (Corbet and Morgan (1992)) demonstrates how difficult it is to achieve flat power regulation (constant power versus wind speed) in high winds with passive methods alone. The report does not examine aeroelastic tailoring through composite lay up structure because it is judged too difficult to produce in a reliable manner given current hand-lay up techniques of blade manufacturing. They infer that manufacturing improvements are needed before aeroelastic tailoring based on material coupling can be fully implemented on utility scale machines.

Here we examine more modest twist angles intended to produce load alleviation and perhaps power regulation or enhancement through bending twist-coupling. It seems quite possible to reduce the rotor dynamic response by enhancing aeroelastic damping in critical modes of vibration. Eggers, et al.(1996) have shown how a simple control system, in some ways similar to coupling between root bending and blade pitch, can reduce low frequency blade loads substantially. However, when modifications that influence aeroelastic behavior are introduced into a rotor there is always the possibility of also introducing instabilities. Stability is studied here by mapping out regions of potential coupling, creating a finite element formulation for coupled blades, and evaluating an example blade with added twist coupling. The load alleviating capabilities are not evaluated here, but will be the topic of follow-on studies.

Introduction

Before the aeroelastic behavior of adaptive blades is studied, an investigation into the limits of the magnitude of the coupling is required. Aeroelastic stability computations are then completed within the range of these limits. Two types of aeroelastic instability are investigated, divergence and classical flutter.

Divergence is a static phenomenon wherein the blade relative velocity is great enough so that the aerodynamic load produced for an incremental angle of attack change (due to blade twisting) is greater than the reaction load produced by elastic restoring forces. The result is an effective loss of stiffness so the blade twists without bound, leading to catastrophic failure. Classical flutter is a dynamic phenomenon characterized by an interaction between blade bending and twisting oscillations. As the flow velocity increases, the aerodynamic loading causes the vibratory phase between these two motions to change, eventually leading to a negative damping situation and catastrophic failure. Both of these phenomena can occur at low angle of attack. A third type of aeroelastic instability, which will not be addressed in this paper, is stall flutter. It is characterized by predominantly torsional blade oscillation and normally occurs at high angle of attack near stall.

The finite element model used for this study includes centrifugal stiffening of the blades and rotating coordinate system effects in a manner similar to that done by Lobitz (1984). The "tennis racket" effect, wherein the blade tends to flatten into the plane of rotation due to the chordwise distribution of mass loaded by centrifugal forces, is modeled by distributing the blade mass fore and aft along the chord at each node as two equal lumped masses. The masses are equidistant from the node and the distance between them is adjusted so that the correct torsional inertia is obtained. The incorporation of aeroelasticity terms is based on Theodorsen's equations (Bisplinghoff (1955)) for the lift and moment on an oscillating airfoil in terms of its plunging and pitching motions (bending and twisting for a HAWT blade). The principle of virtual work is employed to cast them into the finite element framework (see Lobitz and Ashwill (1985)). The MSC NASTRAN commercial finite element code is used for this analysis, incorporating the special effects mentioned above and the special couplings described in the next paragraph through the Direct Matrix Input at Grids (DMIG) input option. Special purpose software computes the necessary matrix input values and generates required data records for the input stream.

Coupling between extension and twist, and bending and twist is implemented in the beam element used to model the HAWT blades and will be discussed in greater detail in the next section. The third section of this paper contains results of the aeroelastic instability study for the bending-twist-coupled blade. Conclusions and recommendations are presented in the last section.

Coupling Terms for Beam Elements

The coupling terms for the beam elements are generated starting with beam "stress-strain" relations. Coupling terms are developed for extension twist-coupling and bending twist-coupling, followed by a static demonstration of the bending twist-coupling for the Combined Experiment Blade (CEB).

Extension Twist-Coupling

For the extension twist-coupling the beam "stress-strain" relations at a point are given in matrix form below:

$$\begin{bmatrix} EA & -g \\ -g & GK \end{bmatrix} \begin{bmatrix} \frac{\partial u}{\partial x} \\ \frac{\partial \varphi}{\partial x} \end{bmatrix} = \begin{bmatrix} F \\ M_t \end{bmatrix} \qquad (4.1)$$

As shown in Figure 4.1, u is the axial displacement, φ is the axial twist, F is the axial force, M_t is the twisting moment, and K is the geometric torsional stiffness factor (for a circular cross section, K is equal to J, the polar moment of inertia of the cross section). E, G and A are the Young's Modulus, the shear modulus and

the cross sectional area of the beam, respectively. The quantity, g, is the coupling term, which is zero for the standard beam where no coupling is present between extension and twist. In order for this system to be positive defnite,

$$|g| < \sqrt{EAGK} \tag{4.2}$$

To investigate intermediate values of the coupling term, it is taken to be:

$$g = \alpha\sqrt{EAGK}\,, \quad -1 < \alpha < 1 \tag{4.3}$$

There are, of course, additional bending terms in the beam "stress-strain" relations, but only the above terms impact the development of the coupling term for this type of coupling.

Taking u and φ to vary linearly along the element length and using the principle of virtual work, the finite element representation of Equation 4.1 becomes:

$$\frac{1}{l}\begin{bmatrix} EA & -g & -EA & g \\ -g & GK & g & -GK \\ -EA & g & EA & -g \\ g & -GK & -g & GK \end{bmatrix}\begin{bmatrix} u_1 \\ \varphi_1 \\ u_2 \\ \varphi_2 \end{bmatrix} = \begin{bmatrix} F_1 \\ M_{t_1} \\ F_2 \\ M_{t_2} \end{bmatrix} \tag{4.4}$$

Here l is the length of the element. For illustrative purposes it is instuctive to examine the behavior of a one element beam. If the "1" end of this element is held fixed, the displacements at the "2" end can be obtained in terms of the applied forces at that end, yielding:

$$\begin{bmatrix} u_2 \\ \varphi_2 \end{bmatrix} = l\begin{bmatrix} \frac{1}{1-\alpha^2}\left(\frac{1}{EA}\right) & \frac{\alpha}{1-\alpha^2}\left(\frac{1}{\sqrt{EAGK}}\right) \\ \frac{\alpha}{1-\alpha^2}\left(\frac{1}{\sqrt{EAGK}}\right) & \frac{1}{1-\alpha^2}\left(\frac{1}{GK}\right) \end{bmatrix}\begin{bmatrix} F_2 \\ M_{t_2} \end{bmatrix} \tag{4.5}$$

The coefficients in the matrix involving a $[1/(1-\alpha^2)$ and $\alpha/(1-\alpha^2)]$ are plotted in

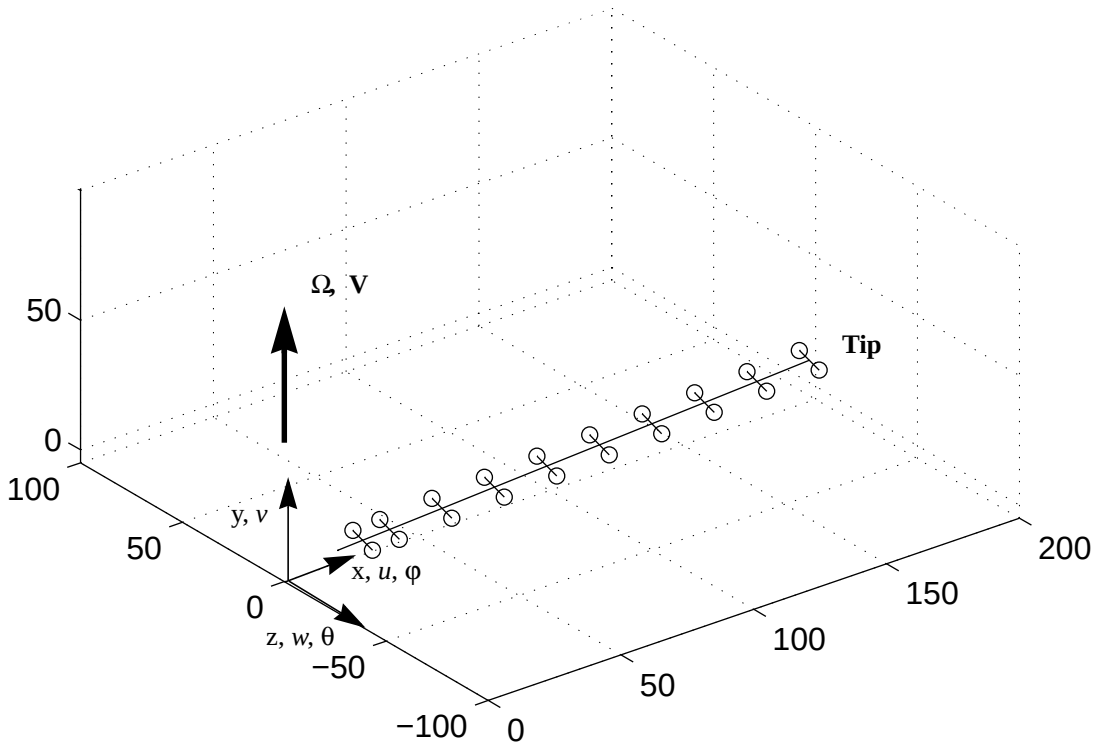

Figure 4.1. Untwisted Combined Experiment Blade (CEB) Model.

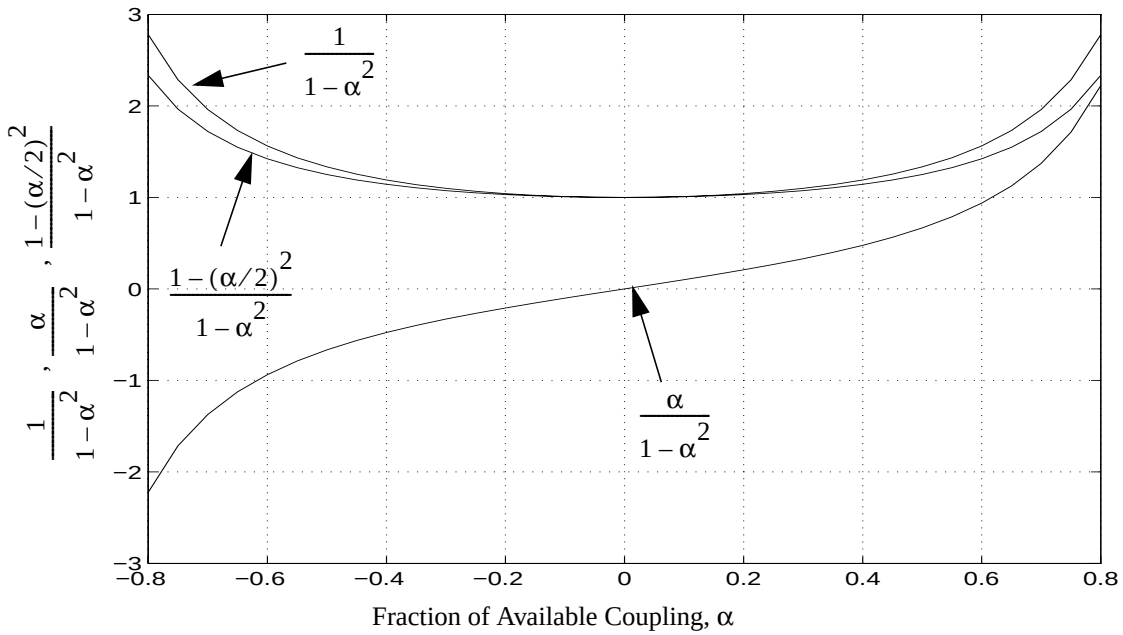

Figure 4.2. Coefficients of matrix elements involving α.

Figure 4.2. This figure along with Equation 4.5 indicate how the various forces affect the coupled motion for the extension twist-coupling. From Equation 4.5, if F_2>0 and M_{t_2}=0, the extension and the twist are positive.

Extension-Twist Demonstration

To exercise this coupled element, the uniform CEB shown in Figure 4.1 is modeled. The "tennis racket" effect is modeled as described above by distributing the mass fore and aft as shown and the blade is pitched toward stall $12°$. A small amount of coning ($3.5°$) is apparent in Figure 4.1. With the rotor turning in still air at 72 rpm (1.2 Hz), the tip rotation and axial extension are shown in Figure 4.3 as a function of the coupling coefficient. In this figure, positive tip rotation corresponds to twisting toward stall. For this loading condition, at 80% of the available coupling, tip rotations of approximately $1.0°$ towards stall and $0.1°$ toward feather are obtained. Part of the reason for this difference in magnitude is the aeroload differences that occur due to the twisting of the blade (the model includes these aeroelastic effects). Axial extension of the tip varies between .0019 and .0163 inches. The tip flapwise deflection (not shown in Figure 4.3) varies between 2.86 and 3.06 inches. It is anticipated that at least several degrees of twist will be required for effective load alleviation .

Bending Twist-Coupling

For the bending twist-coupling the "stress strain" relations at a point are given by:

$$\begin{bmatrix} EI & -g \\ -g & GK \end{bmatrix} \begin{bmatrix} \frac{\partial \theta}{\partial x} \\ \frac{\partial \varphi}{\partial x} \end{bmatrix} = \begin{bmatrix} M_b \\ M_t \end{bmatrix} \qquad (4.6)$$

Referring to Figure 4.1, $\theta = \partial v/\partial x$ (v is the flapwise displacement) and M_b is the bending moment. In order for this system to be positive definite, g is taken to be:

$$g = \alpha\sqrt{EIGK}, \quad -1 < \alpha < 1 \qquad (4.7)$$

The quantity, α, serves the same function here as in the extension twist-coupling. Only bending in the flapwise direction is accounted for in Equation 4.6. Bending in the edgewise direction is considered to be small relative to the

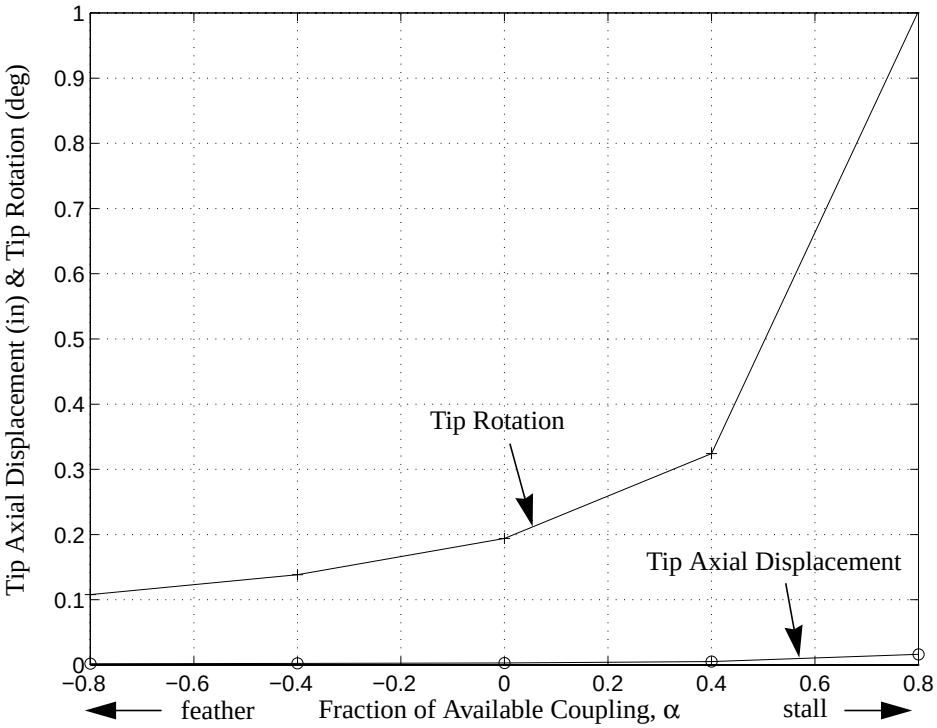

Figure 4.3. Tip Motion of the Extension-Twist Coupled CEB Turning at 72 rpm in Still Air.

flapwise direction, yielding minimal coupling. The axial extension term in the beam "stress-strain" relations does not impact this type of coupling.

Taking v to vary quadratically and φ to vary linearly along the element length (a customary practice for beam element development), and using the principle of virtual work, the finite element representation of Equation 4.6 becomes:

$$\frac{1}{l}\begin{bmatrix} 12EI/l^2 & 6EI/l & 0 & -12EI/l^2 & 6EI/l & 0 \\ 6EI/l & 4EI & -g & -6EI/l & 2EI & g \\ 0 & -g & GK & 0 & g & -GK \\ -12EI/l^2 & -6EI/l & 0 & 12EI/l^2 & -6EI/l & 0 \\ 6EI/l & 2EI & g & -6EI/l & 4EI & -g \\ 0 & g & -GK & 0 & -g & GK \end{bmatrix}\begin{bmatrix} v_1 \\ \theta_1 \\ \varphi_1 \\ v_2 \\ \theta_2 \\ \varphi_2 \end{bmatrix} = \begin{bmatrix} F_1 \\ M_{b_1} \\ M_{t_1} \\ F_2 \\ M_{b_2} \\ M_{t_2} \end{bmatrix} \tag{4.8}$$

The quantities, F_1 and F_2 are transverse forces at the ends of the beam element. As before, if the "1" end of this element is held fixed, the displacements at the "2" end can be obtained in terms of the applied forces at that end, yielding:

$$\begin{bmatrix} v_2 \\ \theta_2 \\ \varphi_2 \end{bmatrix} = \begin{bmatrix} \frac{1-(\alpha/2)^2}{1-\alpha^2}\left(\frac{l^3}{3EI}\right) & \frac{1}{1-\alpha^2}\left(\frac{l^2}{2EI}\right) & \frac{\alpha}{1-\alpha^2}\left(\frac{l^2}{2\sqrt{EIGK}}\right) \\ \frac{1}{1-\alpha^2}\left(\frac{l^2}{2EI}\right) & \frac{1}{1-\alpha^2}\left(\frac{l}{EI}\right) & \frac{\alpha}{1-\alpha^2}\left(\frac{l}{\sqrt{EIGK}}\right) \\ \frac{\alpha}{1-\alpha^2}\left(\frac{l^2}{2\sqrt{EIGK}}\right) & \frac{\alpha}{1-\alpha^2}\left(\frac{l}{\sqrt{EIGK}}\right) & \frac{1}{1-\alpha^2}\left(\frac{l}{GK}\right) \end{bmatrix}\begin{bmatrix} F_2 \\ M_{b_2} \\ M_{t_2} \end{bmatrix} \tag{4.9}$$

The coefficients in the matrix of Equation 4.9 involving α, $1/(1-\alpha^2)$, $\alpha/(1-\alpha^2)$ and $(1-(\alpha/2)^2)/(1-\alpha^2)$, two of which are equivalent to those of Equation 4.5, are plotted in Figure 4.2. For $F_2>0$ and $M_{b_2}=M_{t_2}=0$, the flapwise displacement, the slope and the twist are all positive.

Bending-Twist Demonstration

As for the extension-twist element, the uniform CEB shown in Figure 4.1 is used to exercise the bending-twist element. As before, the

"tennis racket" effect is modeled as described by distributing the mass fore and aft as shown in Figure 4.1, and the blade is pitched toward stall $12°$. With the rotor turning in still air at 72 rpm (1.2 Hz), the tip flapwise displacement and axial rotation are shown in Figure 4.4 as a function of the coupling coefficient. Also shown in Figure 4.4 is the twist toward feather resulting from the "tennis racket" effect, which, for this relatively stiff blade, is negligible compared to that due to the coupling. In this figure, positive tip rotation corresponds to twisting toward stall. The curves for both the tip displacement and rotation appear to be roughly a linear combination of those of Figure 4.3, which is reasonable because the loading consists of a combination of forces, bending moments and twisting moments. For this loading condition, at 80% of the available coupling, tip rotations of approximately $10°$ towards stall and $3°$ toward feather are obtained. As before, part of the reason for this difference in magnitude is the aeroload differences that occur due to the twisting of the blade (the model includes these aeroelastic effects). For load alleviation it is anticipated that at least several degrees of twist will be required.

In addition to the tip motions of the blade, the distribution of the motion along the blade is of interest for ascertaining the magnitudes of the total loads on the blade due to the coupling. In Figure 4.5 , this distribution is shown for the case of α = -0.8. It is apparent for this blade that the coupling produces twist towards feather within 90% of the tip value over the outer third of its span where the aerodynamic loading is the greatest.

In Figure 4.6 the effect of the coupling on the first flap and torsional natural frequencies (also computed using NASTRAN) is presented. These two modes of vibration have significant impact on the aeroelastic stability problem. As indicated, the effect is symmetric with α, and as the magnitude of α increases, the frequencies of the two modes tend toward each other. This is generally considered to be destabilizing.

To investigate the coupled behavior of softer blades, a simplified version of Equation 4.6 can be obtained. For the case of $M_t = 0$ (a reasonable approximation), the following equa-

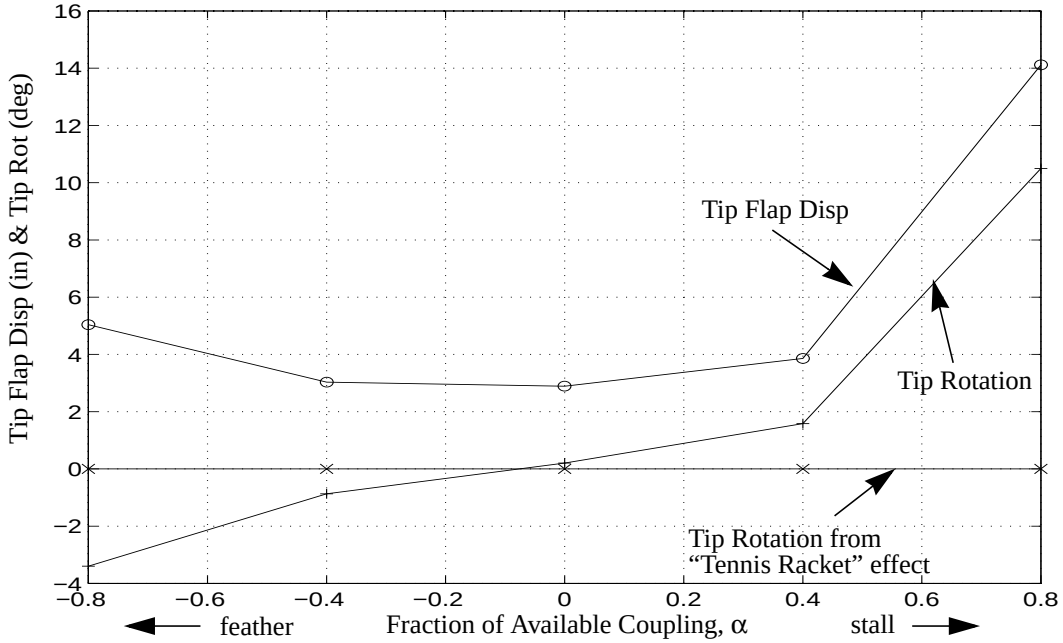

Figure 4.4. Tip Motion of the bending twist-coupled CEB Turning at 72 rpm in Still Air.

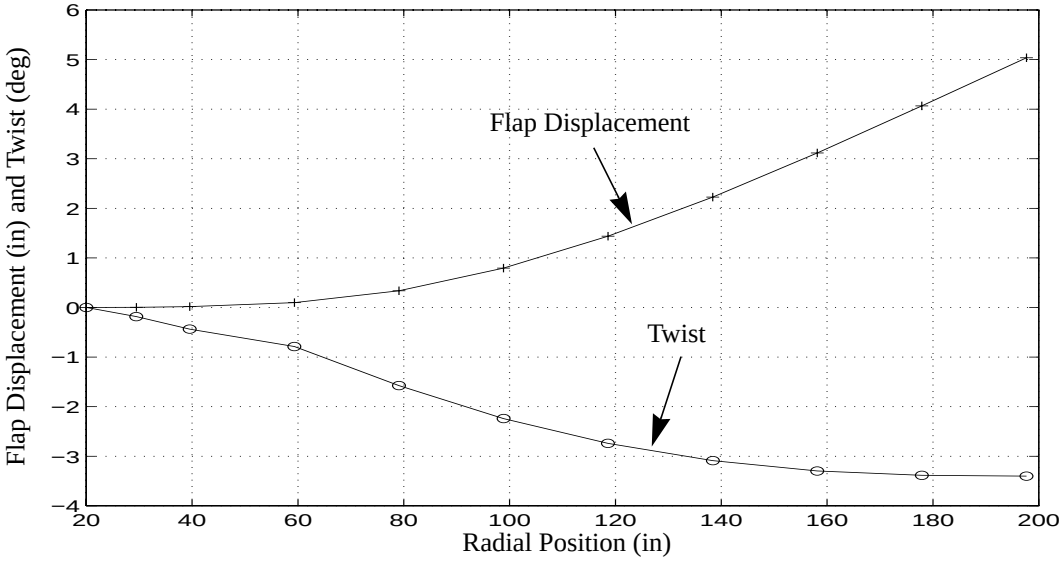

Figure 4.5. Distribution of Flap Displacement and Twist for the Bending Twist-Coupled CEB, α=-0.8 (feather).

tion relating the rate of change of twist with length to the curvature of the blade is obtained:

$$\frac{\partial \varphi}{\partial x} = \alpha\left(\frac{EI}{GK}\right)^{1/2}\frac{\partial \theta}{\partial x} \qquad (4.10)$$

A blade with a given cross section can be softened by simply reducing Young's Modulus, in which case the square root term will remain unchanged. However, for the same loading the curvature of the blade will be greater because of the softer material, and the twist per unit length will also be proportionately greater.

Aeroelastic Stability Results

As discussed in the introduction, this investigation of aeroelastic stability is based on the classical theory developed by Theodorsen[11]. These computations include the effects of centrifugal stiffening, rotational coordinate system effects (i.e. Coriolis forces, etc.), and the "tennis racket" effect, in addition to the aeroelas-

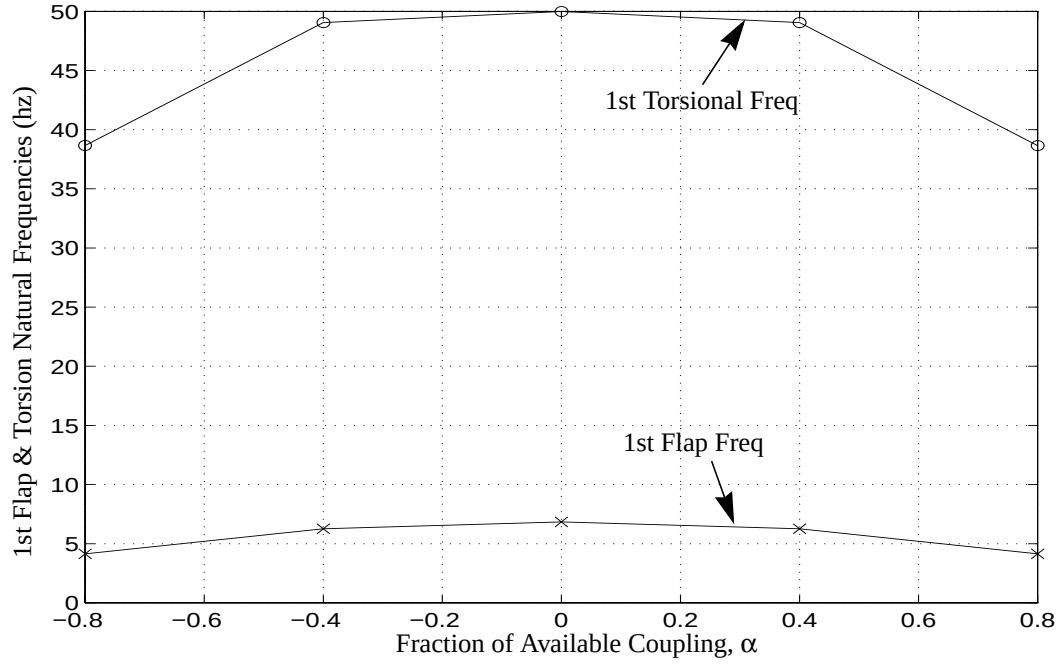

Figure 4.6. Natural Frequencies of the 1st Torsional and Flap Modes Versus Coupling Coefficient.

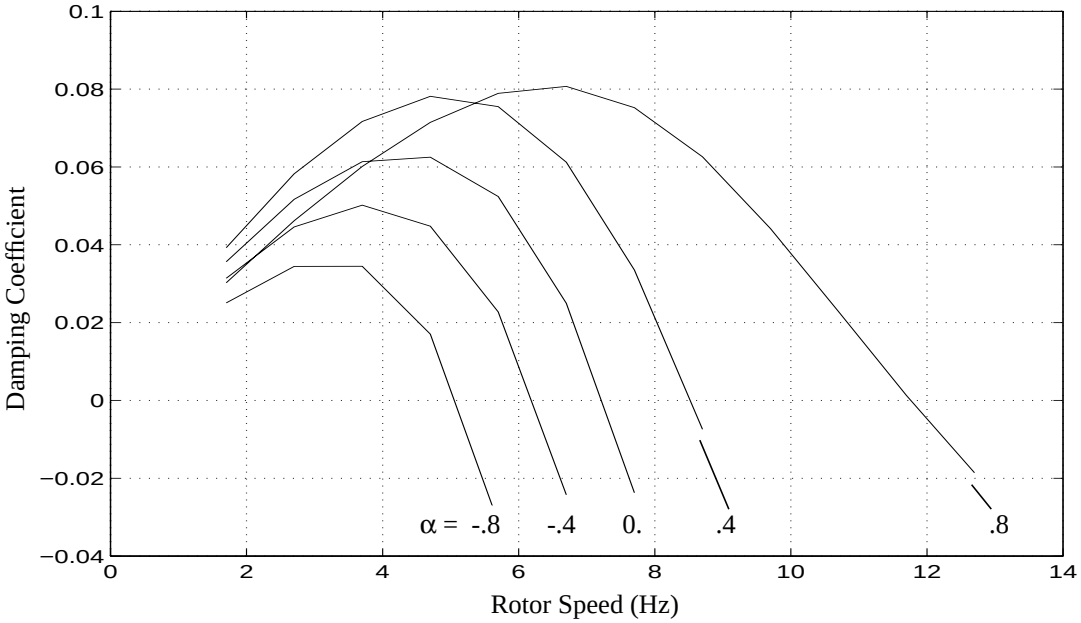

Figure 4.7. Damping Coefficient for the 1st Torsional Mode of the bending twist-coupled CEB.

ticity and coupling terms that are required for the analysis. In general, for aeroelastic stability analyses the airflow is increased until the instability point is reached. For HAWTs the airflow is made up of a component due to the rotation of the rotor and a component due to the ambient wind. In this analysis the component due to the ambient wind is neglected (i.e. the rotor is assumed to be turning in still air) and the rotor speed is simply increased until the system becomes unstable. The remainder of this section will address the aeroelastic stability for bending twist-coupling only.

Analyses are completed for both divergence and classical flutter as a function of the coupling coefficient, α. For flutter, the damping coefficient for the first torsional mode (the first mode to go unstable) of the blade is shown in Figure 4.7 as a function of rotor speed. The various curves correspond to different values of the coupling coefficient. All of the curves show the characteristic increase in the damping coefficient with rotor speed before they fall off to negative values, which indicate instability. The critical rotor speed (where the damping-coefficient curve crosses the axis) appears to be monotonically decreasing with as the coupling coefficient decreases. Incidentally, for this vibrational mode, damping coefficients near the operating speed (1.2 Hz.) are larger for the smaller magnitude coupling coefficients (α equal to -0.4 and 0.4) in Figure 4.7) and smaller for the extreme coupling coefficients (α equal to -0.8 and 0.8), an undesirable characteristic for load reduction.

These critical rotor speeds are plotted in Figure 4.8 along with the divergence rotor speeds as a function of the coupling coefficient. As expected, divergence occurs at lower rotor speeds as the coupling coefficient increases. For positive α, as the blade bends downwind it also twists toward stall, increasing angle of attack and therefore the aeroloads. Conversely for negative α, the blade twists toward feather reducing the aeroloads. In fact as α becomes more negative it is increasingly difficult to get the blade to diverge. For this particular blade the area below the combined flutter and divergence curves represents the region of aeroelastic stability. The horizontal dashed line is the rotor design speed. The blade appears to be less stable at the extreme values of the coupling coefficient and particularly as the blade twists toward stall.

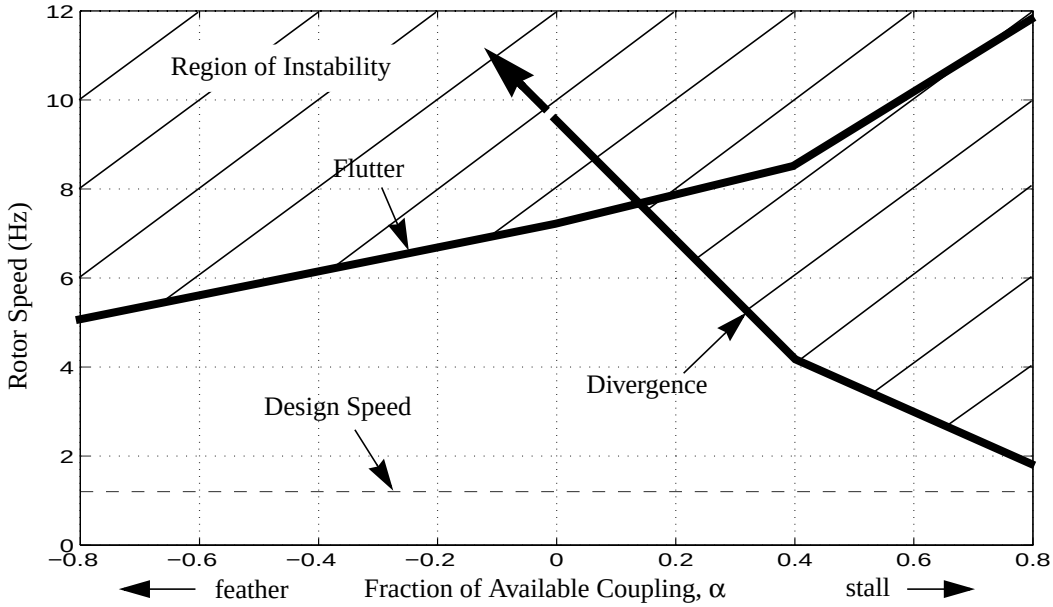

Figure 4.8. Aeroelastic Stability Boundaries for the Bending-Twist Coupled CEB.

Conclusions and Recommendations

In the development of the coupled elements, limits on the amount of coupling are required to preserve the positive definiteness of the system. These limits are established for both the extension-twist and bending-twist beam elements. For the CEB with the bending twist-coupling, these limits proved not to be overly restrictive in that the blade-tip twist ranged from $-3°$ to $10°$ for the coupling coefficient varying from -0.8 to 0.8, under loading from the blade rotating at its design speed. Of course there will be practical limits that might be more restrictive than these theoretical ones. For the extension twist-coupling the theoretical limits proved to be much more severe, with tip twist ranging from $0.1°$ to $1.0°$ for the coupling coefficient range noted above.

The aeroelastic instabilities investigated for the bending twist-coupled blade were divergence and classical flutter, which are based on linear aerodynamic theory (i.e. blade stall is not considered). Results indicate that this CEB blade is less stable as the extreme values of the coupling coefficient are approached. For blades that twist toward stall ($\alpha > 0$) the instability is driven by divergence, and for twist toward feather ($\alpha < 0$), by flutter. The divergence end of the spectrum is significantly more critical than flutter end. Over the range of coupling coefficients examined, the computed critical rotor speeds were always above the rotor's design speed.

Recommendations for further work include completing the aeroelastic stability analysis for the case of extension twist-coupling for variable speed applications, completing a parameter study to obtain optimal levels of aerodynamic damping for transient load reduction, fabricating test articles to examine the practical limits of bending twist-coupling and initiating an effort to investigate stall-flutter instability for coupled blades that are designed to twist toward stall. Additionally, it is recommended that the ability of these coupled blades to alleviate transient loading without seriously compromising performance be studied, this in an effort to increase fatigue life.

Load Mitigation with Twist-Coupled Blades on a Constant Speed Stall-Controlled Rotor

Chapter 5

Introduction

In the process of improving HAWT performance, new methods are continually being sought for capturing additional amounts of energy, alleviating loads and controlling the rotor. One such technique employs the use of an adaptive blade that can sense the wind velocity or rotational speed in some fashion and accordingly modify its aerodynamic configuration to meet a desired objective. This could be achieved in either an active or passive manner, although the passive approach is much more attractive due to its simplicity and economy. For example, a blade might employ coupling between bending (and/or extension), and twisting so that, as it bends (and extends) in response to aerodynamic and inertial loads, it also twists and modifys aerodynamic performance in some way. Previous work has investigated increased energy capture for a constant-speed rotor having twist-coupled blades. Lobitz and Veers (1998) investigated the aeroelastic stability of these blades. Results of that study, which focused on the Combined Experiment Blade (CEB), indicated that although the coupling generally had a destabilizing effect, the operating speed of that rotor was always below the speed at the predicted stability boundary.

Bolstered by these results, the current investigation addresses the load mitigation prospects of a blade that twists toward feather as it bends. Of course stall regulation will be more difficult if not impossible with this blade and therefore some other means of regulation is recommended. One possibility is variable-speed operation which is becoming increasingly popular with wind turbine designers.

As with the previous work, the analysis for the bending twist-coupled blade is carried out within the confines of beam finite element theory. The coupling terms for the beam elements are generated starting with beam "stress-strain" relations. For bending twist-coupling the "stress-strain" relations at a point along the blade span are given by Equation 4.6 and are reproduced here for convenience

$$\begin{bmatrix} EI & -g \\ -g & GK \end{bmatrix} \begin{bmatrix} \frac{\partial \theta}{\partial x} \\ \frac{\partial \varphi}{\partial x} \end{bmatrix} = \begin{bmatrix} M_b \\ M_t \end{bmatrix} \qquad (5.1)$$

Here, $\theta = \partial v / \partial x$ is the flapwise slope of the blade (v is the flapwise displacement, with x measured along the blade span), M_b is the flapwise bending moment, φ is the blade twist, and M_t is the twisting moment. The material parameters E and G are the Young's modulus and the shear modulus respectively; I represents the moment of inertia of the cross section and K the torsional moment of inertia (equal to the polar moment of inertia for circular sections). The quantity, g, is the coupling term, and has a value of zero for the standard beam where no coupling is present. In order for this system to be positive definite (i.e., the determinant of the matrix of Equation 5.1 must be greater than zero) g is taken to be:

$$g = \alpha \sqrt{EIGK}\ , \quad -1 < \alpha < 1 \qquad (5.2)$$

The coupling coefficient, α, provides for variable coupling within the designated limits. Only bending in the flapwise direction is accounted for in Equation 5.1. Bending in the edgewise direction is considered to be small relative to the flapwise direction, yielding min-

imal coupling. Axial extension is also ignored for this type of coupling.

For this analysis the ADAMS/WT software (ADAMS/WT User's Guide, 1997) is used to create rotor models for subsequent analysis with ADAMS (ADAMS/SOLVER Reference Manual, 1994), which has been coupled to Aerodyn (Hansen, 1998). To incorporate the coupling in the "tapered beam" stiffness matrix modifications to the ADAMS/WT software have been implemented. These modifications involve replacing the k_{46} and k_{64} elements of the matrix, which are normally zeroed, with the expression given below:

$$\frac{-(\alpha_L+\alpha_0)[(EI_L+EI_0)(GK_L+GK_0)]^{1/2}}{4L} \quad (5.3)$$

The subscripts *L* and 0 refer to the quantities evaluated at either end of the element. Further explanation of the other parameters in this expression can be found in the ADAMS/WT User's Guide (1997). The parameter α is also added to the "Rotor Blade Data File" to facilitate model input and provide for a coupling coefficient that varies with blade span. The above expression provides a mean value for the coupling in each blade element. As the mean value is only exact for the case of a uniform blade, the positive definiteness of the stiffness matrix may not be preserved for non-uniform blades with high absolute values of the coupling coefficient ($|\alpha| > 0.9$).

To verify that the coupling is incorporated in ADAMS/WT correctly, results for the CEB reported by Lobitz and Veers (1998) have been reproduced with ADAMS. These results are associated with the CEB turning in still air over a range of bending twist-coupling levels. Blade tip rotations and deflections are shown in Figure 5.1 as a function of α for both the previously generated NASTRAN results and the current ADAMS results. The favorable

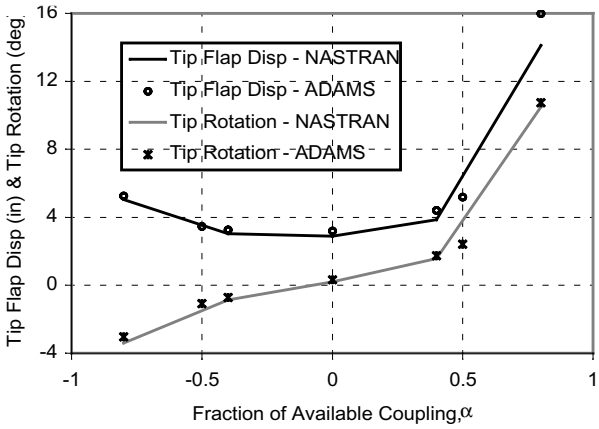

Figure 5.1. ADAMS/NASTRAN comparison for the CEB with bending-twist coupling

agreement between the two provides confidence that the ADAMS modeling is correct.

Using a twist-coupled model of a representative stall-regulated rotor operating at a constant speed, ADAMS is exercised using stochastic wind time series generated with SNLWIND-3D (Kelley, 1993) for hub-height mean wind speeds of 8 m/s, 14 m/s and 20 m/s. These wind speeds represent the linear aerodynamic, stall and post stall regions of the power curve, respectively. Two turbulence levels are used in the simulations, one representing the current IEC standard (Safety of Wind Turbine Generator Systems, 1998) and the other at 50% of that standard. These levels represent a relatively turbulent site and a relatively benign one. With these wind loadings, computations are completed for several values of the bending twist-coupling coefficient within a range that assures positive definiteness of the structural stiffness. These are α = -0.6, -0.3, 0.0, 0.3, 0.6, with α = 0.0 corresponding to the uncoupled case. Load histories and power output are computed and stored for all of the above cases for subsequent processing.

Fatigue-damage estimates are computed for these load histories assuming that damage is proportional to the load-cycle amplitude raised to a material exponent, *b*. The parameter *b* is

often used to define the fatigue behavior of a material that follows the trend:

$$N \propto S^{-b} \qquad (5.4)$$

where S is the stress amplitude and N is the number of cycles to failure.

Values for b of 3, 6, and 9 are used to represent a range of materials from welded steel to aluminum to composites. The damage is assumed to be cumulative, and therefore Miner's Rule is invoked. Damage results for the various levels of bending twist-coupling are compared to the uncoupled case. Average power levels and maximum load levels are also compared.

The remaining sections of the chapter contain a description of the rotor model and wind inputs, computed results, and concluding remarks.

Rotor and Turbulence Models

The rotor model created using ADAMS/WT employs flexible blades comprised of 20 elements each. All other model parts and interconnections are rigid. Parameters for the basic model are presented in Table 5.1.

Table 5.1. Model Configuration Sumary.

Parameter	**Value**
Number of blades	3
Rotor configuration	upwind
Yaw configuration	fixed
Blade length	14.9 m
Rotor hub radius	1.5 m
Rotor precone angle	0 deg
Rotor radius	16.4 m
Rotor hub height	50.0 m
Rotor tilt angle	0 deg
Rotor rotational speed (constant)	32 rpm

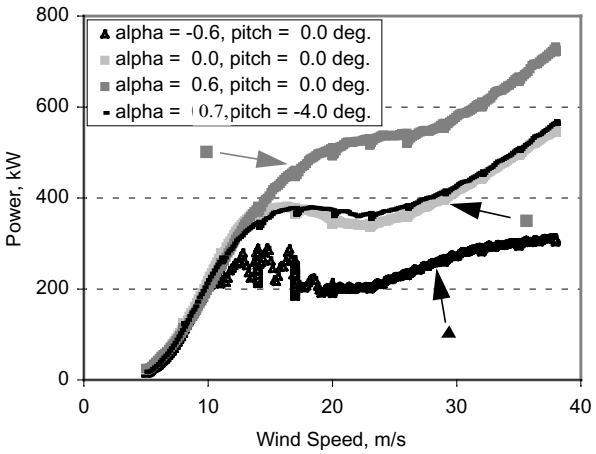

Figure 5.2. Power curves for 4 models showing effect of twist-coupling and pitch angle.

The rotor blade is based on an existing 15-meter blade design, modified only to include the twist-coupling. No attempt was made to optimize this blade.

Models were created in ADAMS/WT for each of the five twist-coupling values of α discussed earlier. The pitch angle of the majority of these models is a constant 0.0 degrees. Power curves for three of these models are shown in Figure 5.2. Because α affects blade twist, and therefore stall, it also affects the power curve for the model, as shown in Figure 5.2. An additional model was created for $\alpha = 0.7$ with a blade pitch of -4 degrees, to limit the peak power, and hence drivetrain loading, to that of the $\alpha = 0.0$ model. The power curve for this model is also shown in Figure 5.2.

An interesting feature of the $\alpha = -0.6$ power curve in Figure 5.2 is the instability near peak power (12 – 18 m/s), which apparently results from the onset of stall flutter. The effect of this instability on fatigue life will be discussed in the Results section.

Simulated turbulence was created using SNL-WIND-3D for 3 average wind speeds as discussed earlier. Inputs to the program were chosen to duplicate conditions specified in the IEC standard. Shear velocity input was used to

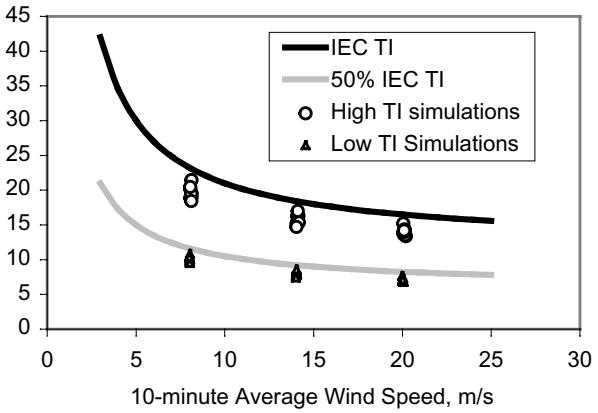

Figure 5.3. Turbulence intensity of simulated turbulence compared to IEC standard criteria.

vary turbulence intensity. Ten 10-minute wind data sets were created at each wind speed for IEC turbulence intensity level, each using a different seed or initiation point for the random process utilized in generating the time series. Ten additional 10-minute turbulence files were created at each wind speed with the turbulence intensity set to 50% of IEC levels. Figure 5.3 compares the turbulence intensities of the simulated turbulence with the IEC criteria.

In all, a total of 100 minutes of simulated turbulence at each mean wind speed and turbulence level were created. Thus, with the six models investigated, a total of 3600 simulated minutes – comprised of 360 10-minute simulations – are used in this analysis.

Results

Simulation results discussed in this section include fatigue damage, average power and maximum load for the various cases. In addition to the damage estimates, sample load-spectra are provided. A sample load-time-history is also included that shows the development of a possible stall flutter instability.

Figures 5.4 (a, b, and c) and 5.5 (a, b, and c) summarize the fatigue damage for most of the simulations, Figure 5.4 is for the high turbulence intensity corresponding to the IEC Standard and Figure 5.5 is for half of that turbulence level. The damage is computed for the out-of-plane root bending moment only as the loads are generally highest at that location. Loads due to blade twist are not considered in the damage computation. For each turbulence intensity the damage is normalized to the damage that occurs for the 14 m/s wind speed and $\alpha = 0.0$. Thus in Figures 5.4b and 5.5b the damage associated with the $\alpha = 0.0$ bar is set to unity for all three values of the material exponent. In all cases positive α indicates twisting toward feather, and negative α indicates twisting toward stall.

It is immediately apparent from Figures 5.4b and 5.5b that twisting to stall dramatically increases fatigue damage for the 14 m/s wind speed. This is probably the result of an apparent stall flutter instability that occurs for negative α in the stall and post stall wind regimes. As mentioned earlier, the power curve for $\alpha = -0.6$ in Figure 5.2 shows a region of instability from approximately 12 m/s out to 18 m/s. This instability is also apparent in the time series plot of Figure 5.6 for the out-of-plane moment. Here the frequency of the instability is approximately 1.7 hz, which is close to the frequency of the first bending twist-coupled mode of the $\alpha = -0.6$ blade, as listed in Table 5.2. For the 8 m/s and 20 m/s wind speeds, coupling toward stall still carries a high damage penalty although not as dramatic as that for the 14 m/s wind speed, where stall events occur more often.

Table 5.2. Non-Rotating Blade 1st Flap Freqs.

α	-0.6	-0.3	0.0	0.3	0.6
Freq (hz)	1.69	2.25	2.39	2.22	1.65

Comparing damage results for $\alpha = 0.0$ and $\alpha = 0.6$ (twisting toward feather), there is at least a factor of two reduction in damage in almost all cases, with significantly greater reductions for the 8 m/s wind speed. For the

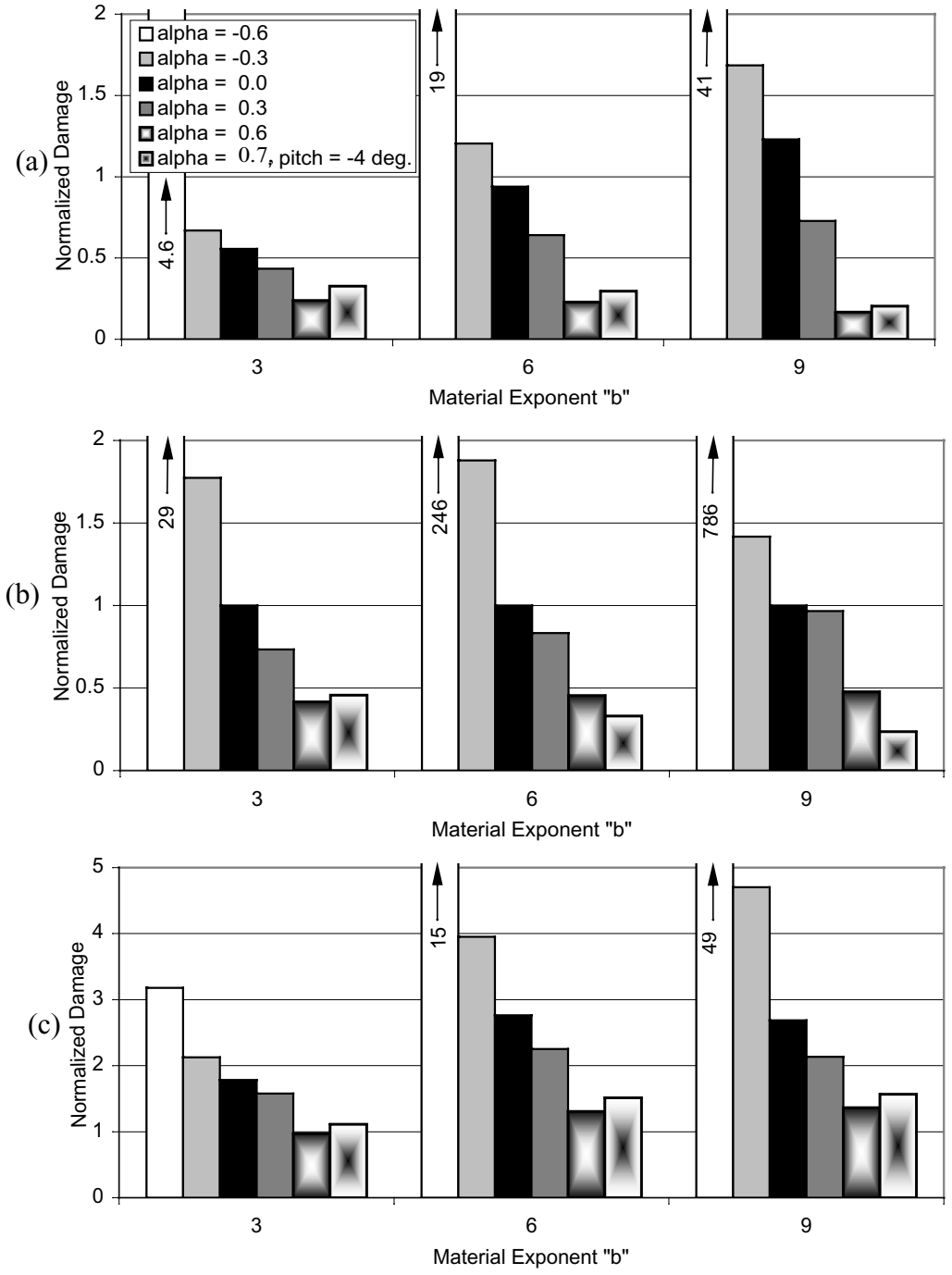

Figure 5.4. Comparison of relative fatigue damage for 6 blade models and 3 material exponents for 100 simulated minutes at (a) 8, (b) 14, and (c) 20 m/s average wind speeds with the IEC turbulence intensity.

case of $\alpha = 0.3$ the reductions in damage are proportionately much less than for those of $\alpha = 0.6$, especially for the 20 m/s wind speed. In general, the trend of reduced relative damage with increasing α is roughly independent of the material exponent.

Figure 5.5a and b show the curious result that the relative damage for $b = 6$ and 9 is greater

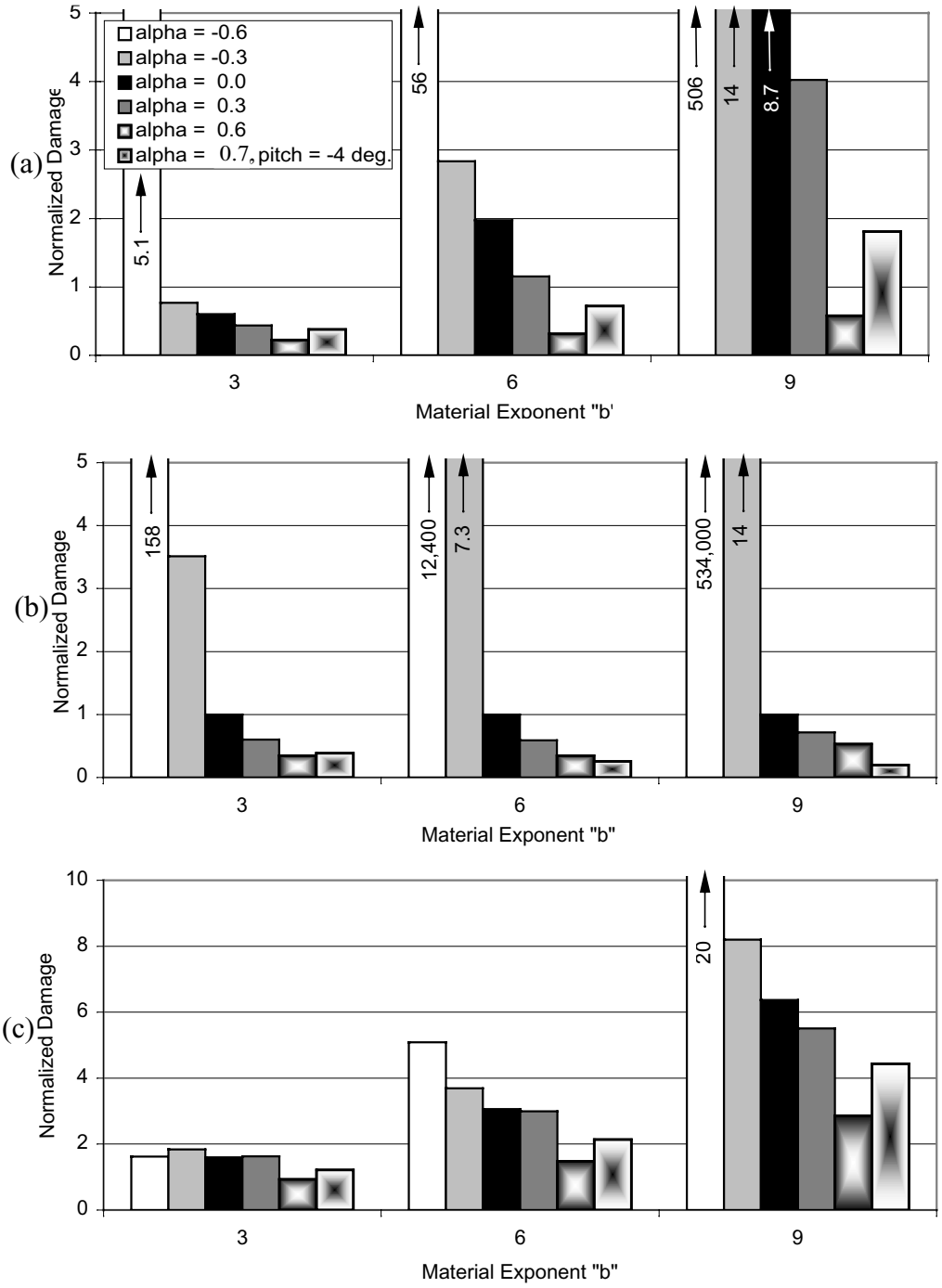

Figure 5.5. Comparison of relative fatigue damage for 6 blade models and 3 material exponents for 100 simulated minutes at (a) 8, (b) 14, and (c) 20 m/s average wind speeds with 50% of the IEC turbulence intensity.

for some α's at 8 m/s than at 14 m/s. This is due to differences in the range of lift coefficient realized at different wind speeds and turbulence levels, as shown in Figure 5.7. For low turbulence, Figure 5.7a shows that at 8 m/s the blade operates in the linear part of the lift curve, covering a range from 0.6 to 1.4. At 14 m/s the blade operates in stall transition covering the smaller range from 1.2 to 1.6. Therefore, although the loads are in general greater

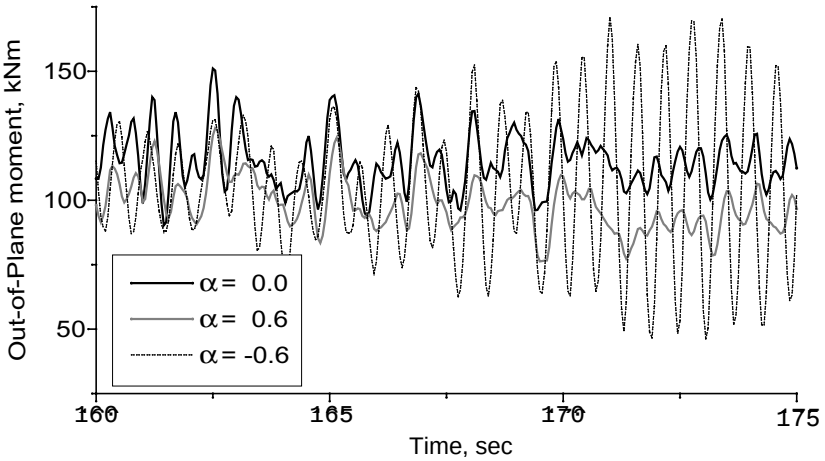

Figure 5.6. Time series plot of blade bending moment showing the instability at $\alpha = -0.6$.

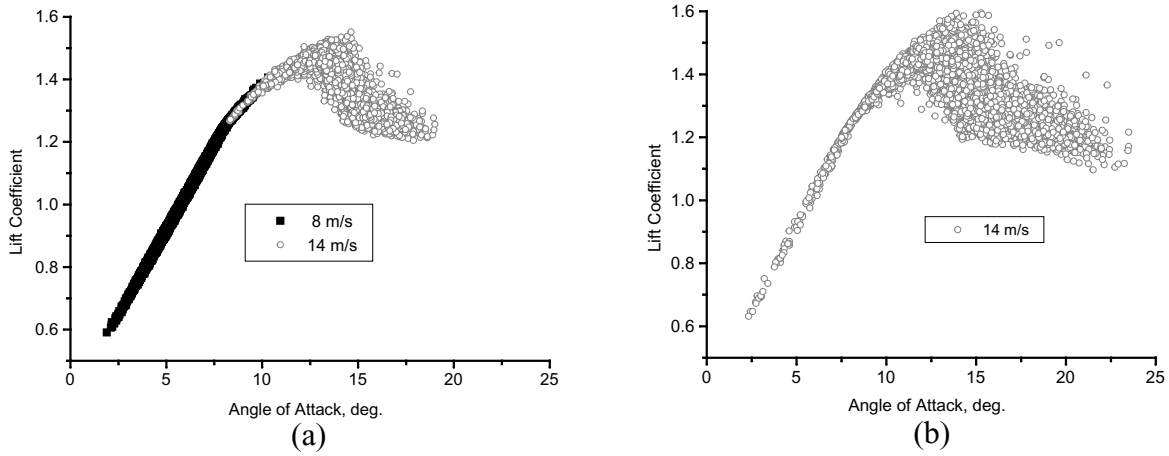

Figure 5.7. Coefficient of lift plots showing that the range for 8 m/s (solid black squares) is greater than that for 14 m/s (open gray circles) for the low turbulence case (a), and both are smaller than for the 14 m/s high turbulence case (b).

at 14 m/s, loads cycles are actually larger at 8 m/s. Figure 5.7b shows that the lift curve range for 14 m/s is much greater for the higher turbulence level – 0.6 to 1.6 – than for the lower turbulence level, hence this result of higher damage at lower wind speed is not evident in Figure 5.4.

Figure 5.8 shows load spectra for $\alpha = -0.6$, 0.0, 0.6 for the 14 m/s average wind speed with IEC turbulence intensity. Cycle amplitude clearly increases with decreasing α, and the effect of the instability for $\alpha = -0.6$ discussed above is dramatic.

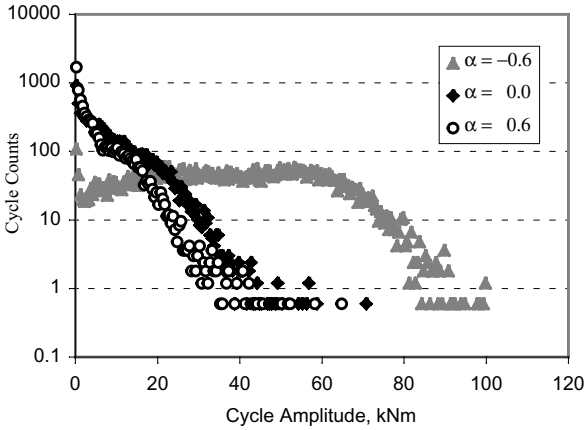

Figure 5.8. Comparison of cycle counted out-of-plane bending moments at 14 m/s average wind speed with IEC turbulence intensity.

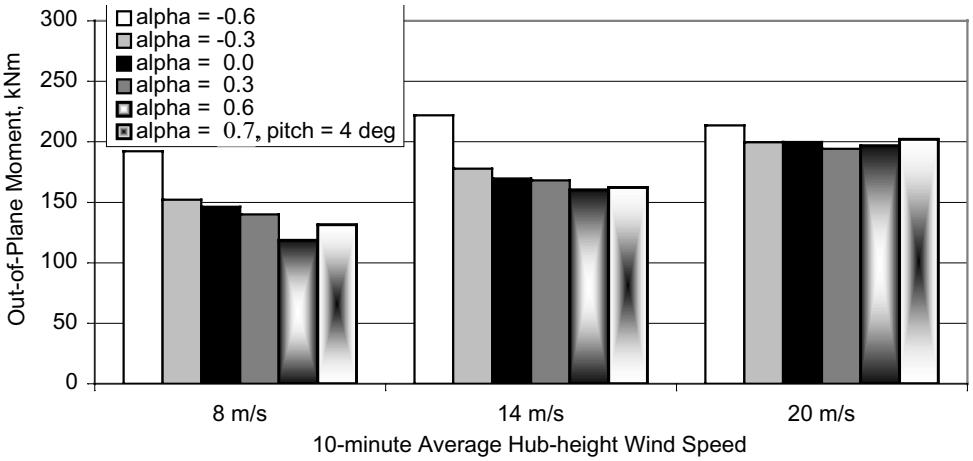

Figure 5.9. Comparison of maximum out-of-plane moments over all simulations for all models and wind speeds.

Figure 5.9 provides comparisons of the maximum bending moments that occur in each time series for the various α's and average wind speeds. For each wind speed the maximum load for $\alpha = 0.6$ is somewhat less than that for $\alpha = 0.0$. The random nature of the turbulence can make such a direct comparison of maximum values misleading. A better way to compare the maxima is using probability of exceedence curves. These were calculated using a Gumbel distribution fit from the FITS routine (Kashef and Winterstein, 1998) and are shown in Figure 5.10 for the 20 m/s case. It is clear that the probability of exceeding a given maximum load tends to decrease with increasing α.

In Figure 5.11 the average power is displayed for the various cases and, except for the average wind speed of 8 m/s, the average power is greater for $\alpha = 0.6$ than for $\alpha = 0$. This result is consistent with the power curves of Figure 5.2.

In short summary, for a blade that twists to feather as it bends with a bending twist-coupling coefficient of $\alpha = 0.6$, the rotor produces

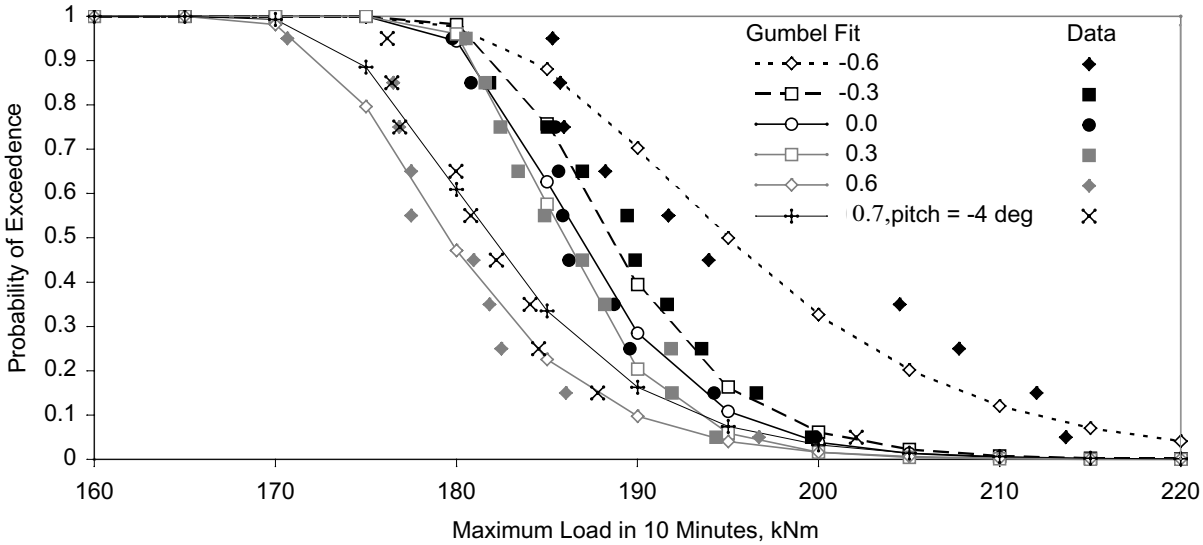

Figure 5.10. Comparison of curves of probability of exceedence in 10 minutes at 20 m/s average wind speed and associated simulation data points for maximum out-of-plane moment for all 6 wind turbine models.

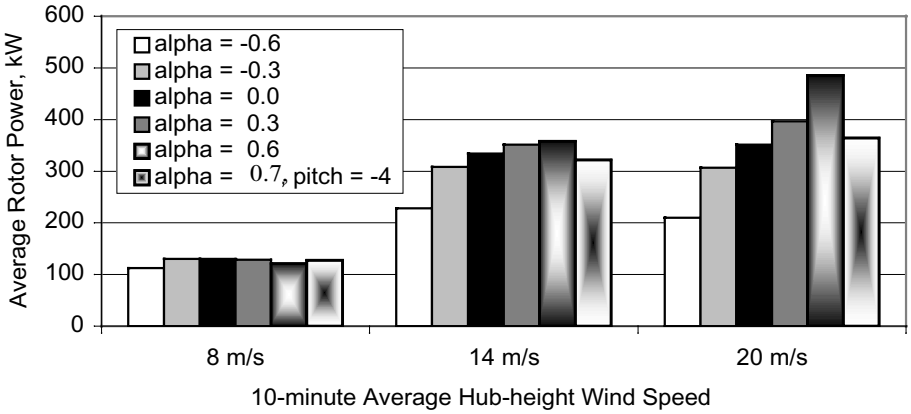

Figure 5.11. Comparison of average rotor power over all simulations for all models and wind speeds.

greater average power and simultaneously experiences smaller maximum loads and half the fatigue damage compared to the uncoupled blade. While these are all very desirable improvements, a higher capacity gearbox and generator would be required to accommodate the higher power of this twist-coupled rotor. Additionally, as observed from its power curve in Figure 5.2, this rotor does not stall regulate and therefore some other means of regulation would be necessary.

To obtain a more rigorous comparison, the blade pitch of the above twist-coupled rotor was adjusted toward stall to obtain a power curve similar to the one for the uncoupled rotor. This is accomplished by setting the pitch of the twist-coupled rotor to -4.0 degrees. The resulting power curve, shown in Figure 5.2, is now in reasonable agreement with the one for the uncoupled rotor. As shown in Figure 5.9, the maximum loads for the pitched blade with $\alpha = 0.7$ have crept a little higher than those of the unpitched $\alpha = 0.6$ model, and are now roughly equivalent to those for the uncoupled rotor. The probability of exceedence for a given maximum load also increases slightly for the pitched blade as shown in Figure 5.10. Likewise, as shown in Figure 5.11, the average power levels have crept down some and are also roughly equivalent to those for the uncoupled rotor (this is expected since the two power curves are now roughly equivalent). However, referring to Figures 5.4 and 5.5 (a, b, and c), the fatigue damage levels for nearly all cases shown are still down by at least a factor of two when compared to those of the uncoupled rotor. Thus, it is apparent that the primary improvement provided by the twist-coupled blade is a substantial reduction in fatigue damage.

Conclusions and Recommendations

The ADAMS software is employed to investigate the feasibility of using blades that twist as they bend to mitigate fluctuating loads. Time-series calculations are made for three average hub-height wind speeds, two wind turbulence settings and five levels of twist-coupling. Fatigue damage is computed from the load histories using material exponents that represent materials ranging from welded steel to composites.

Results show that twist-coupling toward stall produces significant increases in fatigue damage, and for a range of wind speeds in the stall regime, apparent stall flutter behavior is observed. For twist-coupling toward feather with a coupling coefficient of 0.6 fatigue damage is decreased by at least a factor of two for almost all of the cases investigated. The damage reductions seemed to be relatively independent of the material exponent.

Concurrent with lower fatigue damage estimates for positive twist-coupling, maximum loads decreased modestly and average power increased due to elevations in the power curve in the stall region. When the pitch is altered to bring the power curve into agreement with that of the uncoupled rotor, fatigue-damage levels remain at the same reduced levels, while differences in maximum load and average power are reduced.

There is evidence in the power curve that pitching the coupled rotor may reduce overall energy capture. However, for a new rotor, twist-coupled blades would be carefully designed to minimize this reduction. Also, the use of twist-coupling along with active power control could better take advantage of the increased energy capture seen in these results, while maintaining the fatigue-load mitigation observed.

The turbine model used was a simple one, making it difficult to extrapolate results to machines incorporating variable speed, pitch control, or non-zero rotor coning. The substantial fatigue damage reductions that have been predicted call for additional investigation, and turbines incorporating these increasingly common characteristics should be included. The combination of rotor coning and variable speed is especially interesting, as twist will vary with rotor speed due to flap loading caused by centrifugal force.

The fatigue benefits of twist-coupling can only be realized if blades incorporating this trait can be built. Composite, uniform, D-spars have already been designed and fabricated (Ong and Tsai, 1999) that possess coupling coefficients in the range of 0.6. The next step involves the design and fabrication of a much more complex twist-coupled blade with a coupling coefficient in this same range. Design factors such as spanwise variance of coupling coefficient, and optimization of blade geometry to make the most of the advantages of twist-coupling need to be investigated. The ultimate goal is to design and produce a rotor blade that provides maximum benefit to turbine performance with minimal additional production cost.

LOAD MITIGATION WITH TWIST-COUPLED BLADES ON ROTORS USING MODERN CONTROL STRATEGIES

CHAPTER 6

INTRODUCTION

The prospect of installing blades that twist as they bend and/or extend on horizontal axis wind turbines provides opportunities for enhanced energy capture and/or load mitigation. Although this coupling could be achieved in either an active or passive manner, the passive approach is much more attractive due to its simplicity and economy. As an example, a blade design might employ coupling between bending and twisting, so that as the blade bends due to the action of the aerodynamic loads, it also twists modifying the aerodynamic performance in some way.

Previous works have focused on the application of blades with this bending twist-coupling to constant speed rotors, investigating increased energy capture, aeroelastic stability, and enhanced load mitigation. Results indicate that energy capture can be increased significantly by configuring the coupled blades to twist toward stall while increasing the rotor diameter to maintain the maximum power at its design value (Lobitz et al., 1996). However subsequent simulations with the rotor turning in turbulent winds showed substantial increases in fatigue damage when the coupled blades (i.e. blades with bending twist-coupling) twist toward stall as they bend (Lobitz and Laino, 1999). Moreover, for a range of wind speeds in the stall regime, stall-flutter is observed (Lobitz and Laino, 1999). Twisting toward stall also destabilizes divergence, although not critically for reasonable levels of coupling (Lobitz and Veers, 1998). In contrast, when the blades twist toward feather, fatigue damage is reduced by approximately a factor of two, stall-flutter is not observed and divergence is stabilized (Lobitz et al., 1998, 1999). Classical flutter, however, is destabilized, although not critically for reasonable levels of coupling (Lobitz and Veers, 1998). There is evidence from the simulated power curve of a constant speed rotor that energy capture may be somewhat reduced when the blades twist toward feather (Lobitz and Laino, 1999). It should be noted that these blades were originally designed to operate without the twist-coupled feature and were pitched as a rigid body toward stall to limit the maximum power to its design value. However, twist-coupled blades carefully designed to eliminate this preset pitch would tend to minimize this reduction and possibly even increase performance in low winds. Active turbine power control also serves to eliminate this degradation.

As with the previous work, the analysis for the bending twist-coupled blade is carried out within the confines of beam finite element theory using the ADAMS software (ADAMS/SOLVER Reference Manual, 1994). The coupling terms for the beam elements are generated starting with beam "stress-strain" relations. For bending twist-coupling the "stress-strain" relations at a point along the blade span, x, are given by Equation 4.6, and are reproduced here for convenience:

$$\begin{bmatrix} EI & -g \\ -g & GK \end{bmatrix} \begin{bmatrix} \frac{\partial \theta}{\partial x} \\ \frac{\partial \varphi}{\partial x} \end{bmatrix} = \begin{bmatrix} M_b \\ M_t \end{bmatrix} \qquad (6.1)$$

Here, $\theta = \partial v / \partial x$ is the flapwise slope of the blade (v is the flapwise displacement), M_b is the flapwise bending moment, φ is the blade twist, and M_t is the twisting moment. The quantities EI and GK are the flexural rigidity and torsional stiffness respectively, and g is the

coupling term which has a value of zero for the standard beam where no coupling is present. For this system to be positive definite g is taken to be:

$$g = \alpha\sqrt{EIGK}, \quad -1 < \alpha < 1 \qquad (6.2)$$

The coupling coefficient, α, provides for variable coupling within the designated limits. Practical experience (Ong et al.,1999) suggests that α may be limited to $-0.6 < \alpha < 0.6$. Only bending in the flapwise direction is accounted for in Equation 6.2 above. Bending in the edgewise direction is considered to be small relative to the flapwise direction, yielding minimal coupling. Axial extension is also ignored for this type of coupling. For ease of model generation the ADAMS/WT (ADAMS/WT User's Guide, 1997) software is modified to incorporate the bending twist-coupling as described in Chapter 5, page 52.

The current work focuses on the application of bending twist-coupled blades to rotors that use three different control strategies. A constant speed stall-controlled rotor is included in this set as a baseline. The two more modern control strategies investigated are variable speed stall-control and variable speed pitch-control. The blades of each of these rotors are first optimized by setting the pre-twist such that a desirable twist distribution is achieved at rated power. In each case this procedure produces power curves for the twist-coupled rotors that are nearly identical to those of the uncoupled rotors to which they are being compared.

A separate study for the variable speed stall-controlled rotor is presented wherein the twist-coupled rotor efficiency is compared to that of the uncoupled one in a steady wind environment. In this study, the peak rotor efficiency is determined at each windspeed by optimally adjusting the rotor rpm. This peak efficiency is plotted versus wind speed and compared to that for blades with no twist-coupling.

For the three rotors, simulations are completed for turbulent winds to compare the associated fatigue damage reductions for the twist-coupled blades to the uncoupled ones. Power degradations are also presented.

As twist-coupling tends to soften the blades, additional simulations are completed to assess the degree to which the softening alone reduces the fatigue damage. In this investigation, the variable speed stall-controlled rotor blades are softened to have the equivalent stiffness of the twist-coupled ones, but without the twist-coupling.

Using twist-coupled models of a representative rotor and the three different control strategies, ADAMS is exercised using turbulent wind time series generated with SNLWIND-3D (Kelley, 1993) for hub-height mean windspeeds of 8 m/s, 14 m/s and 20 m/s, each approximately 90 minutes in length. For the stall-controlled rotors, these windspeeds represent the linear aerodynamic, stall and deep stall regions of the power curve, respectively. Two turbulence levels are used in these simulations, the current IEC Class I standard (Safety of Wind Turbine Generator Systems, 1998) and 50% of that standard. These levels represent a relatively turbulent site and a relatively benign one. Using the wind loadings defined above, computations are completed for blades with the optimal pre-twist and a value of the bending twist-coupling coefficient of $\alpha = 0.6$, where $\alpha = 0.0$ corresponds to the uncoupled case. Load histories and power output are computed and stored for all of the above cases for subsequent processing.

Fatigue-damage estimates are computed for these load histories assuming that damage is proportional to the load-cycle amplitude raised to a material exponent, b, namely:

$$D \propto S^b \qquad (6.3)$$

where S is the stress amplitude and D is fatigue

damage.

Values for b of 3, 6, and 9 are used to represent a range of materials from welded steel to aluminum to composites. Results are also presented for a value of b=1, which represents the average cyclic load. The damage is assumed to be cumulative and therefore Miner's Rule is invoked, resulting in the following expression for the total damage, D_T:

$$D_T = \sum_{i=1}^{N} S_i^b , \qquad (6.4)$$

where N is the total number of stress cycles. An additional damage measure, the damage equivalent load, D_{EL}, is also provided, given by:

$$D_{EL} = (D_T)^{1/b} \qquad (6.5)$$

Damage results for the various control strategies for both the bend twist-coupled rotor and the incoupled one are compared. Maximum load levels and average power levels are also compared.

The remaining sections of the chapter contain a description of the rotor models and wind inputs, computed results, and concluding remarks.

ROTOR AND TURBULENCE MODELS

The rotor models created using ADAMS-WT employ flexible blades comprised of 20 elements each. All other model parts and interconnections are rigid. Parameters for the basic model are presented in Table 6.1. The rotor blade is based on an existing 15-meter blade design, modified to include twist-coupling. Models were developed for coupling coefficients of $\alpha = 0.6$ and $\alpha = 0.0$. For the uncoupled case the pre-twist varies as indicated in Figure 6.1 by the solid curve (the negative sign indicating twist toward feather). For the twist-coupled rotor the pre-twist was set so that this twist distribution was achieved at rated power.

Table 6.1. Model Configuration Summary.

Parameter	Value
Number of blades	3
Rotor configuration	upwind
Yaw configuration	fixed
Blade length	14.9 m
Rotor hub radius	1.5 m
Rotor precone angle	0.0 deg
Rotor radius	16.4 m
Rotor hub height	50 m
Rotor tilt angle	0.0 deg
Sling (dist from yaw axis to hub)	4.0 m
Rotor rotational speed (variable)	0 - 32 rpm

This pre-twist is determined by building a rotor with two blades in the same azimuthal location, one uncoupled and one with twist-coupling. Pointers in the ADAMS/Solver dataset are then modified so that aeroloads from AERODYN (Hansen, 1998) computed for the uncoupled blade were also applied to the coupled one (in lieu of the aeroloads AERODYN would normally compute for the

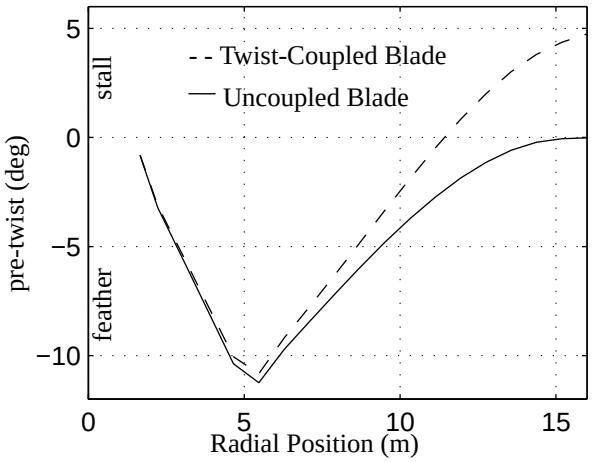

Figure 6.1: pre-twist for the twist-coupled and uncoupled blades.

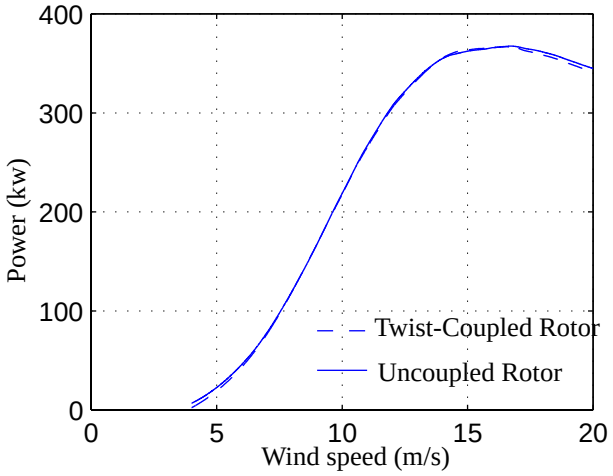

Figure 6.2: Power curves for the uncoupled rotor and the twist-coupled one with optimal pre-twist.

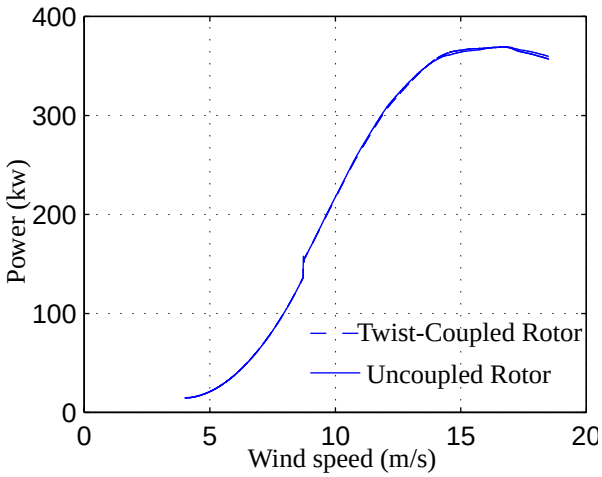

Figure 6.3: Power curves for the variable speed stall-controlled rotor with uncoupled blades and twist-coupled one with optimal pre-twist.

coupled blade). The blade twist distribution that occurs due to the twist-coupling under this loading is then subtracted from the desired twist distribution providing the optimal pre-twist. Thus when the aeroelastic twists are included in the aeroload computations, the twist distribution at the rated power will coincide with the desired one. The accuracy of this technique depends on the linearity of the blade twist with the aeroloads in the range of interest.

For the rotor turning at 32 rpm the windspeed at rated power was defined to be 13 m/s. This value was chosen in part to bring the peak power of the twist-coupled rotor into compliance with that of the uncoupled one. The optimal pre-twist for the twist-coupled blade under the load associated with this windspeed is shown in Figure 6.1 by the dashed curve. To be more consistent with convention, this pre-twist could be recast by shifting the distribution so that the pre-twist is zero at the tip and then specifying a full blade pitch of 4.85 degrees toward stall. The power curves for the coupled rotor with optimal pre-twist and uncoupled rotors operating at a constant speed of 32 rpm are shown in Figure 6.2. Note that the two power curves are essentially equivalent with the uncoupled rotor generating slightly more power than the twist-coupled one at the extremes of the windspeed range.

Variable speed operation was effected by applying a reactive torque to the rotor at the low-speed shaft. For the linear aerodynamics range of the power curve this torque was made proportional to the rpm squared with the coefficient selected to balance the torque produced by the wind loads, thereby allowing the rotor to operate at maximum efficiency. The coefficient for the torque equation in the linear range was computed using data from the peak of the C_p curve for the uncoupled rotor. This coefficient was also used for the twist-coupled rotor although it may not be optimal.

For the variable speed stall-controlled rotor, variable speed transitions to constant speed at 32 rpm. The tip-speed ratio at peak C_p combined with this rotor speed indicate that the corresponding wind speed for the onset of constant speed operation is approximately 8.6 m/s. Constant speed operation was accomplished by significantly increasing the reactive torque when the rpm exceeds the desired constant speed value. Power curves for the uncoupled rotor and the twist-coupled one are shown in Figure 6.3, with the pre-twist of Figure 6.1 applied to the twist-coupled blades. From the jump in the curve in Figure 6.3 where the

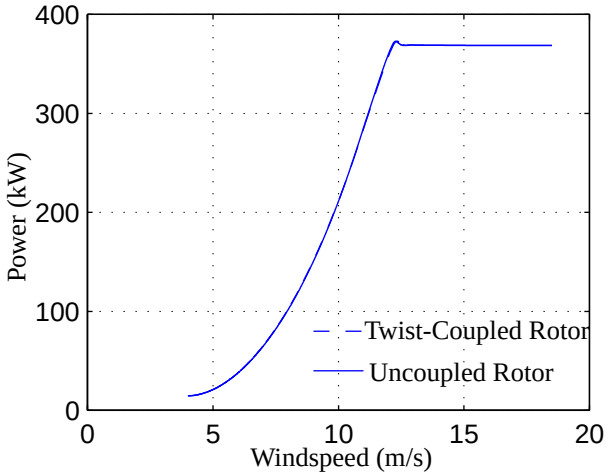

Figure 6.4: Power curves for the variable speed stall-controlled rotor with uncoupled blades and twist-coupled ones with optimal pre-twist.

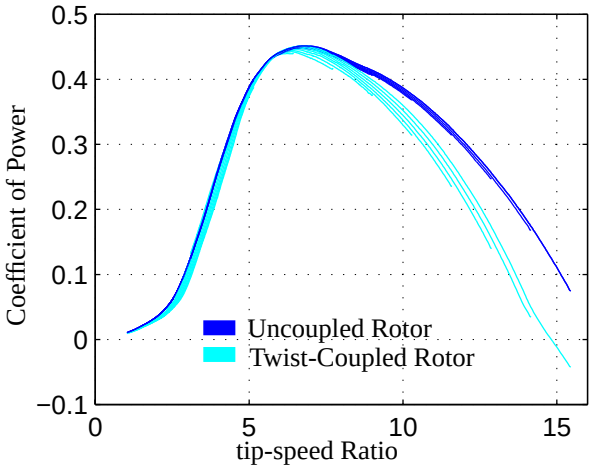

Figure 6.5: C_p curve families for rotor speeds from 12 to 36 rpm for the twist-coupled and uncoupled rotors.

rotors transition from variable speed to constant speed operation, it is evident that the coefficient in the torque equation is sub-optimal.

For the variable speed pitch-controlled rotor, variable speed operation continues until peak power is achieved. This occurs at an rpm of approximately 43.5 with a corresponding wind speed of 12 m/s. For higher wind speeds the rotor speed is held at this value and power is also held constant through active full-span pitch control. An adaptive control scheme developed by K. Pierce at the National Renewable Energy Laboratory was modified for this application. Power curves for the uncoupled rotor and the twist-coupled one are shown in Figure 6.4, with the pre-twist of Figure 6.1 applied to the twist-coupled blades.

Simulated turbulence was created using SNLWIND-3D for 2 average wind speeds as discussed earlier. Inputs to the program were chosen to duplicate conditions specified in the IEC standard. Shear velocity input was used to vary turbulence intensity. Nine 10-minute wind data sets, each with a different seed, were created at each wind speed for IEC turbulence intensity levels. Nine additional 10-minute turbulence files were created at each wind speed with the turbulence intensity set to 50% of IEC levels. Generally, turbulence intensities for the simulated winds at 8, 14 and 20 m/s came out slightly less than the target values.

RESULTS

Steady Wind Results for a Variable Speed Stall-Controlled Twist-Coupled Rotor

For an uncoupled variable speed stall-controlled rotor, the efficiency of the rotor in the linear aerodynamic range can be maximized by running at the tip-speed ratio associated with the peak of the power coefficient curve. For the twist-coupled case, however, the location of the peak of the power coefficient curve changes modestly with rotor rpm due to the twisting of the blades. Thus the maximum rotor efficiency must be represented as a function of windspeed (or rpm) and the rpm-windspeed schedule required to achieve maximum efficiency must be altered from that of the uncoupled rotor.

Using the ADAMS software for both the twist-coupled and uncoupled rotors, power curves were generated for rotor speeds from 12 to 36 rpm in intervals of 3 rpm for windspeeds varying from 4 to 20 m/s. The families of C_p curves shown in Figure 6.5 were developed from these power curves. For the uncoupled

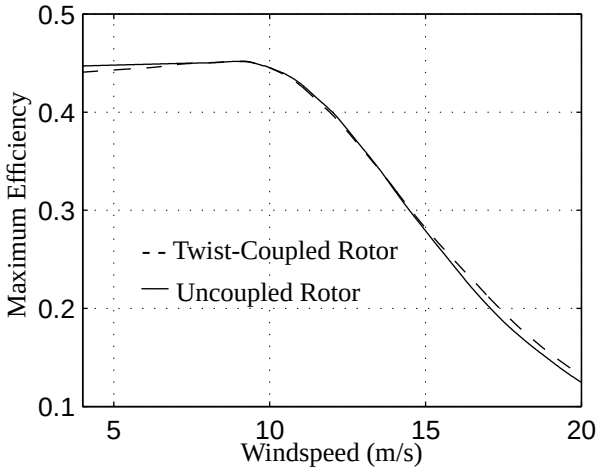

Figure 6.6: Comparison of the efficiencies of the twist-coupled and uncoupled rotors.

rotor, these curves are nearly coincident as expected, but for the twist-coupled one there is some degree of spread due to the induced blade twisting. Plots of the maximum efficiency versus windspeed shown in Figure 6.6 were also developed from the power curves. It is apparent from these curves that over a significant portion of the windspeed range associated with linear aerodynamics, the maximum rotor efficiencies are essentially identical. At lower windspeeds the uncoupled rotor operates at modestly higher efficiencies than the twist-coupled one. The rpm-windspeed schedules required to achieve these efficiencies are shown in Figure 6.7. Note that the schedule for the uncoupled rotor is approximately linear

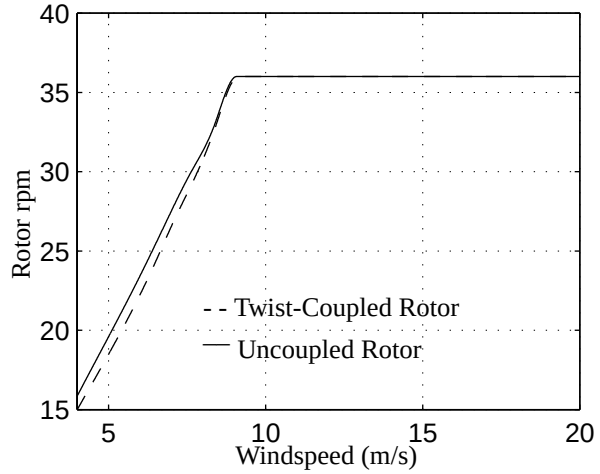

Figure 6.7: Comparison of the maximum efficiency rpm schedules for the twist-coupled and uncoupled rotors.

with windspeed, representing a constant tip-speed ratio. The C_p curves of Figure 6.5 indicate that those for the twist-coupled rotor tend to have sharper peaks than those for the uncoupled rotor. This may result in reduced energy capture in a turbulent wind environment. This issue will be investigated in the next segment of this section

Turbulent Wind Results for Twist-Coupled Rotors Using Three Control Strategies

Simulation results discussed in this segment include normalized fatigue damage and average power for uncoupled and twist-coupled constant speed stall-controlled, variable speed stall-controlled and variable speed pitch-controlled rotors driven by the various turbulent wind loadings.

The fatigue damage is computed for the out-of-plane root bending moment only, as the loads are generally highest for that moment at that location. Loads due to blade twist are not considered in the damage computation.

Figure 6.8 summarizes the fatigue damage results for the baseline constant speed stall-controlled rotor. For each turbulence intensity

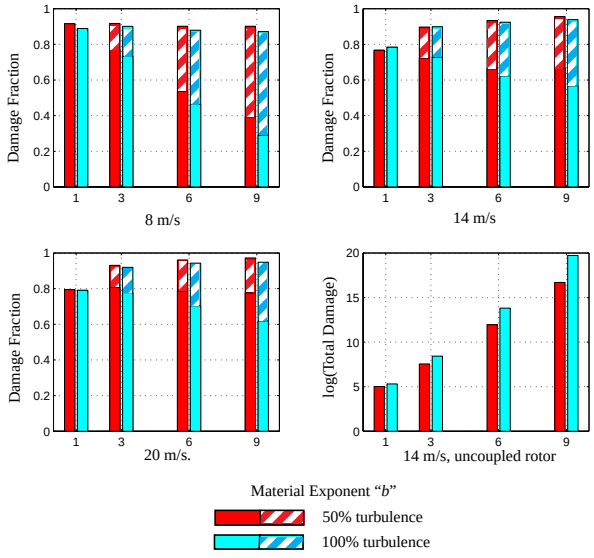

Figure 6.8. Damage (solid) and damage equivalent load (striped) fractions for the constant speed stall-controlled rotor.

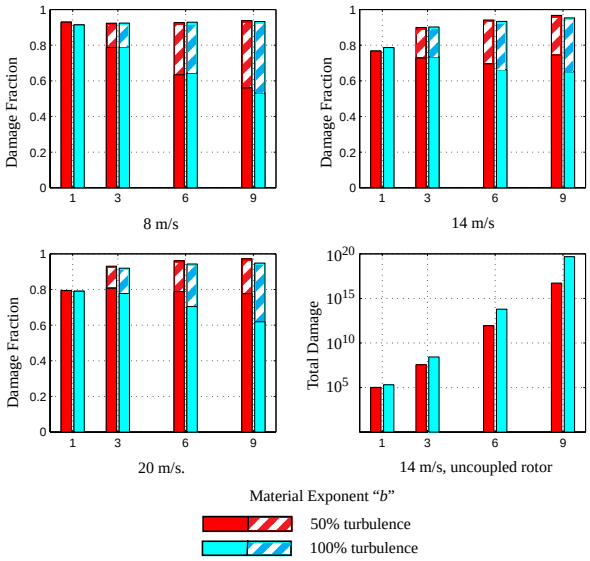

Figure 6.9. Damage (solid) and damage equivalent load (striped) fractions for the variable speed stall-controlled rotor.

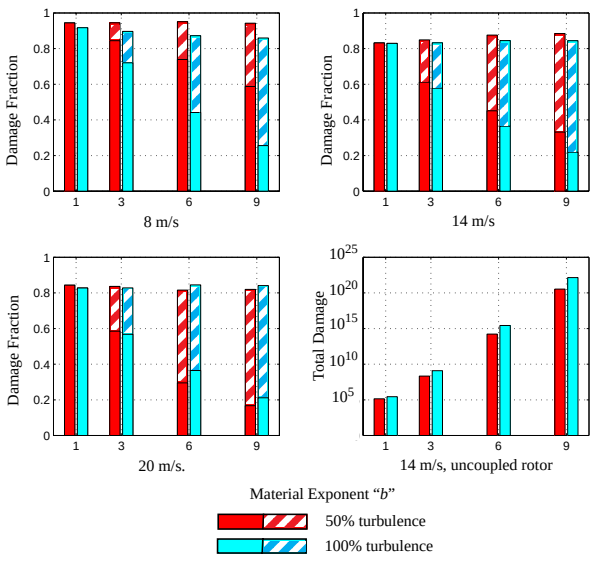

Figure 6.10. Damage (solid) and damage equivalent load (striped) fractions for the variable speed pitch-controlled rotor.

and wind speed the damage fraction (solid bars), which is the ratio of the damage incurred by the twist-coupled rotor to the uncoupled one, is provided. Damage equivalent load fractions (striped bars), which are the ratio of the damage equivalent load for the twist-coupled rotor to the uncoupled one, are also provided. Although not apparent from the damage fractions, the magnitude of the damage reductions is markedly greater for the higher material exponents as indicated by the "log(Total Damage)" bar chart of Figure 6.8. Generally the damage fractions run from 0.6 to 0.8, except for the higher exponents at the 8 m/s average wind speed where they are significantly lower. This is the result of the higher load ranges that occur when the rotor is operating in the linear aerodynamic range, providing a greater opportunity for damage reduction. The damage fractions are generally smaller for 100% turbulence when compared to 50% turbulence, as expected. The bars for the material exponent of 1 signify the average cyclic load fractions that occur for the twist-coupled rotor relative to the uncoupled one. They are approximately 0.9 at 8 m/s and near 0.8 for the higher wind speeds.

Fatigue damage results for the variable speed stall-controlled rotor shown in Figure 6.9 are quite similar to those for the baseline constant speed rotor presented in Figure 6.8. One minor difference, for which there is no immediate explanation, is that the significantly lower damage fractions noted in the baseline constant speed case for the higher exponents at 8 m/s are somewhat larger for the variable speed rotor.

For the variable speed pitch-controlled rotor the damage fractions and damage equivalent load fractions shown in Figure 6.10 are generally lower than those for the previous two cases. At the average wind speed of 8 m/s results are similar to prior solutions, but for the higher wind speeds the fractional damage measures are substantially smaller. This is a consequence of the pitch-control which keeps the rotor operating in the linear aerodynamic range regardless of wind speed. As for the 8 m/s windspeed, the higher load ranges that occur when the rotor is operating in this range provide greater opportunity for damage reduction. Generally, but not always, the higher turbulence level produced smaller damage fractions.

In Figure 6.11, power fractions, which are the ratios of the power produced by the twist-cou-

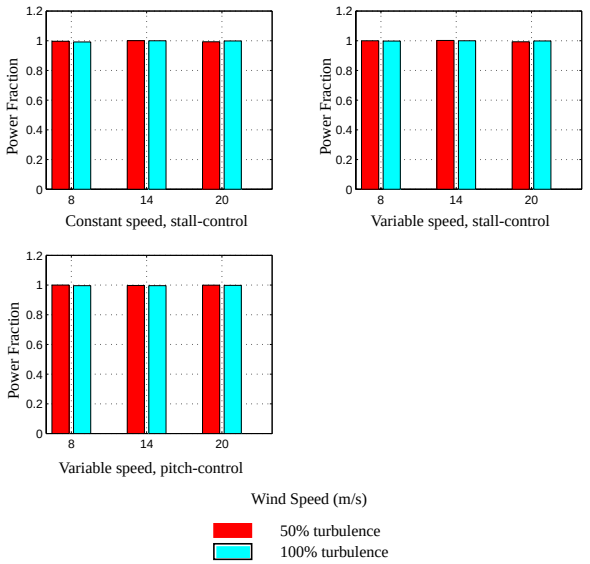

Figure 6.11. Power fractions for the twist-coupled rotor with the three control strategies.

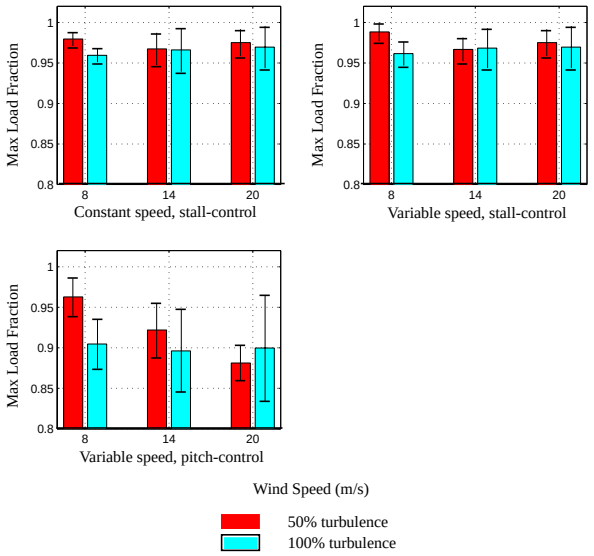

Figure 6.12. Maximum load fractions for the twist-coupled rotor with the three control strategies.

pled rotor to the uncoupled one, are provided for the three control strategies. As indicated, differences in power output between the uncoupled and twist-coupled rotors are negligible for all three control strategies. Maximum power degradations are 0.8%, 0.7% and 0.5% for the constant speed stall-controlled, variaable speed stall-controlled and the variable speed pitch-controlled rotors, respectively.

In Figure 6.12, maximum load fractions are provided for the three control strategies. These are computed by first forming the maximum load fractions (ratios of the maximum load experienced by the twist-coupled rotor to the uncoupled one) for each of the nine ten-minute records. The mean (solid bar) and standard deviations (error bands) for each of these sets of data are displayed in the figure. Maximum load fractions are similar for the constant speed and variable speed stall-controlled rotors, but significantly smaller for the variable speed pitch controlled one.

Turbulent Wind Results for a Variable Speed Stall-Controlled Softened Uncoupled Rotor

In Lobitz and Veers (1998) and Ong et al. (1999), mathematical expressions are presented indicating that the introduction of off-diagonal terms in the beam stiffness matrix, required to model twist-coupling causes the beam to become softer in bending, even though the terms representing the flexural rigidity are not altered. This softening is also apparent in the current simulations where blade tip deflections for the twist-coupled rotor exceed those of the uncoupled one by approximately 50%, as shown in the histograms of Figure 6.13, which correspond to a windspeed of 14 m/s and a turbulence level of 100% of the

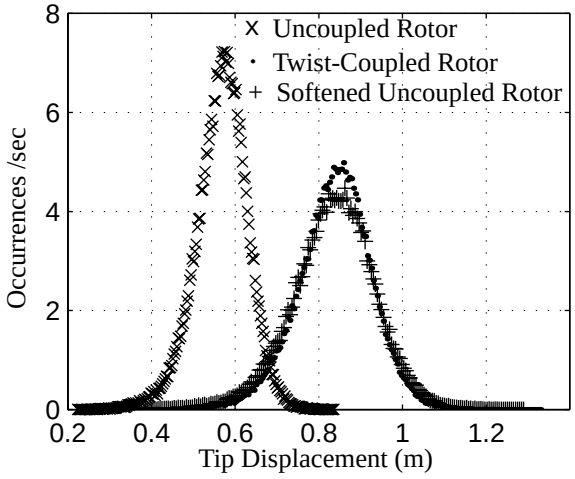

Figure 6.13: Histograms of tip displacements for the uncoupled, twist-coupled and softened uncoupled rotors (14m/s, 100% IEC turbulence intensity).

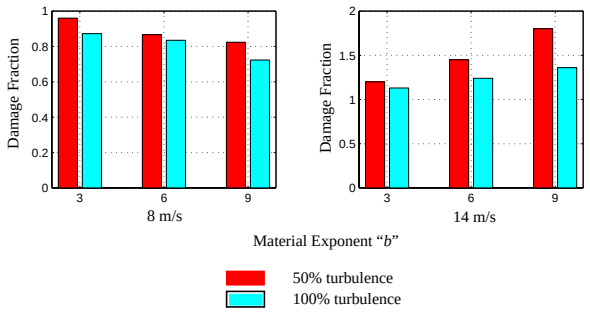

Figure 6.14. Damage fractions for the variable speed stall-controlled softened uncoupled rotor.

IEC Standard. To determine the role this softening plays in the damage reduction, an additional uncoupled model was developed where both the blade flexural rigidity and torsional stiffness were reduced to be commensurate with those of the twist-coupled model. Variable speed, stall control was used to control the rotor. Resulting blade tip deflections for this new model are equivalent to those of the twist-coupled one (see Figure 6.13).

Fatigue damage comparisons for this new softer uncoupled model relative to the previous uncoupled one are shown in Figure 6.14 using the damage fraction defined as the ratio of the damage incurred by the softer uncoupled rotor to that of the original uncoupled one. The bar charts for the 8 m/s windspeed show that there is indeed a damage reduction associated with the softer uncoupled model, although not as large as that of the twist-coupled rotor shown in Figure 6.9. For 14 m/s windspeed, where the rotor has entered the stall aerodynamic range, the damage for the softer uncoupled rotor actually increases relative to the stiffer one. Thus, just softening the blades produces mixed results with regard to fatigue damage reduction and at best provides only a fraction of the damage reduction produced when twist-coupling is incorporated.

CONCLUSIONS AND RECOMMENDATIONS

The ADAMS software is employed to investigate the feasibility of using HAWT blades that twist as they bend to mitigate fluctuating loads for a variable speed rotor. The twist coupling coefficient for the blades was set at $\alpha = 0.6$ (twisting toward feather), and the blades were pre-twisted toward stall to match the constant speed power curve for uncoupled blades. Power control is achieved using three different strategies. The first, used as a baseline, is just stall control with a constant speed rotor. In the second, variable speed is implemented by imposing a reactive torque on the low-speed shaft proportional to the rpm squared, with the coefficient specified so that the rotor operates at peak efficiency in the linear aerodynamic range. At higher wind speeds, the maximum rpm is limited so as to take advantage of the stall controlled nature of the rotor. The third strategy also employs variable speed, but pitch control is implemented at the higher wind speeds enabling the rotor to continue operating in the linear aerodynamic range.

Prior to running turbulent wind simulations, steady wind results were obtained showing that for variable speed stall-controlled operation the twist-coupled rotor described above can be almost as efficient as the uncoupled one if a slightly altered rpm-windspeed schedule is followed.

Turbulent wind simulations were made for three average hub-height wind speeds and two wind turbulence settings. Fatigue damage is computed from the load histories using material exponents that represent materials ranging from welded steel to composites. In most cases significant fatigue damage reductions (20-80%) were exhibited by the twist-coupled rotor. For the constant speed and variable speed rotors that employed stall-control, significant damage reductions were observed at the higher material exponents for the 8 m/s average wind speed where the rotor operates primarily in the linear aerodynamic range. For the variable speed pitch-controlled rotor, significant reductions were observed at the higher wind speeds as well due to its ability to con-

tinue to operate in the linear aerodynamic range even at the higher windspeeds. In all cases power production for the twist-coupled rotor was equivalent to the uncoupled one. Thus, for this twist-coupled rotor, substantial fatigue damage reductions prevail for the rotor in variable speed operation as in the case for constant speed, and with no loss in power output. Maximum loads for the twist-coupled rotors were also reduced, especially for the variable speed pitch-controlled one.

The turbine model used was a simple one, making it difficult to extrapolate results to machines incorporating free yaw and/or non-zero rotor coning. The combination of rotor coning and variable speed is especially interesting, as twist will vary with rotor speed due to flap loading caused by centrifugal force. The substantial fatigue-damage reductions that have been predicted call for additional study, and twist-coupled rotors incorporating these increasingly common characteristics should be investigated not only for load mitigation but also to determine the impact of twist-coupling on various rotor control forces.

The fatigue benefits of twist-coupling can only be realized if blades incorporating this trait can be built. Composite, uniform, D-spars have already been designed and fabricated[6] that possess coupling coefficients in the range of 0.6. The next step involves the design and fabrication of a much more complex twist-coupled blade with a coupling coefficient in this same range. Design factors such as spanwise variance of coupling coefficient and optimization of blade geometry to take advantage of twist-coupling need to be investigated. The ultimate goal is to design and produce a rotor blade that provides maximum benefit to turbine performance with minimal additional production cost.

ACKNOWLEDGEMENTS

The authors wish to express their gratitude to Marshall Buhl for his assistance in getting the PC version of ADAMS up and running at Sandia, Craig Hansen for his guidance in developing a simple variable speed control system for stall controlled rotors, and Kirk Pierce for providing his control system for variable speed, pitch-controlled rotors.

Conclusions

The incorporation of twist-coupled blades in rotor design can be beneficial to energy production or load reduction, and possibly both simultaneously. For reducing loads, the blades are designed to twist toward feather as they bend. For variable speed pitch-controlled rotors twist-coupling substantially decreases fatigue damage over all wind speeds, without reducing average power. Maximum loads also decrease modestly. For constant speed stall-controlled and variable speed stall-controlled rotors significant decreases in fatigue damage are observed at the lower wind speeds and smaller decreases at the higher wind speeds. Maximum loads also decrease slightly. As a general observation, whenever a rotor is operating in the linear aerodynamic range (lower wind speeds for stall-control and all wind speeds for pitch-control), substantial reductions in fatigue damage are realized.

For blades that are designed to twist toward stall as they bend fatigue damage loads dramatically increase as do the maximum loads. In addition, time series computations for both steady and turbulent inflow indicate stall-flutter behavior with this type of twist-coupling.

As twist-coupling may promote aeroelastic instability, classical flutter and divergence were investigated for the Combined Experiment Blade rotating in still air. For a wide range of twist-coupling it was found that twist-coupling toward stall tends to render the blade less stable in divergence and twist-coupling toward feather tends to render the blade less with regard to classical flutter. However, in both cases, these destabilizing effects are not critical to the stable operation of the rotor.

For improving energy production, the blades are designed to moderately twist toward stall as they bend or extend. For a stall-controlled rotor this has the effect of advancing stall and pulling the power curve down below rated power. The power curve can then be restored by increasing the diameter of the rotor. Depending on twist-coupling parameters and inflow environments, energy production increases between 5% and 10% can be realized. For a variable speed stall-controlled rotor, by optimally selecting blade pitch and twist-coupling parameters, the optimal energy capture of a variable speed variable-speed-controlled rotor can be approached. However, as mentioned above, twist-coupling toward stall is associated with significantly higher fatigue and maximum loads, and a greater proclivity for stall-flutter.

Although some preliminary work has been done in designing and manufacturing a D-spar with bending twist-coupling to determine practical limits, future efforts will focus on the design and manufacture of actual blades with bending twist-coupling. The goal is for these blades to meet performance and reliability objectives without being prohibitively expensive.

References

ADAMS/SOLVER Reference Manual, Version 8.0, Mechanical Dynamics, Inc., Ann Arbor, November 15, 1994.

ADAMS/WT User's Guide, Version 1.50, Mechanical Dynamics, Inc., Ann Arbor, February 1997.

Bielawa, R. L. (1971) "Techniques for Stability Analysis and Design Optimization with Dynamic Constraints of Nonconservative Linear Systems," AIAA Paper 71-388.

Bir, G., Chopra, I., Nguyen, K. (1990) "Development of UMARC (University of Maryland Advanced Rotor Code)," *Proc. of the 46th Annual National Forum of the AHS*, Washington, D.C., May 1990.

Bir, G., and Chopra, I. (1994) "Aeroelastic Stability of Rotorcraft with Advanced Geometry Blades," *Mathematical and Comp. Modeling*, Vol. 19, No. 34, Feb. 1994.

Bischof, C. et al. (1995) " ADIFOR 2.0 User's Guide," Mathematics and Computer-Science Division, Technical Memoradum No. 192, Argonne National Laboratory, Argonne, IL, August 1995.

Bisplinghoff, R. L., Ashley, H. and Halfman, R. L. (1955) *Aeroelasticity*, Addison-Wesley Publishing Company, 1955, p.272.

Blackwell, R. H. (1983) "Blade Design for Reduced Helicopter Vibration," *Journal of the American Helicopter Society*, Vol. 28, No. 3, pp. 33-41.

Bottrell, G. W. (1981) "Passive Cyclic Pitch Control for Horizontal Axis Wind Turbines," Proceedings of Wind Turbine Dynamics, NASA Conf. Pub. 2185, DOE Pub. CONF-810226, Cleveland, OH.

Carlin, P. (1997) "Analytical Expressions for Maximum Wind Turbine Average Power in a Rayleigh Wind Regime," *1997 ASME Wind Energy Symposium* held at 35th AIAA Aerospace Sciences Meeting and Exhibition, Reno, NV, Jan. 6-9, 1997.

Celi, R. (1987) "Aeroelasticity and Structural Optimization of Helicopter Rotor Blades with Swept Tips," *Ph.D. Dissertation*, Mechanical, Aerospace and Nuclear Engineering Dept., UCLA.

Celi, R., and Friedman, P. P. (1988) "Structural Optimization with Aeroelastic Constraints of Rotor Blades with Straight and Swept Tips," *AIAA Paper 88-2297*; also, *AIAA Journal*, Vol. 28, No.5.

Celi, R. (1989) "Optimum Design of Helicopter Rotors for Longitudinal Handling Qualities Improvement in Forward Flight," AIAA Paper 89-1270.

Chandra, R., and Chopra, I. (1991) "Experimental and Theoretical Analysis of Composite I-Beams with Elastic Couplings," *AIAA Journal*, Vol. 29, No. 12.

Chandra, R., and Chopra, I. (1992) "Structural Behavior of Two-Cell Composite Rotor Blades with Elastic Couplings," *AIAA Journal*, Vol. 30, No. 12.

Cheney, M. C. and Speirings, P. S. M. (1978) "Self Regulating Composite Bearingless Wind Turbine," *Solar Energy*, Vol. 20.

Corbet, D. C. and Morgan, C. A. (1992) "Report on the Passive Control of Horizontal Axis Wind Turbines," ETSU WN 6043, Garrad Hassan and Partners, Bristol, UK.

Currin, H. (1981) "North Wind 4kW `Passive' Control System Design," Proc. *Wind Turbine Dynamics*, NASA Pub. 2185, DOE Pub. CONF-810226, Cleveland, OH.

Daughaday, H., DuWaldt, F., and Gates, C. (1957) "Investigation of Helicopter Blade Flutter and Load Amplification

Problem," *J. of the American Helicopter Soc.*, Vol. 2, No. 3, pp. 27-45.

Davis, M. W., and Weller, W. H. (1988) "Application of Design Optimization Techniques to Rotor Dynamics Problems," *J. of the AHS*, Vol. 33, No. 3, July, pp. 42-50.

Eggers, A. J. Jr., Ashley, H., Rock, S. M., Chaney, K., and Digumarthi, R. (1996) "Effects of Blade Bending on Aerodynamic Control of Fluctuating Loads on Teetered HAWT Rotors," *J. of Solar Energy Engr.*, Vol. 118, No. 4, Nov. 1996.

Eisler, G. R. and Veers, P. S. (1998) "Optimization Applied to Adaptive Blade Use on a Variable-Speed Wind Turbine," Sandia National Laboratories, to be published.

Eldred, M.S. et al (1996) "Utilizing Object-Oriented Design to Build Advanced Optimization Strategies with Generic Implementation," paper AIAA-96-4164 in *Proceedings of the 6th AIAA/USAF/NASA/ISSMO Symposium on Multi-Disciplinary Optimization*, Bellevue, WA, Sept 4-6, 1996, pp. 1568-1582.

Feuchtwang, J. B. and D. G. Infield (1995) "Aerofoil profile section for passive pitch control using self-twisting blades," Wind Energy Conversion, Proc. 17th BWEA Wind Energy Conf., ed. J. Halliday, BWEA, Warwick, July 19-21, 1995.

Fingersh, L. and Carlin, P. (1998) "Results from the NREL Variable-Speed Test Bed," AIAA-98-0050, Proc. *1998 ASME Wind Energy Symposium* held at 36th AIAA Aerospace Sciences Meeting and Exhibition, Reno, NV, Jan. 12-15, 1998.

Friedmann, P. P., and Shanthakumaran, P. (1983) "Aeroelastic Tailoring of Rotor Blades for Vibration Reduction in Forward Flight," *AIAA Paper 83-0916*,.

Friedmann, P. P., and Shanthakumaran, P. (1984) "Optimum Design of Rotor Blades for Vibration Reduction in Forward Flight," *Journal of the AHS*, Vol. 29, No. 4, pp. 70-80.

Friedmann, P.P., Venkatesan, C., and Yuan, K. (1992) "Development of a Structural Optimization Capability for the Aeroelastic Tailoring of Composite Rotor Blades with Straight and Swept Tips," *4th AIAA Symp. on Multidisciplinary Analysis and Optimizations*, Cleveland, Ohio, Sept. 1992.

Ganguli, R., and Chopra, I. (1992) "Aeroelastic Optimization of a Composite Helicopter Rotor," *Fourth AIAA Symposium on Multidisciplinary Analysis and Optimizations*, Cleveland, Ohio, Sept. 1992.

Ganguli, R., and Chopra, I. (1993) "Aeroelastic Optimization a Helicopter Rotor with Composite Tailoring," *Proceedings of the 49th Annual Forum and Technology Display of the American Helicopter Society*, St. Louis, Missouri, May 19-21, 1993.

Ganguli, R., and Chopra, I. (1994) "Multi-Objective Optimization of a Composite Helicopter Rotor," Presented at *the 35th Structures, Structural Dynamics and Materials Conference and Adaptive Structures Forum*, April 1994.

Ganguli, R., and Chopra, I. (1997) "Aeroelastic Tailoring of Composite Couplings and Blade Geometry of a Helicopter Rotor Using Optimization Methods," *Journal of the AHS*, Vol. 42, No. 3.

Hansen, A. C. (1998) AeroDyn for ADAMS User's Guide, Version 11.0, University of Utah, Salt Lake City, August 31, 1998.

Hirch, H., Dutton, R. E., and Rasamoff, A. (1956) "Effects of Spanwise and Chordwise Mass Distribution on Rotor Blade Cyclic Stresses," *Journal of the AHS*, Vol. 1, No. 2, pp. 37-45.

Hohenemser, K. H. and Swift, A. H. P. (1981) "Dynamics of an Experimental Two Bladed Horizontal Axis Wind Turbine with Blade Cyclic Pitch Variation," *Wind Turbine Dynamics*, NASA Pub. 2185, DOE Pub. CONF-810226, Cleveland, OH.

Hong, C.H., and Chopra, I. (1985) "Aeroelastic Stability of a Composite Blade," *Journal of the AHS*, Vol. 30, No. 2.

Infield D. G. and J. B. Feuchtwang (1995) "Design criteria for passive pitch control of wind turbines using self-twisting blades," International Journal of Ambient Energy, Vol. 16, No. 3, July 1995.

Infield, D. G., Feuchtwang, J. B. and Fitches, P. (1999) "Development and Testing of a Novel Self-Twisting Wind Turbine Rotor," Proceedings of the 1999 European Wind Energy Conference, pp329-332, Nice, France, Mar 1-5, 1999.

Joose, P. A. and van den Berg, R. M. (1996) "Development of a TenTorTube for Blade Tip Mechanisms," P7.17, Proc., *1996 European Union Wind Energy Conf. and Exhib.*, Götegorg, May 20-24, 1996.

Karaolis, N. M., Mussgrove, P. J., and Jeronimidis, G. (1988) "Active and Passive Aeroelastic Power Control using Asymmetric Fibre Reinforced Laminates for Wind Turbine Blades," Proc. *10th British Wind Energy Conf.*, D. J. Milbrow Ed., London, March 22-24, 1988.

Karaolis, N. M., Jeronimidis, G., and Mussgrove, P. J. (1989) "Composite Wind Turbine Blades: Coupling Effects and Rotor Aerodynamic Performance," Proc., *EWEC'89*, European Wind Energy Conf., Glasgow, Scotland, 1989.

Kashef, T. and Winterstein, S. R. (1998) Moment Based Modeling and Extreme Response Estimation – The FITS Routine, Report No. RMS-31, Civil Engineering Dept., Stanford University, 1998.

Kelley, N. D. (1993) "Full-Vector (3-D) Inflow Simulation in Natural and Wind Farm Environments Using an Expanded Version of the SNLWIND (Veers) Turbulence Code," Proceedings of the 12th ASME Wind Energy Symposium, Houston, 1993.

Klimas, P. C. (1984) "Tailored Airfoils for Vertical Axis Wind Turbines," SAND84-1062, Sandia National Laboratories, Albuquerque, NM.

Kooijman, H. J. T. (1996) "Bending-Torsion Coupling of a Wind Turbine Rotor Blade," ECN-I--96-060, Netherlands Energy Research Foundation ECN, Petten the Netherlands.

Lim, J., and Chopra, I. (1987) "Design Sensitivity Analysis for an Aeroelastic Optimization of a Helicopter Rotor," AIAA Paper 87-0923.

Lim, J., and Chopra, I. (1988) "Aeroelastic Optimization of a Helicopter Rotor," Proc., *44th Annual Forum of the AHS*, Washington DC, June 1988, pp. 545-558.

Lobitz, D. W. (1984) "A NASTRAN-Based Computer Program for Structural Dynamic Analysis of Horizontal Axis Wind Turbines," Proceedings of the *Horizontal Axis Wind Turbine Technology Workshop*, Department of Energy and NASA-Lewis, Cleveland, May 1984.

Lobitz, D. W. and Ashwill,T. D. (1985) "Aeroelastic Effects in the Structural Dynamic Analysis of Vertical Axis Wind Turbines," Proceedings of the *Windpower 85 Conference*, San Francisco, August 1985.

Lobitz, D. W., Veers, P. S., and Migliore, P. G. (1996) "Enhanced Performance of HAWTs Using Adaptive Blades," Proc. *Wind Energy '96, ASME Wind Energy Symposium*, Houston, Jan. 29 - Feb. 2, 1996.

Lobitz, D. W. and Veers, P. S. (1998) "Aeroelastic Behavior of Twist-Coupled HAWT Blades," AIAA-98-0029, Proc. *1998 ASME Wind Energy Symposium* held at 36th AIAA Aerospace Sciences Meeting and Exhibition, Reno, NV, Jan. 12-15, 1998.

Lobitz, D. W. and Laino, D. J. (1999) "Load Mitigation with Twist-Coupled HAWT Blades," Proc. *1999 ASME Wind Energy Symposium* held at 37th AIAA Aerospace Sciences Meeting and Exhibition, Reno, NV, Jan. 11-14, 1999.

Lobitz, D. W., Veers, P. S. and Laino, D. J. (2000) "Performance of Twist-Coupled Blades on Variable Speed Rotors," Proc. *2000 ASME Wind Energy Symposium* held at 38th AIAA Aerospace Sciences Meeting and Exhibition, Reno, NV, Jan. 10-13, 2000.

McCarthy, J. L., and Brooks, G. W. (1955) "A Dynamic Model Study of the Effect of Added Weights and Other Structural Variations on the Blade Bending Strains of an Experimental Two-Blade Jet-Driven Helicopter in Hovering and Forward Flight," *NACA TN-3367*.

Middleton, V., Fitches, P. Jeronimidis, G. and Feuchtwang, J. (1998) "Passive Blade Pitching for Overspeed Control of an HAWT," Wind Energy 1998, Proceedings of the 20th British Wind Energy Association Conference, Cardiff University of Wales, Sept 2-4, 1998.

Miller, R.H., and Ellis, C.W. (1956) "Helicopter Blade Vibration and Flutter," *Journal of the American Helicopter Society*, Vol. 1, No. 3, pp. 19-38.

Miura, H., and Schmit, L. A. (1979) "NEWSUMT- A Fortran Program for Inequality Constrained Function Minimization-User's Guide." *NASA CR- 159070*.

Moriarty, P. J., Eggers,A. J., Chaney, K. and Holley, W. E. (2001) "Scale and Lag Effects on Control of Aerodynamic Power and Loads on a HAWT Rotor," Proc. *2001 ASME Wind Energy Symposium* held at 39th AIAA Aerospace Sciences Meeting and Exhibition, Reno, NV, Jan. 8-11, 2001.

Muljadi, E., C. P. Butterfield, and P. Migliore (1996) "Variable Speed Operation of Generators with Rotor-Speed Feedback in Wind Power Applications," Proc. *Energy Week '96*, *Book VIII Wind Energy*, (ASME Wind Energy Symposium) Houston, Texas, Jan. 29-Feb. 2, 1996.

Muljadi, E., C. P. Butterfield, and M. L. Buhl (1997) "Effects of Turbulence on Power Generation for Variable-Speed Wind Turbines," Proc. *1997 ASME Wind Energy Symposium*, AIAA-97-0963, held at the 35th AIAA Aerospace Sciences Meeting and Exhibit, Reno, Nevada, January 6-9,1997.

Ong, C. H. and Tsai, S. W. (1999) "Design, Manufacture and Testing of a Bend-Twist D-Spar," Proceedings of the 1999 ASME Wind Energy Symposium, Reno, January 11-14, 1999.

Panda, B., and Chopra, I. (1987) "Dynamics of Composite Rotor Blades in Forward Flight*," Vertica*, Vol. 11, No. 1-2.

Peters, D. A., Rossow, M. P., Korn, A., and Ko, T. (1986) "Design of Helicopter Rotor Blades for Optimum Characteristics," *Computers and Mathematics with Appls.,* Vol. 12A, No.1, pp. 85-109.

Peters, D. A., and Cheng, Y. P. (1988) "Optimization of Rotor Blades for Combined Structural Performance and Aeroelastic Constraints," Proc., *Recent Advances in Multidisciplinary Analysis and Optimization*, NASA CP-3031, Pt. 1, pp. 163-180.

Pierce, K. G. and Migliore, P. G. (2000) "Maximizing Energy Capture of Fixed-Pitch Variable-Speed Wind Turbines," Proceedings of the 2000 ASME Wind Energy Symposium, Reno, January 10-13, 2000.

Safety of Wind Turbine Generator Systems, International Electrotechnical Commission, IEC 61400-1, Second Edition, 1998.

Shanthakumaran, P. (1982) "Optimum Design of Rotor Blades for Vibration Reduction in Forward Flight," *Ph.D. Dissertation*, Mechanics and Structures Dept. UCLA.

Smith, E. C., and Chopra, I. (1991) "Formulation and Evaluation of an Analytical Model for Composite Box Beams," *Journal of the American Helicopter Society.*

Stoddard, F., Nelson, V., Starcher, K., Andrews, B. (1989) "Determination of Elastic Twist in Horizontal Axis Wind Turbines," AEI, West Texas State Univ., SERI Cntr. RL-6-06013, NREL, Golden, CO.

Tangler, J. (1987) "A Horizontal Axis Wind Turbine Performance Prediction Code for Personal Computers," Solar Energy Research Institute, Golden, CO.

Tangler, J. (1990) "Atmospheric Performance of the SERI Thin Airfoil Family: Final Report," Proc. *Windpower '90*, American Wind Energy Association, Washington DC, Sept. 24-28, 1990.

Tangler, J., Smith, B., Kelley, N. and Jager, D., (1991) "Measured and Predicted Rotor Performance for the SERI Advanced Wind Turbine Blades," *Proceedings of Windpower '91*, AWEA/DOE /SERI, Palm Springs, CA.

Tangler, J. and Somers, D. (1995) "NREL Airfoil Families for HAWTs," *Proc. Windpower `95*, American Wind Energy Association, Washington D. C.

Taylor, R. B. (1982) "Helicopter Vibration by Rotor Blade Modal Shaping," Proc., *38th Annual Forum of American Helicopter Society*, Anaheim, CA, May, pp. 90-101.

The Math Works Inc., (1992) "MATLAB - High Performance Numeric Computation and Visualization Software," Natick, MA.

Tsai, S. and Ong, C-H. (1998) , "D-Spar Blade Design and Manufacture," unpublished contractor reports, Sandia National Laboratories contract BB-6066 Stanford University.

Veers, P. S., Bir, G. and Lobitz, D. W. (1998) "Aeroelastic Tailoring in Wind-Turbine Blade Applications," Proc. Windpower '98, AWEA Annual Conference and Exhibition, Bakersfield, Apr. 27 - May 1, 1998.

Vanderplaats Research and Development Inc., 1995 DOT Users Manual, Version 4.20, Colorado Springs, CO.

van den Berg, R. M., P. A. Joosse, and B. J. C. Visser (1994) "Passive Power Control by Self Twisting Blades," Proc., European Wind Energy Association Conf. and Exhib., Thessaloniki, Oct. 10-14, 1994.

Weller, W. H., Davis, M. W. (1988) "Experimental Verification of Helicopter Blade Design Optimized for Minimum Vibration, "Proc., *44th Annual National Forum of the American Helicopter Society* , Washington, DC, June 1988, pp. 263-279.

Weller, W. H., Davis, M. W. (1989) "Wind Tunnel Tests of Helicopter Blade Design Optimized for Minimum Vibration," *Journal of the AHS, Vol. 34, No. 3, July 1989,* pp. 40-50.

Windpower Monthly (1998) February Windtech Notes, compiled by D. Milborrow, pp. 42-43.

Distribution

T. Almeida
TPI Composites Inc.
373 Market Street
Warren, Rhode Island 02885

H. Ashley
Dept. of Aeronautics and
Astronautics Mechanical Engr.
Stanford University
Stanford, CA 94305

K. Bergey
University of Oklahoma
Aero Engineering Department
Norman, OK 73069

G. Bir (3)
NREL
1617 Cole Boulevard
Golden, CO 80401

R. Blakemore
Enron Wind Corp.
13681 Chantico Road
Tehachapi, CA 93561

G. Bywaters
Northern Power Systems.
Box 999
Waitsfield,VT 05673

J. Cadogan
Office of Geothermal & Wind
Technology
EE-12
U.S. Department of Energy
1000 Independence Avenue SW
Washington, DC 20585

D. Cairns
Montana State University
Mechanical & Industrial Engineering Dept.
220 Roberts Hall
Bozeman, MT 59717

S. Calvert
Office of Geothermal & Wind
Technology
EE-12
U.S. Department of Energy
1000 Independence Avenue SW
Washington, DC 20585

J. Chapman
OEM Development Corp.
840 Summer St.
Boston, MA 02127-1533

Kip Cheney
PS Enterprises
222 N. El Segundo, #576
Palm Springs, CA 92262

C. Christensen
Enron Wind Corp.
13681 Chantico Road
Tehachapi, CA 93561

R. N. Clark
USDA
Agricultural Research Service
P.O. Drawer 10
Bushland, TX 79012

J. Cohen
Princeton Economic Research, Inc.
1700 Rockville Pike
Suite 550
Rockville, MD 20852

C. Coleman
Northern Power Systems
Box 999
Waitsfield, VT 05673

K. J. Deering
The Wind Turbine Company
515 116th Avenue NE
No. 263
Bellevue, WA 98004

A. J. Eggers, Jr.
RANN, Inc.
744 San Antonio Road, Ste. 26
Palo Alto, CA 94303

D. M. Eggleston
DME Engineering
1605 W. Tennessee Ave.
Midland, TX 79701-6083

P. R. Goldman
Director
Office of Geothermal & Wind Technology
EE-12
U.S. Department of Energy
1000 Independence Avenue SW
Washington, DC 20585

G. Gregorek
Aeronautical & Astronautical Dept.
Ohio State University
2300 West Case Road
Columbus, OH 43220

D. Griffin
GEC
5729 Lakeview Drive NE, Ste. 100
Kirkland, WA 98033

C. Hansen
Windward Engineering
4661 Holly Lane
Salt Lake City, UT 84117

C. Hedley
Headwaters Composites
105 E. Adams St.
Three Forks, MT 59752

C. Hiel
W. Brandt Goldsworthy & Assoc.
23930 Madison Street
Torrance, CA 90505

S. Hock
Wind Energy Program
NREL
1617 Cole Boulevard
Golden, CO 80401

Bill Holley
3731 Oakbrook
Pleasanton, CA 94588

K. Jackson
Dynamic Design
123 C Street
Davis, CA 95616

E. Jacobsen
Enron Wind
13000 Jameson Rd.
Tehachapi, CA 93561

G. James
NASA-JSC
2101 NASA Rd. 1
Mail Code ES2
Houston, TX 77058-3696

M. Kramer
Foam Matrix, Inc.
PO Box 6394
Malibu CA 90264

D. Laino (3)
Windward Engineering
4661 Holly Lane
Salt Lake City, UT 84117

D. Malcolm
GEC
5729 Lakeview Drive NE, Ste. 100
Kirkland, WA 98033

J. F. Mandell
Montana State University
302 Cableigh Hall
Bozeman, MT 59717

T. McCoy
GEC
5729 Lakeview Drive NE, Ste. 100
Kirkland, WA 98033

L. McKittrick
Montana State University
Mechanical & Industrial Engineering Dept.
220 Roberts Hall
Bozeman, MT 59717

P. Migliore (3)
NREL
1617 Cole Boulevard
Golden, CO 80401

E. Mroz
Enron Wind Corp.
13681 Chantico Road
Tehachapi, CA 93561

NWTC Library (5)
NREL
1617 Cole Boulevard
Golden, CO 80401

V. Nelson
Department of Physics
West Texas State University
P.O. Box 248
Canyon, TX 79016

J. W. Oler
Mechanical Engineering Dept.
Texas Tech University
P.O. Box 4289
Lubbock, TX 79409

T. Olsen
Tim Olsen Consulting
1428 S. Humboldt St.
Denver, CO 80210

J. Richmond
MDEC
3368 Mountain Trail Ave.
Newbury Park, CA 91320

Michael Robinson
NREL
1617 Cole Boulevard
Golden, CO 80401

D. Sanchez
U.S. Dept. of Energy
Albuquerque Operations Office
P.O. Box 5400
Albuquerque, NM 87185

L. Schienbein
CWT Technologies, Inc.
4006 S. Morain Loop
Kennewick, WA 99337

R. Sherwin
Atlantic Orient
PO Box 1097
Norwich, VT 05055

Brian Smith
NREL
1617 Cole Boulevard
Golden, CO 80401

K. Starcher
AEI
West Texas State University
P.O. Box 248
Canyon, TX 79016

F. S. Stoddard
79 S. Pleasant St. #2a
Amherst, MA 01002

A. Swift
University of Texas at El Paso
320 Kent Ave.
El Paso, TX 79922

R. W. Thresher
NREL
1617 Cole Boulevard
Golden, CO 80401

S. Tsai
Stanford University
Aeronautics & Astronautics
Durand Bldg. Room 381
Stanford, CA 94305-4035

W. A. Vachon
W. A. Vachon & Associates
P.O. Box 149
Manchester, MA 01944

C. P. van Dam
Dept of Mech and Aero Eng,
Univ. of CA, Davis
One Shields Avenue
Davis, CA 95616-5294

B. Vick
USDA, Agricultural Research Service
P.O. Drawer 10
Bushland, TX 79012

R. E. Wilson
Mechanical Engineering Dept.
Oregon State University
Corvallis, OR 97331

S. R. Winterstein
Civil Engineering Department
Stanford University
Stanford, CA 94305

M. Zuteck
MDZ Consulting
931 Grove Street
Kemah, TX 77565

M.S. 0557 T. J. Baca, 9125
M.S. 0557 T. G. Carne, 9124
M.S. 0708 H. M. Dodd, 6214 (25)
M.S. 0708 T. D. Ashwill, 6214
M.S. 0708 D. E. Berg, 6214
M.S. 0708 R. R. Hill, 6214
M.S. 0708 P. L. Jones 6214
M.S. 0708 D. L. Laird, 6214
M.S. 0708 M. A. Rumsey, 6214
M.S. 0708 H. J. Sutherland, 6214
M.S. 0708 P. S. Veers, 6214 (3)
M.S. 0708 J. Zayas, 6214
M.S. 0847 D. W. Lobitz, 9125 (3)
M.S. 0847 D. R. Martinez, 9124
M.S. 0958 M. Donnelly, 1472
M.S. 1003 G. R. Eisler, 15211 (3)
M.S. 1490 A. M. Lucero, 12660
M.S. 0612 Review & Approval Desk, 9612
For DOE/OSTI
M.S. 0899 Technical Library, 9616 (2)
M.S. 9018 Central Technical Files, 8945-1